



Department für Chemie

Lehrstuhl für biomolekulare NMR-Spektroskopie

NMR characterization of the membrane-localized interaction network between the kinase TOR, the GTPase Rheb and the FKBP12-like protein FKBP38.

Maristella De Cicco

Vollständiger Abdruck der von der Fakultät für Chemie der Technischen Universität München zur Erlangung des akademischen Grades eines

Doktors der Naturwissenschaften (Dr. rer.nat)

genehmigten Dissertation.

Vorsitzender: Prof. Dr. Michael Sattler

Prüfer der Dissertation:

1. Priv. Doz. Dr. Sonja A. Dames

2. Prof. Dr. Aymelt Itzen

Die Dissertation wurde am 19.09.2017 bei der Technischen Universität München eingereicht und durch die Fakultät für Chemie am 09.11.2017 angenommen

Dedicated to Davide

Declaration

I hereby declare that parts of this thesis are already submitted to scientific international journals or already published:

- De Cicco M., Rahim M.S., Dames S.A., Regulation of the Target of Rapamycin and Other Phosphatidylinositol 3-Kinase-Related Kinases by Membrane Targeting. *Membranes*. 2015 Sep 29; 5(4):553-75.
- De Cicco M., Kiss L., Dames S.A., NMR analysis of the backbone dynamics of the small GTPase Rheb and its interaction with the regulatory protein FKBP38. *Febs Letters*. In press
- De Cicco M., Milroy L., Dames S.A., Target of rapamycin FATC domain as a general membrane anchor: the FKBP-12 like domain of FKBP38 as a case study. *Peptide Science*. 2017

Abbreviations

1D, 2D, 3D	One, two, three Dimensional
Ca ²⁺	Calcium ion
CaaX	C = cysteine, a = aliphatic, X = terminal amino acid
DEPTOR	DEP-domain-containing mTOR-interacting protein
DihepPC	1,2-diheptanoyl- <i>sn</i> -glycero-3-phosphocholine
DMPC	1,2-dimyristoyl- <i>sn</i> -glycero-3-phosphocholine
DPC	Dodecylphosphocholine
EDTA	Ethylenediaminetetraacetic acid
FKBP38	FK506-binding protein of 38 kDa (also known as FKBP-8)
GAP	GTPase Activating Protein
GDP	guanosine diphosphate
GEF	Guanine exchange factor
GppCp	guanosine-5'-[(β,γ)-methylene]triphosphate, sodium salt
GppNHp	guanosine-5'-[(β,γ)-imido]triphosphate, trisodium salt
GTP	guanosine triphosphate
HSQC	Heteronuclear single quantum coherence spectroscopy
IPTG	Isopropyl β -D-1-thiogalactopyranoside
LST8	mammalian lethal with SEC13 protein 8
Mg ²⁺	Magnesium
mTOR	Mammalian target of rapamycin
mTORC1	Mammalian target of rapamycin complex 1
mTORC2	Mammalian target of rapamycin complex 2
OD	Optical Density at 600 nm Wavelength
PA	Phosphatidic acid

PI3K	Phosphatidylinositol 3-kinase
PLD1	Phospholipase D1
ppase	Phosphatase
PRAS40	Proline-rich Akt substrate 40 kDa
Raptor	Regulatory associated protein of mTOR
Rheb	Ras homolog enriched in brain
S6K	p70 ribosomal protein S6 kinase
SDS-PAGE	Sodium dodecyl sulfate-polyacrylamide gel electrophoresis
TBC1D7	TBC1 domain family, member 7
TCTP	translationally controlled tumor protein
TM	Transmembrane
TPR	Tetratricopeptide repeats
TSC	Tuberous sclerosis complex
V-ATPase	Vacuolar ATPase
y1FATC	y1FATC, residues 2438-2470 of <i>S. cerevisiae</i> TOR1

Abstract (English)

Ras homolog enriched in brain (Rheb) belongs to the Ras GTPase superfamily. The typical GTPase fold consists of a mixed of six strand beta sheet with five helices packing around it. Three different motifs are conserved in GTPases. The phosphate binding loop (P-loop) interacts with the α - and β -phosphates from the bound nucleotide, whereas the two switch motifs, switch I and switch II, coordinate the γ -phosphate group if GTP is bound.

Rheb exists in the guanosine 5'-triphosphate (GTP)-bound form and the guanosine diphosphate (GDP)-bound form, active and inactive states respectively. Rheb is involved in the mammalian/mechanistic target of rapamycin (mTOR) signaling pathway and thereby plays a critical role in regulating cell cycle and growth. Rheb has been suggested to directly bind to the N-terminal region of mTOR kinase domain and to activate it in a GTP-dependent manner. Based on co-immunoprecipitation and *in vitro* binding assays, Rheb interacts further with FKBP38, a member of the FK506-binding protein (FKBP) family, and prevents its association with mTOR in a GTP-dependent manner. Another immunoprecipitation study confirmed the interaction between Rheb and FKBP38 but did not show any effect of the bound nucleotide on the interaction. The interaction between Rheb and FKBP38 could not be detected by *in vitro* binding assays done by another group .

In this work the NMR binding studies between the biochemically defined binding regions of Rheb and FKBP38 are presented. For human Rheb a C-terminal truncated version lacking the CaaX box needed for farnesylation was used (Rheb Δ CT) and for human FKBP38 the FKBP12-like domain (FKBP38-BD). The results showed that Rheb Δ CT-GDP does not significantly interact with FKBP38-BD. Titration of 15 N-FKBP38-BD with a 13-mer peptide, corresponding to the Rheb switch I region, did also not result in spectral changes. However, a weak interaction between Rheb Δ CT bound to a GTP analogue (GppNHp) and FKBP38-BD has been observed. This weak or transient interaction of Rheb Δ CT-GppNHp and FKBP38-BD stimulates the GDP-GTP exchange if FKBP38-BD is present at rather equimolar concentrations.

Another part of this work shows that the 33 residue long FATC domain of the serine/threonine kinase target of rapamycin 1 (y1fatc) can be applied as membrane anchoring unit for other proteins. As a case study it has been demonstrated that the FKBP12-like domain (FKBP38-BD) of the FK506-binding protein of 38 kDa in the cell localizes to the outer mitochondrial membrane and the endoplasmic reticulum by a short transmembrane domain. Based on NMR monitored interaction

studies, the FKBP38-BD-y1fatc fusion protein binds to all tested membrane mimetics. Using chemically synthesized peptides corresponding to the C-terminal 11-17 residues of y1fatc, it is further shown that they also interact with all tested membrane mimetics and may be used as membrane anchoring unit if the full y1fatc sequence is too long or shall be differently labeled, e.g. by attaching unlabeled y1fatc peptide to a ^{15}N -labeled target protein by native ligation. The fact that the y1fatc membrane anchoring unit is water-soluble can be exploited to titrate a target protein 1-y1fatc fusion to an already membrane mimetic attached interaction partner of target protein 1.

Abstract (Deutsch)

Ras-homologue-enriched-in-brain (Rheb) gehört zur Superfamilie der Ras-GTPasen. Die typische Struktur einer GTPase besteht aus einem Beta-Faltblatt mit sechs Strängen, das von fünf Helices umgeben ist. Drei verschiedene Sequenzmotive sind in GTPasen konserviert. Die Phosphatbindungsschleife (P-Schleife) interagiert mit α - und β -Phosphaten aus dem gebundenen Nukleotid, während die beiden Sequenzmotive Switch I und Switch II die γ -Phosphatgruppe koordinieren, wenn GTP gebunden ist. Rheb liegt in der Guanosin-5'-triphosphat (GTP)-gebundenen Form und der Guanosindiphosphat (GDP)-gebundenen Form vor, beziehungsweise dem aktiven und inaktiven Zustand.

Rheb ist an der Regulation des Ziels des Rapamycins im Säugetier (mTOR) beteiligt und spielt daher eine entscheidende Rolle bei der Regulierung von Zellzyklus und Wachstum. Es wurde vorgeschlagen, dass Rheb direkt an die N-terminale Region der mTOR-Kinase-Domäne bindet und sie in einer GTP-abhängigen Weise aktiviert. Basierend auf Co-Immunpräzipitation und *In vitro*-Bindungstests wechselwirkt Rheb weiterhin mit FKBP38, einem Mitglied der FK506-bindenden Protein (FKBP) Familie, was seine GTP-abhängige Bindung an mTOR verhindert. Eine weitere Immunpräzipitationsstudie bestätigte die Wechselwirkung zwischen Rheb und FKBP38, zeigte jedoch keine Wirkung des gebundenen Nukleotids auf die Interaktion. Die Wechselwirkung zwischen Rheb und FKBP38 konnte nicht durch *In vitro*-Bindungstests, die von einer anderen Gruppe durchgeführt wurden, nachgewiesen werden. In dieser Arbeit werden NMR-Bindungsstudien zwischen den biochemisch definierten Bindungsregionen von Rheb und FKBP38 vorgestellt.

Für menschliches Rheb wurde eine C-terminal verkürzte Version, ohne die für die Farnesylierung nötige CaaX-Box, verwendet (Rheb Δ CT), und für menschliches FKBP38 die FKBP12-ähnliche Domäne (FKBP38-BD). Die Ergebnisse zeigten, dass Rheb Δ CT-GDP nicht signifikant mit FKBP38-BD interagiert. Die Titration von ^{15}N -FKBP38-BD mit einem 13-mer-Peptid, das dem Rheb-Switch-1-Bereich entspricht, führte ebenfalls nicht zu spektralen Veränderungen. Es wurde jedoch eine schwache Wechselwirkung zwischen Rheb Δ CT, das an das GTP-Analogon GppNHp gebunden ist, und FKBP38-BD, beobachtet.

Diese schwache oder transiente Interaktion von Rheb Δ CT-GppNHp und FKBP38-BD stimuliert den GDP-GTP-Austausch, wenn FKBP38-BD in etwa äquimolaren Konzentrationen vorliegt.

Ein weiterer Teil dieser Arbeit zeigte, dass die 33 Reste lange FATC-Domäne der Serin / Threonin-Kinase- Target of Rapamycin 1 aus *S. cerevisiae* (y1fatc) als Membranverankerungseinheit für andere Proteine angewendet werden kann. Dies wird als Fallstudie für die FKBP38-BD, die sich in der Zelle auf die äußere mitochondriale Membran und das endoplasmatische Retikulum durch eine kurze Transmembran-Domäne lokalisiert, gezeigt. Basierend auf NMR-beobachteten Interaktionsstudien wechselwirken das FKBP38-BD-y1fatc-Fusionsprotein mit allen getesteten Membranmimetika. Unter Verwendung von chemisch synthetisierten Peptiden, die den C-terminalen 11-17 Resten von y1fatc entsprechen, konnte ferner gezeigt werden, dass diese auch mit allen getesteten Membranmimetika wechselwirken und als Membranverankerungseinheit verwendet werden können, wenn die volle y1fatc-Sequenz zu lang ist oder anders markiert werden soll, z.B durch Anfügen von unmarkiertem y1fatc-Peptid an ein ¹⁵N-markiertes Zielprotein durch native Ligation. Der Umstand, dass die y1fatc-Membranverankerungseinheit wasserlöslich ist, kann ausgenutzt werden, um einen bereits an ein Membranmimetikum gebundenen Interaktionspartner von Zielprotein 1 mit einer Zielprotein 1-y1fatc-Fusionsprotein zu titrieren.

LIST OF CONTENTS

Chapter 1.....	11
1.1 Biological background.....	12
1.2 Regulation of mTORC1 by relocalization to the lysosomal membrane.....	14
1.3 Regulation of mTORC1 by relocalization of mTORC1 to mitochondria/mitochondrial membranes.....	16
1.4 Structure and function of the small GTPase Rheb.....	17
1.5 Structure and function of the human FK506-binding protein 38 (FKBP38).....	21
1.6 The FAT C-terminal domain of TOR as membrane anchor.....	23
1.7 Scope of this study.....	25
Chapter 2.....	27
2. Nuclear Magnetic Resonance (NMR) Spectroscopy.....	28
2.1 Basic principles of NMR.....	28
2.2 Relaxation.....	31
2.3 $\{^1\text{H}\}$ - ^{15}N Heteronuclear NOE.....	31
2.4 Protein NMR.....	32
2.4.2 Chemical exchange.....	36
2.4.3 Real time NMR.....	38
2.5 Fingerprint spectra and biomolecular resonance assignment.....	38
2.6 Circular Dicroism.....	40
Chapter 3.....	42
3.1 Materials.....	43
3.1.1 Bacterial strains and plasmids.....	43
3.1.2 Cell growth media.....	43
3.2 Methods.....	44
3.2.1 Protein expression and purification.....	44
3.2.2 Rheb Δ ACT expression purification.....	44
3.2.3 FKBP38-(BD) expression and purification.....	44
3.2.4 FKBP38-fatc.....	45
3.2.4.1 Plasmid cloning.....	45
3.2.4.2 Protein expression and purification.....	46
3.2.5 Preparation of the Rheb Switch-1 peptide.....	47
3.2.6 Synthesis of y1fatc-peptides.....	47
3.2.7 Preparation of membrane mimetics.....	48
3.3 NMR sample preparation.....	49

3.3.1 Rheb Δ CT and FKBP38-BD	49
3.3.2 FKBP38-y1fatc	50
3.3.3 Y1fatc derived peptides	50
3.4 NMR spectroscopy	51
3.5 CD spectroscopy	53
Chapter 4.....	54
4. Results.....	55
4.1 Backbone assignment of Rheb Δ CT-GDP	55
4.2 Analysis of ¹⁵ N relaxation data	58
4.6 Analysis of the interactions between the FKBP38-BD-y1fatc chimeric protein and membrane mimetics ..	76
4.7 Membrane interaction studies with 11 to 17 residue long y1fatc peptides	82
Chapter 5.....	89
5.1 Summary and Discussion.....	90
References	98
Appendix	107
Acknowledgements	136
Curriculum vitae	137

CHAPTER 1

1.1 BIOLOGICAL BACKGROUND

Several GTPases of the Rat Sarcoma, Ras, family have been implicated in many cancer diseases. Ras itself has been discovered to be an oncoprotein that was found to be mutationally activated in 1/3 of all cancers, with the highest frequency seen in pancreatic (90%), colorectal (50%) and lung (30%) cancer.[1-5]

The Ras family includes Rheb (Ras homolog enriched in brain), an activator of the mammalian target of Rapamycin (mTOR) signaling pathway, which responds to a plethora of cellular signals to regulate protein translation, cell size, and cell cycle progression.[6]

MTOR is a serine/threonine kinase belonging to the PIKKs (phosphatidylinositol-3-kinase-related kinases) family of kinases with other five members: ataxia-telangiectasia mutated (ATM), ataxia- and rad3-related (ATR), DNA-dependent protein kinase catalytic subunit (DNA-PKcs), suppressor of morphogenesis in genitalia-1 (SMG-1), and transformation/transcription domain-associated protein (TRRAP). They all play vital roles in the regulation of cell growth, proliferation, survival, and consequently metabolism, as well as in the cellular response to stresses such as ionizing radiation or redox changes. The regulation of the localization of signaling proteins allows for generating a locally specific output. The current knowledge about the regulation of the localization of PIKKs at different cellular (membrane) compartments by a network of interactions has been reviewed in [7].

TOR is named for the naturally abundant macrolide antibiotic, rapamycin or sirolimus, discovered 42 years ago. It was isolated from *Streptomyces Hygroscopicus* cultures originating in soil samples, which have been discovered to have immunosuppressive and autoproductive properties.[8] Most of the initial knowledge regarding the pathway in mammals (mTOR) and its function originated from studies in budding yeast, where two TOR genes, TOR1 and TOR2 were identified as targets of the immunosuppressant rapamycin.[9]

In *S. cerevisiae* two different signaling complexes containing TOR1 and/or TOR2 have been characterized: TORC1 and TORC2. The first complex, TORC1, is rapamycin sensitive and involved in the regulation of cell growth, cell cycle progression and amino acid uptake. The second one, TORC2, is instead involved in the regulation of the actin cytoskeleton, and appears to be rapamycin insensitive.[10]

In mammalian cells only one TOR gene is present (mTOR). However, recent works have demonstrated that also here mTOR functions in two distinct complexes: mammalian target of

rapamycin complex 1 (mTORC1) and 2 (mTORC2). The best characterized complex and main focus of this introduction, mTORC1, is involved in cell growth, translation, autophagy and metabolism and is regulated by insulin, growth factors, nutrients, hypoxia and energy stress (reviewed in [11]) (Figure 1.1). The mTORC1 complex itself consists of mTOR, Regulatory-associated protein of mTOR (Raptor), LST8/G-protein β -subunit like protein (mLST8/G β L), the proline-rich Akt-substrate (PRAS40) and the DEP-domain containing interactor of mTOR (DEPTOR). [12, 13]

The main substrates of mTORC1 are the ribosomal protein S6 kinase beta1 (S6K1) and the eukaryotic translation initiation factor 4E-binding protein 1 (4E-BP1) [14], which are most often used as readout for mTORC1 activity. The importance of this complex is underscored by the involvement of overactive mTOR signalling in multiple cancers (reviewed in e.g.[15]).

The other complex, mTORC2, is less well characterized but is thought to be regulated by growth factors through an unknown mechanism (Figure 1.1). In contrast to mTORC1, this complex is not regulated by nutrients and is involved in the regulation of the cytoskeleton, survival, proliferation, metabolism and translation.[16-18].

mTOR localizes to many different cellular compartments such as the outer membranes of lysosomes, the Golgi, the ER, mitochondria, and swollen vacuolar structures, as well as to the plasma membrane and the nucleus [19-27], which seems to be mediated by a network of interactions, the exact nature of which may depend on the cell type as well as the signaling state. Besides the mentioned mTOR localization and activation places, signaling to mTORC1 may further occur from the peroxisome to which Rheb has also been localized [28].

To current knowledge, Rheb seems to be solely involved in the regulation of the TORC1 complex.[29] Activation of mTORC1 leads to a shift from catabolic to anabolic metabolism leading to increased protein synthesis, cell growth and proliferation and inhibition of autophagy.

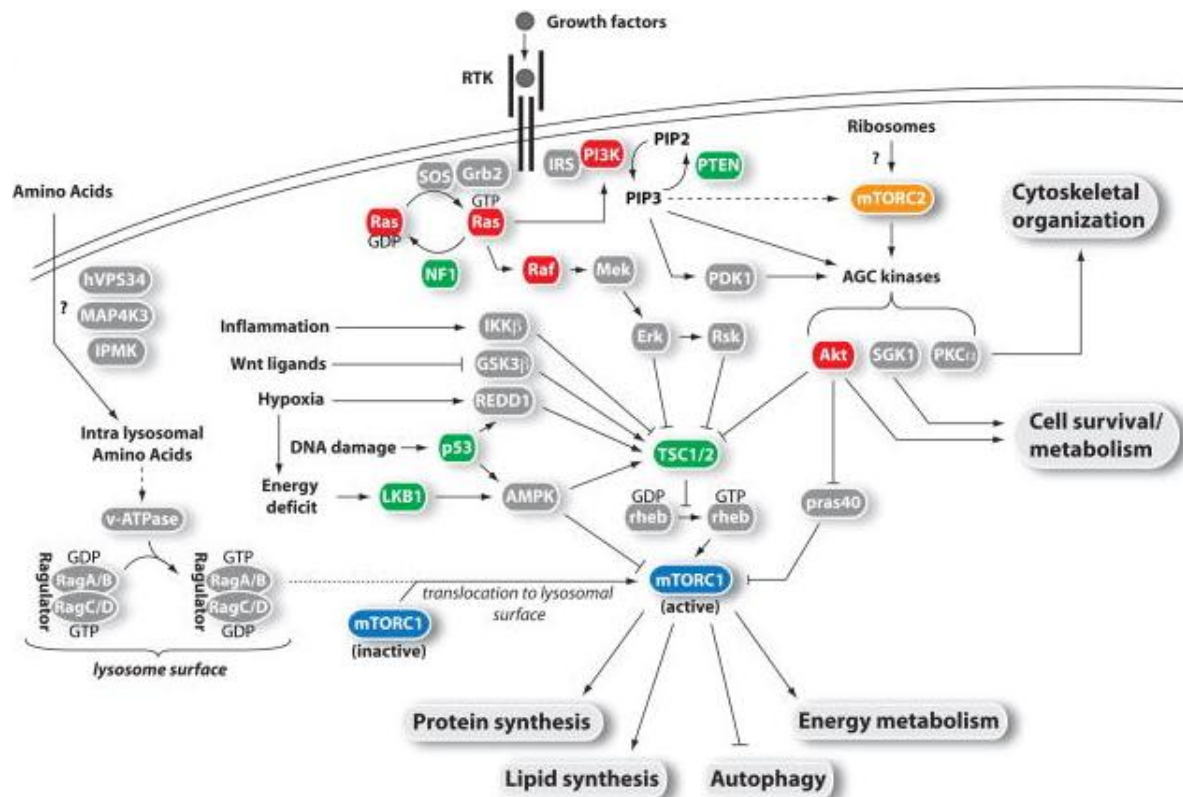


Figure 1.1: mTOR signaling pathway. The regulation of mTOR activity by growth factors is mediated by the PI3K/Akt signaling pathway leading to phosphorylation and inhibition of TSC2 by Akt and to the subsequent activation of Rheb, which activates mTOR by an as yet unknown mechanism. In addition, TSC2 is activated by AMPK (see text for details). Adapted from [30].

1.2 REGULATION OF mTORC1 BY RELOCALIZATION TO THE LYSOSOMAL MEMBRANE

Relocalization of mTORC1 within the cell is an important mechanism of regulation for mTORC1 activation. The localization and regulation of mTORC1 at the outer membranes of lysosomes/late endosomal structures have been studied in rather great detail. It has been revealed that these processes happen in a highly choreographed manner (reviewed in [12, 31, 32] and they are important mechanisms of regulation for mTORC1 activation.

mTORC1 is activated by the small GTPase Rheb, located on the lysosomal membrane [33, 34]. Unlike yeast TORC1, mTORC1 activity is partially moderated by its translocation onto the lysosomal membrane, where Rheb resides [22, 35, 36].

It has been known for many years that amino acid deprivation leads to the inhibition of mTORC1 [37-39]. However, although amino acid deprivation leads to a reduced association between mTOR

and Rheb, it does not alter the Rheb nucleotide binding status [33]. Overexpression of Rheb is able to completely reverse the effects of amino acid deprivation on mTORC1 signalling, probably via mislocalization of overexpressed Rheb that activates mTORC1 on different locations in the cell than endogenous Rheb [40].

The mechanism behind the amino acid regulation of mTORC1 has been unknown for many years, but the identification of the Rag (Ras related GTP-binding protein) GTPases as important players of this regulation has pushed this field forward [20, 22]. The GTPase Rag recruits mTORC1 to the lysosome, together with Rheb (Figure 1.2) by interacting with a regulatory-associated protein of mTOR, raptor [20, 22].

In *Drosophila* and mammalian cells, heterodimeric Rag GTPases (RagAB/CD) belong to the Ras superfamily. In contrast to other family members, they contain a long carboxyl-terminal domain, lack a membrane-targeting motif, and can form heterodimers (A/C or B/D) [31, 41]. The Rag GTPases transmit the amino acid signal to mTORC1, thereby promoting cell growth and inhibition of autophagy. Maximum binding to mTORC1 occurs if A/B are GDP- and B/D GTP-bound [31]. The Rag GTPases are localized on the lysosome via their interaction with the so-called Ragulator complex [35], which has GEF activity towards RagA and RagB [42]. The Ragulator interacts further with the vacuolar-H⁺-ATPase (V-ATPase) and is additionally tethered to the lysosomal outer membrane by its lipidated p18 protein subunit [35].

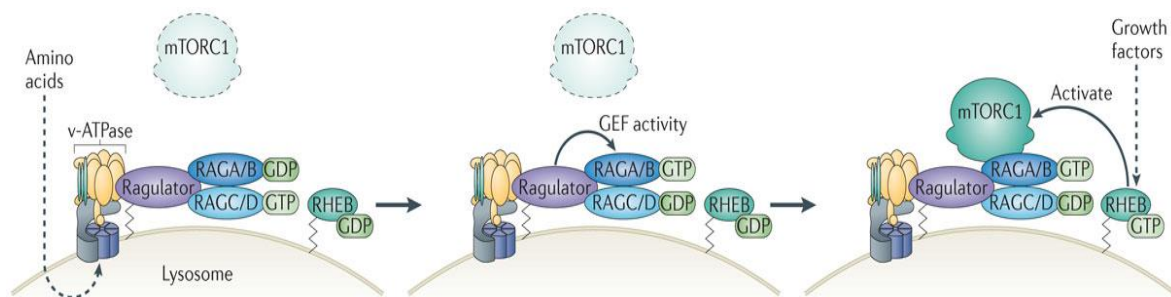


Figure 1.2: Mammalian cells have four Rag GTPases which form heterodimers; RagA or RagB associates with RagC or RagD. V-ATPase controls RAG GTPase–Ragulator binding, and therefore Ragulator guanine exchange factor (GEF) activity. When active, RagA/RagB is bound to GTP whilst RagC/RagD is bound to GDP. When amino acids accumulate within the lysosomal lumen and signal to vacuolar H⁺-ATPase (v-ATPase) through an ‘inside–out’ mechanism, the Rag GTPases promote TORC1 activity by relocating mTORC1 to lysosomes containing active Rheb. The Rag GTPases are tethered to the lysosomal membrane via interaction with the Ragulator complex. Adapted from [12]

RagA and RagB are inactivated by the GAP complex GATOR1 [43]. The current model is that if cells are amino acid depleted, the inactivation of the Rag GTPase complex results in cytoplasmic localization of mTORC1. When cells are replenished with amino acids, the Rag GTPase complex becomes activated and targets mTOR to the lysosome via a GTP-dependent interaction with Raptor. Since Rheb is also thought to localize at the lysosome membrane, mTORC1 can now be activated. Although these studies identified important players in the regulation of mTORC1 by amino acids, they still do not explain how the amino acid signal is transmitted from the V-ATPase to the regulator complex, which activates the Rag GTPases.

1.3 REGULATION OF mTORC1 BY RELOCALIZATION OF mTORC1 TO MITOCHONDRIA/MITOCHONDRIAL MEMBRANES

Subcellular fractionation data revealed that mTOR as well as the mTOR–raptor complex and thus mTORC1 can be purified from the mitochondrial fraction [44].

The mitochondrial FK506-binding protein 38, FKBP38, was found as a Rheb-interacting protein in a yeast-two-hybrid screen. Moreover, FKBP38 is a negative regulator of mTOR in response to growth factor stimulation and nutrient availability [45]. FKBP38 has been suggested to interact by its FKBP12-like domain (FKBP-C) with a region encompassing the FRB (FKBP12-rapamycin-binding)-like domain and the N-terminal kinase domain region on mTOR (amino acids 1967–2191)[45]. Thus the determined binding site of mTOR overlaps with one earlier determined for Rheb [33].

Follow-up experiments suggested that Rheb binds the mTOR interacting protein FKBP38 in a GTP-dependent manner through its switch I segment and that this interaction displaces FKBP38 from mTOR, thereby releasing the inhibition on the kinase domain of mTOR by FKBP38 [45, 46]. However, these results are still under discussion since a number of studies confirm the interaction of Rheb with FKBP38, whereas, these studies could not show an effect of FKBP38 overexpression or knockdown on the activation of mTORC1 signalling [47-49].

This lack of effect of FKBP38 overexpression was refuted again and proposed to be an effect of the differences in protein expression in the studies [50]. This was supported by showing in *in vitro* studies that FKBP38 inhibits Rheb and RhebL1 mediated mTORC1 activity in a dose-dependent manner. However, this study did not explain the lack of effect observed upon FKBP38 knockdown.

Finally, it was suggested that FKBP38 does not have an effect on mTORC1 activity, but has an mTOR-independent effect on the inhibition of apoptosis via Rheb [51]. It was proposed that the interaction of the anti-apoptotic proteins Bcl-2 and Bcl-xL with FKBP38 is negatively regulated by Rheb in a GTP-dependent manner. A decrease in GTP loading of Rheb diminishes the interaction with FKBP38, which in turn will recruit Bcl-2 and Bcl-xL to the mitochondria to induce autophagy. Sun *et al.* suggested an alternative model: the mTORC1 activation by Rheb happens via the binding of GTP-loaded Rheb and the phospholipase D1 (PLD1). PLD1 localizes also at endomembranes, where upon mitogenic stimulation it generates phosphatidic acid (PA) [52]. PLD1 activation by a subset of growth factors stimulates PA production and activation of mTORC1 and this activation is essential for cell growth [53, 54]. PA is a positive regulator of mTOR activity that, like FKBP38, also binds to the FRB domain of mTOR. PA can stimulate the p70 ribosomal protein S6 kinase (S6K1) and the 4E-binding protein 1 (4E-BP1) phosphorylation in cells deprived of serum in a PI3K-independent and rapamycin-dependent manner. However, PA is unable to activate mTORC1 in cells deprived of amino acids [55].

Although both scenarios are still under discussion, all studies point to Rheb as an essential activator of the mTORC1 kinase. [35, 56-58].

1.4 STRUCTURE AND FUNCTION OF THE SMALL GTPASE RHEB

Rheb is highly conserved [59-61] and although it was named from its initial identification as a gene rapidly induced in brain by seizures and by receptor-dependent synaptic activity, it is ubiquitously expressed from yeast to mammals [61, 62]. Six years after the discovery of Rheb in neuronal tissue of rats, a first paper described a potential function of Rheb in cell growth. It was shown in the yeast *Schizosaccharomyces pombe* that loss of Rheb leads to small, round cells caused by arrested cell growth and division [63].

In addition, loss of the membrane-targeting signal of Rheb leads to the accumulation of *S. pombe* cells in the G0/G1 phase of the cell cycle, again demonstrating a role for Rheb in cell cycle progression and growth [64].

Rheb exists as two isoforms, Rheb1 and Rheb2. The gene products share 54% identity and 74% similarity in sequence, and perform similar functions [65]. Rheb1, (referred to as Rheb in this dissertation) is ubiquitously expressed, whereas Rheb2 shows more limited expression profile [66].

Rheb encodes a 184 a.a. small GTPase protein that possesses five G-box motifs G1-G5 (Figure 1.3) conserved amongst small GTPases. These motifs mediate nucleotide-binding and hydrolysis, as well as interactions with effectors and regulators [67-69]. The G1 box forms the P-loop, which is responsible for phosphate binding. The G2 box is the effector region and undergoes a conformational change upon GTP or GDP binding. The G3 box is involved in the binding of the nucleotide-associated Mg^{2+} ion. The G4 box forms a hydrogen bond with the guanine ring and stabilizes the protein by interacting with residues in the G1 box. Finally, the G5 box residues make indirect associations with the guanine nucleotide and this box is less well conserved among the Ras superfamily members. The conformational change upon GTP or GDP binding is primarily confined to two loop regions, called the Switch I and the Switch II region, which overlap with the G2 and the G3 box, respectively. If the GTPase is GTP bound, these regions display a binding surface with high affinity for effector proteins. GTP hydrolysis and thus release of the γ -phosphate, will lead to a conformational change that decreases the affinity for the effector protein and thus leads to the attenuation of downstream signaling.

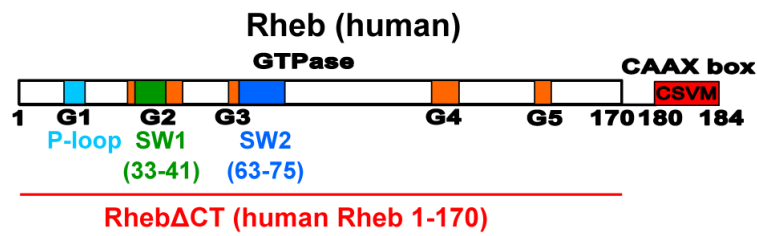


Figure 1.3: Domain organization of human Rheb. The C-terminally truncated fragment (1-170), lacking the CaaX box used within this study is referred to as Rheb Δ CT. The G boxes and the two switch regions (SW1 and SW2) are indicated. Adapted from [70]

The sequence of Rheb also revealed the presence of a C-terminal CaaX, where C=cysteine, A=aliphatic amino acid and X= any amino acid. The CaaX box is subject to farnesylation and it is involved in the localization of Rheb to intracellular membranes [71] (Figure 1.3). The C-terminus of Rheb is unusual among GTPases in that it only contains a farnesylation site but no additional membrane targeting signals. This suggests that the localization of Rheb may not be restricted to lysosomes, to which is the main site where the Rheb localization has been reported [66, 72, 73]. Rheb becomes farnesylated on the endoplasmic reticulum and is subsequently transported to the Golgi complex for signal transduction to mTORC1. This translocation is required for proper signal

transduction, since a farnesylated Rheb mutant that is trapped on the ER has reduced signalling activity. Mutation studies of Rheb have furthermore shown that not only an intact Golgi complex, but also the CaaX box of Rheb and farnesylation of Rheb are essential for its signalling function[72, 74].

The typical fold of a GTPase contains a mixed six-stranded beta sheet with five helices packing around it. Three different motifs are conserved in GTPases: the P-loop, switch I and switch II. [50, 75, 76] (Figure 1.4).

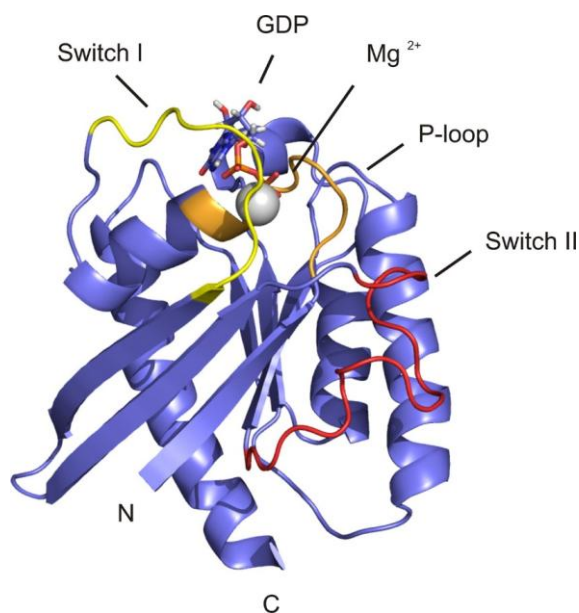


Figure 1.4: Ribbon drawing of a representative member of the ensemble structures of C-terminally truncated version of rat Rheb, residues 6-174.[77]

As a small GTPase, Rheb acts as switch in cellular signaling pathway: it is active GTP-bound state, is able to interact with diverse effector proteins, whereas is considered inactive GDP- bound state is generally inactive (Figure 1.5) [67]. Because the GDP is in general tightly bound and GTP is hydrolyzed very slowly, small GTPases require the helping hand of guanine nucleotide exchange factors (GEFs) that facilitate GDP dissociation and of GTPase activating proteins (GAPs) that stimulate GTP hydrolysis. The actual molecular switch is thus composed of a small GTPase, a GEF, and a GAP, rather than a small GTPase alone.[78]

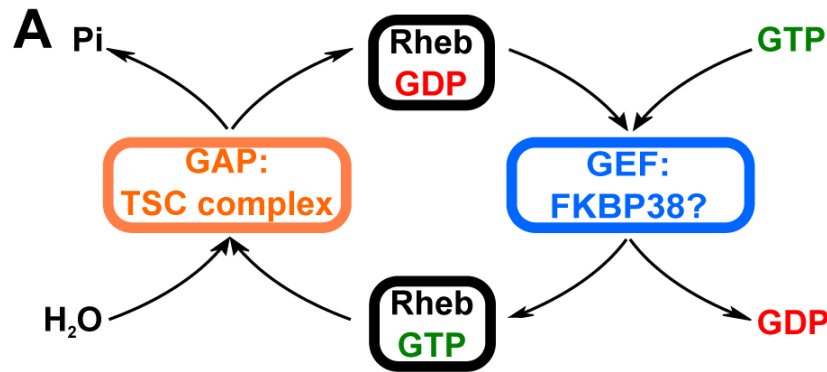


Figure 1.5: The activation and deactivation cycle of Rheb. The TSC complex acts as a GTPase-activating protein (GAP) for Rheb. It has not been analyzed if FKBP38 has some guanine nucleotide exchange factor- (GEF-) like activity on Rheb. Adapted from [70]

During GDP to GTP cycling, the switch 1 region of Rheb undergoes a conformational change while the switch II region adopts a stable, extended conformation that differs significantly from the α -helical conformation seen in other small GTPases. That results in a certain orientation of Q64, which is equivalent to the catalytic Q61 of Ras, that disables GTP hydrolysis thereby explaining its low intrinsic GTPase activity [50] Therefore the regulatory or nucleotide binding motifs show in general an increased flexibility in comparison with the rest of the protein. [79].

An important GAP in the mTOR signalling pathway is tuberin (TSC2), which, in complex with hamartin (TSC1), regulates the inactivation of Rheb [28, 56, 80-82].

It was reported by five independent groups that Rheb activity is regulated by the TSC1/TSC2 complex and that TSC2 is the GAP for Rheb [56, 80-83]. Altogether, these data placed Rheb downstream of the TSC complex and upstream of TOR in the TOR signalling pathway (Figure 1.1). Recently, Tre2-Bub2-Cdc16 (TBC) 1 domain family, member 7 (TBC1D7) was identified as a third component in the TSC complex [32]. TBC1D7 binds the complex through TSC1 and leads to the stabilization of the protein. Knockdown of TBC1D7 decreased the association between TSC1 and TSC2 and results in increased mTORC1 signalling through the release of GAP activity towards Rheb. TBC1D7 is not involved in the amino acid regulation of mTORC1 signalling.[32] Rheb and TSC2 are a special GTPase-GAP pair since the first has a high basal GTP-state level and the latter uses instead of the catalytic arginine-finger found in the Ras-GAP an asparagine-thumb [84]. Based on the crystal structure of human Rheb bound to GTP, shielding of the phosphate moiety by the conserved Y35 of switch 1 appears to disable the insertion of an arginine finger [68].

The GTP loading of small GTPases is stimulated by guanine nucleotide exchange factors (GEFs). Such a factor is not yet known for Rheb and the existence is a matter of debate. It was reported that the *Drosophila* ortholog of human TCTP (translationally controlled tumor protein) acts as a GEF for dRheb [85]. However, it has been difficult to confirm that TCTP functions as a Rheb GEF or to determine whether the *in vitro* detected TCTP's GEF activity on Rheb is physiologically significant [48, 86].

The mechanism by which Rheb regulates mTOR activity is not known. It was shown that Rheb binds to the upper lobe of the mTOR catalytic domain, but surprisingly this binding was independent of the nucleotide loading of Rheb [33, 87]. An increased binding to mTOR was seen for two mutants of Rheb, S20N and D60I, with markedly reduced GTP binding (< 5%) compared to wild type.[33] The Rheb mutants D60V and D60K are unable to bind GTP or GDP.[88, 89] Based on co-immunoprecipitation assays using wild type or mutant Rheb expressed in HEK293 cells, the D60V and D60K mutants could also interact with mTOR complexes, which suggested that the interaction is not dependent on the nucleotide-binding state.[90]

1.5 STRUCTURE AND FUNCTION OF THE HUMAN FK506-BINDING PROTEIN 38 (FKBP38).

The human FKBP38 (gene name FKBP8), member of the FKBP506-binding protein family, was first characterized as a result of a very pronounced expression of its corresponding mRNA in neuronal cells [91].

FKBP belongs to the immunophilin family, which consists of proteins with a variety of protein-protein interaction domains and versatile cellular functions. Analysis of the functions of immunophilins has been the focus of studies in recent years and has led to the identification of various molecular pathways in which FKBP38s play an active role. All FKBP38s contain a domain with prolyl cis/trans isomerase (PPIase) activity.

The peptidyl prolyl cis/trans isomerases (PPIases, Enzyme class 5.2.1.8.) [92] assist the cis/trans interconversion of peptide bonds, which possess partial double bond character due to the delocalization of the lone electron pair of the nitrogen atom across the entire amide group and assists the interconversion of peptide bonds where proline is in the C-terminal position.

PPIases are ubiquitous in life. The subfamilies of this enzyme class are unrelated to each other in their amino acid sequences, have distinct substrate specificities, and prove to be sensitive to different inhibitors.

The protein FKBP38 consists of 412 amino acids, Figure 1.7, organized in the N-terminal glutamate rich region is followed by a FKBP12-like prolyl isomerase (PPIase) domain, referred to as FKBP-C, the structure of which as well as its interaction with FK506 and Bcl-2 have been characterized [76, 93, 94] (Figure 1.6).



Figure 1.6: Solution structure of the FK506-binding (FKBP-C) domain of human FKBP38. The best calculated structures are superimposed in this figure. (PDB-ID: 2F2D)

The tetratricopeptiderepeats (TPR) domain consists of three TPR motifs and an associated calmodulin-binding site, and the C-terminal membrane anchor that is unique among human FKBP38 and leads to the localization of FKBP38 in the membranes of the endoplasmic reticulum and the mitochondria (Figure 1.7) [93, 95].

A remarkable property of FKBP38 is the lack of constitutive FKBP activity of its FKBP domain. [93, 96, 97]. The enzymatic activity of this protein is regulated by CaM/Ca²⁺, which is a unique property among human FKBP38. Only the CaM/Ca²⁺/FKBP38 complex exhibits PPIase activity and is able to bind FK506 [93]. The TPR domain has been shown to interact with the molecular chaperone Hsp90, the anti-apoptotic proteins Bcl-2 and Bcl-XL and the 26S proteasome – each involved in central processes of the cell [93, 98, 99].

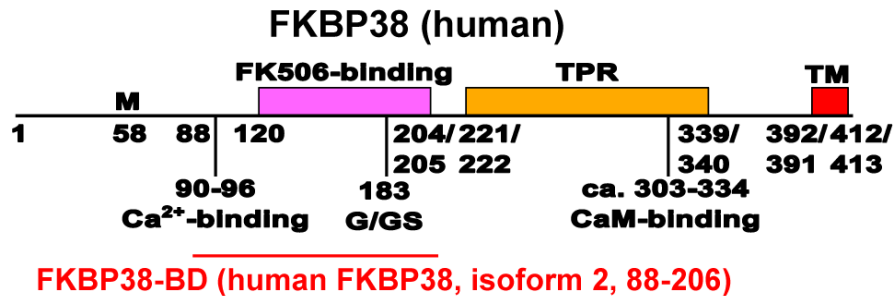


Figure 1.7: Human FKBP38 exists in two isoforms and has different functional regions (TPR – tetratricopeptide repeat domain, TM – transmembrane domain). For this study residues 88-206 of isoform 2 (has GS instead of only G at position 183) encompassing the binding region for Rheb and referred to as FKBP38-BD was used. Adapted from [70]

A number of results have been published suggesting an anti-apoptotic function of FKBP38 in HeLa cells. FKBP38 was suggested to target Bcl-2 to the mitochondria [100], and to play a role in the folding and stabilization of Bcl-2 [94]. It was proposed that the interaction of the anti-apoptotic proteins Bcl-2 and Bcl-xL with FKBP38 is negatively regulated by Rheb in a GTP-dependent manner. A decrease in GTP loading of Rheb diminishes the interaction with FKBP38, which in turn will recruit Bcl-2 and Bcl-xL to the mitochondria to induce autophagy.

Based on GST pull-down assays, the FKBP-C domain of FKBP38 interacts with the same region of human TOR (residues 1967-2191) that had been suggested to interact with Rheb in a GTP-dependent manner through its switch I segment. This latter interaction displaces FKBP38 from mTOR, thereby releasing the inhibition on the kinase domain of mTOR by FKBP38 [45, 46].

These results are contradicted in literature by studies that were unable to confirm the interaction of Rheb with FKBP38 [33].

1.6 THE FAT C-TERMINAL DOMAIN OF TOR AS MEMBRANE ANCHOR

TOR has been detected at different cellular membranes and in the nucleus and based on these observations it has been suggested that its localization depends on the composition of the TOR complexes as well as on the cell type and signaling state and is mediated by a whole network of protein-protein and protein-lipid interactions. [7, 19, 21, 23-25, 35, 101-103]. The FATC domain is shared by all members of the family of the PIKKs, which control cellular signaling pathways in response to stress and nutrients [7, 104, 105].

An initial NMR structural characterization of the FATC domain of yeast TOR1 (y1fatc) showed that the oxidized form consists of an α -helix that is followed by a hydrophobic disulfide-bonded loop, whose reduction causes an increased flexibility of the C-terminal half. The determined redox potential of the single disulfide bond and additional mutagenesis studies (Cys to Ser) in yeast indicated further that the intracellular redox potential can affect the cellular amount of the TOR protein via the FATC domain [106]. In line with this, it has been shown that TORC1 formation and signaling is redox-sensitive [107-109].

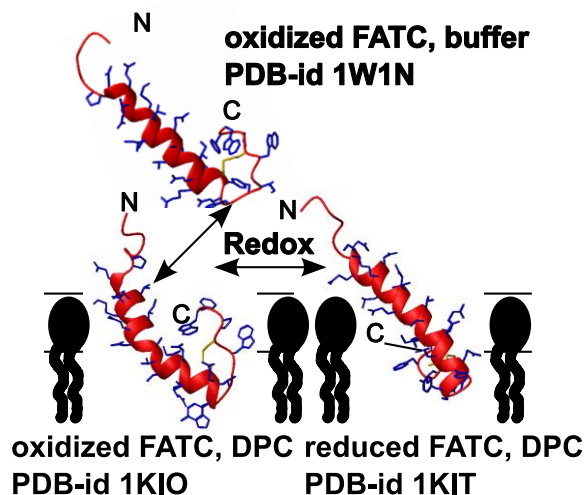


Figure 1.8: The NMR structures of the oxidized FATC domain in the free [106] vs. oxidized and reduced forms in the DPC micelle immersed states [110]; the respective PDB-ids (protein databank identification numbers, [111]) are indicated. Adapted from [7]

Subsequent studies provided the micelle immersed structures of both redox states and showed that they can interact with all tested membrane mimetics including neutral and negatively charged micelles, neutral bicelles, and neutral and negatively charged liposomes of the small unilamellar vesicle (SUV) type.[110, 112]

Whereas replacement of up to 6 or 7 aromatic or aliphatic residues did not abrogate the interaction with neutral micelles and bicelles, replacement of only one aromatic residue (Y1463 or W2466) hampered the interaction with SUVs.[113] This can be explained by the significantly lower sample concentration of SUVs compared to micelles and bicelles as well as their larger radius and thus lower membrane curvature.[114]

1.7 SCOPE OF THIS STUDY

Analysis of the backbone dynamics of Rheb-GDP and -GppNHp and their interaction with FKBP38.

The small GTPase Ras homolog enriched in brain (Rheb) regulates mammalian/mechanistic target of rapamycin complex 1 (mTORC1), a central controller of cellular growth and metabolism in all eukaryotes. In addition, the FK506-binding protein of 38 kDa (FKBP38) has been suggested to interact with Rheb, which regulates its influence on TOR signaling. Some later studies confirmed the interaction between Rheb and FKBP38 but questioned its influence on mTOR; others questioned it completely.

In order to evaluate the influence of cycling between the active GTP and the inactive GDP state on the backbone dynamics, it is interesting to analyze the ^{15}N -relaxation data for a C-terminal truncated fragment of Rheb (Rheb Δ CT) that cannot be farnesylated bound to either GDP or the non-hydrolyzable GTP analogues GppNHp and GppCp. These data are particularly interesting around the well-known regulatory switch I and II regions and the P-loop and suggest a different behavior of Rheb in the GDP and GTP state.

The analysis of the interaction between the proposed binding regions as well as the influence of FKBP38 on the GDP to GTP exchange and the dynamics of Rheb by solution NMR spectroscopy can resolve the conflicting data about the interaction between Rheb and FKBP38.

Since FKBP38 works as an effector in the mTOR signaling pathway, it is also worthy to analyze whether it plays a role as GEF in the Rheb GTPase cycle. With the NMR-based real-time assay it is possible to monitor the rate of GTP hydrolysis, using native GTP and GDP. This methodology requires no chemical modification of the protein or the nucleotide, which can perturb the native structure of the protein and has the ability to sense subtle changes in the rate of catalysis in real-time fashion.

The FATC-terminal domain of target of rapamycin can be used as membrane anchor: FKBP12-like protein FKBP38 as case study.

In the past few years increased efforts have been made to better understand biological processes at membranes. To better understand processes such as the assembly of signaling complexes at membranes and to dissect the specific membrane interactions of the involved proteins, suitable interaction studies have to be performed. In *in vitro* interaction studies, the use of full-length

proteins containing transmembrane domains or a posttranslational prenylation motif to tether proteins of interest to membranes can be challenging due to low expression rates, low solubility and the need of additional purification steps to separate e.g. farnesylated from not farnesylated protein. Thus a membrane anchoring unit that is easy to attach, binds to many different types of membrane mimetics and is also water soluble would find broad application.

Based on earlier NMR binding studies, the FATC domain of the serine/threonine kinase target of rapamycin 1 (y1fatc) can interact with different membrane mimetics, such as differently composed neutral and negatively charged micelles and neutral bicelles. A model of the membrane-binding of y1fatc suggests that the C-terminal hydrophobic bulb-like region of the FATC membrane anchor of both is embedded in the micelle making contact to the hydrophobic fatty acid tails, while a rim of charged residues can interact with the positively and negatively charged parts of the headgroups. First mutagenesis data targeted the two tryptophans W2466 and W2470, since tryptophans play often an important role for the interaction between membranes and proteins. However, replacement of one or both tryptophans by alanine did not abrogate the interaction with DPC micelles, suggesting that the other hydrophobic aromatic and aliphatic residues in the membrane anchor contribute also significantly to the affinity for membrane mimetics

One aim of this work was to demonstrate that the 33 residue long FATC domain of the serine/threonine kinase target of rapamycin 1 (y1fatc) or shorter fragments of it encompassing only the C-terminal 11-17 residue can be applied as membrane anchoring unit for other proteins. As a case study I consider the FKBP12-like domain (FKBP38-BD) of the FK506-binding protein of 38 kDa that in the cell localizes to the outer mitochondrial membrane and the endoplasmic reticulum by a short transmembrane domain. The first step is the cloning of the new fusion protein FKBP3-y1fatc and subsequently the optimization of protein expression and purification. Then the fusion protein can be used for NMR interaction studies with different membrane mimetics such as micelles, bicelles or SUVs.

CHAPTER 2

2. NUCLEAR MAGNETIC RESONANCE (NMR) SPECTROSCOPY

One of the main techniques used to obtain information about the structure and the dynamics of proteins in solution is the nuclear magnetic resonance spectroscopy (NMR). This field of the structural biology has its origins in 1945 when Felix Bloch and Edward Purcell gave a description of the phenomenon. This part of the thesis illustrates some basic ideas of modern NMR spectroscopy, which were used for the work described later. For a more comprehensive understanding of the physical principles of NMR, the reader is referred to the literature [115-118]

2.1 BASIC PRINCIPLES OF NMR

Based on the quantum mechanical description of atoms, nuclei possess the property of spin and the energy of each spin is defined in terms of angular momentum, a vector whose length reflects magnitude and whose orientation reflects direction of the spins. The magnitude of the spin depends also on the spin quantum number, I , which can be zero or a multiple of $\frac{1}{2}$. Only nuclei with a spin number different from zero have a magnetic field. The simplest nuclei to work with have a half-integer spin, i.e. $\frac{1}{2}$, such as ^{15}N , ^{13}C and ^1H . The theory of quantum mechanics suggests that a nucleus of spin I will have $2I + 1$ possible orientations. A nucleus with spin of $\frac{1}{2}$ will have 2 possible orientations. If a magnetic field is applied to this nucleus, the energy levels split. The energy difference ΔE between the two states is called the nuclear Zeeman splitting (Figure 2.1).

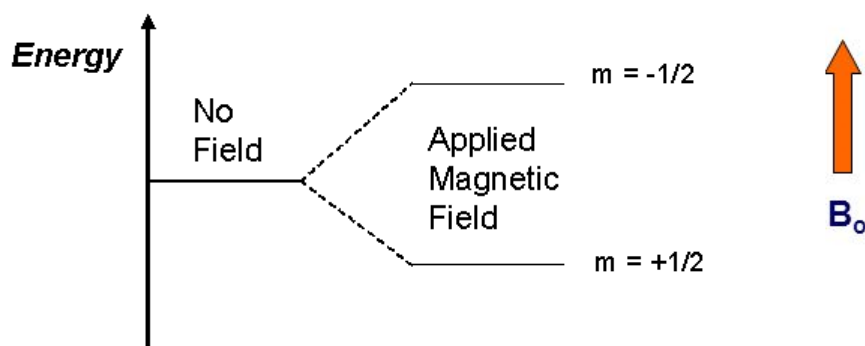


Figure 2.1: NMR energy levels for spin half nuclei in presence of an external magnetic field (B_0).

Each energy level corresponds to a magnetic quantum number m . When the nucleus is in a magnetic field, the energy levels are populated according to the Boltzmann distribution. States

corresponding to lower energy levels will be populated stronger than those at higher levels. Application of a radiofrequency field can induce transition into the higher level. The frequency of the radiation necessary for this change is determined by ΔE :

$$\Delta E = \gamma \hbar B_0 = \hbar \omega_0 \quad [119]$$

where ω_0 is the Larmor frequency.

The difference in spin population between the higher and the lower energy state determines the magnitude of a bulk magnetization vector, M_0 , created by the alignment of nuclear spins along the B_0 magnetic field (Figure 2.3).

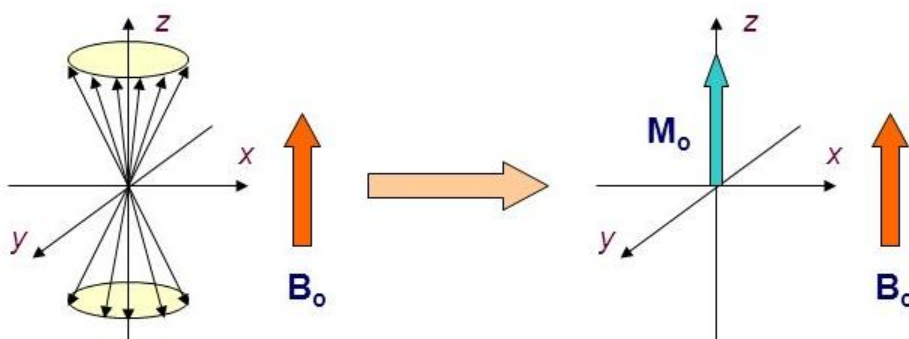


Figure 2.3: The vector model of NMR. Macroscopic magnetization resulting from the sum of individual nuclear magnetic moments. According to the classical picture, a nucleus with $I=1/2$ precesses around the field axis z on the surface of a double cone. If we add the z -components of all nuclear magnetic moments in a sample we obtain a macroscopic magnetization M_0 along the field direction. The vector M_0 plays an important role in the description of all types of pulsed NMR experiments.

Application of an orthogonal energy pulse in the form of radio frequency (RF) imposes a torque on the bulk magnetization vector in a direction that is perpendicular to the direction of the field, which rotates the vector from the z -axis towards the x - y plane. The bulk vector will precess (rotate) around the central z axis, defined by the direction of the B_0 magnetic field, with the Larmor frequency.

This precession of the magnetization vector is detected during an NMR experiment using detection coils and called ‘Free Induction Decay’ (FID). This FID is a time domain signal representing all the Larmor frequencies in the sample. Fourier transformation (FT) can be applied to convert this time domain FID into frequency domain signals which correspond to a spectrum.

In order to ensure ν values as a function of the local chemical environment, chemical shifts are standardized between NMR experiments and NMR spectrometers. The chemical shifts (δ) has been defined in frequencies (which is B_0 field dependent), normalized to a standard (not field dependent), usually to the frequency of tetramethylsilane for ^1H and ^{13}C , and nitric acid for ^{15}N . The chemical shifts has been defined as:

$$\delta_{\text{sample}} = \left(\frac{\nu_{\text{sample}} - \nu_{\text{reference}}}{\nu_{\text{reference}}} \right) * 10^6$$

Where ν_{sample} is the absolute resonance frequency of the sample $\nu_{\text{reference}}$ is the absolute resonance frequency of a standard reference compound, measured in the same applied magnetic field B_0 . Since the numerator is usually expressed in Hz and the denominator in MHz, the chemical shift is expressed in ppm.

In proteins, the ^1H chemical shift typically results from a combination of local magnetic fields due to charges, aromatic ring currents and magnetic anisotropy around bonds [120]. Partial or formal electric charges contribute considerably to the chemical shifts of atoms in different functional groups. In this way the chemical shift is the variation of the resonance frequency of a nucleus experiencing the local chemical environment.

There are two effects: shielding and deshielding, decreasing or increasing the effective external magnetic field. Therefore, the resonance frequencies, ν , values are an indication of the nature of the chemical environment and of the structural geometry of the molecule[120].

Ring currents are important for deviations from average chemical shifts and this makes them a really sensitive tool for identification of binding sites, given that the aromatic rings are present in the majority of drugs .[121] Anisotropic contributions are especially important for backbone amide ^1H , which are close to the anisotropic amide and carbonyl groups. The chemical shift observed in solution-state NMR spectroscopy is the isotropic chemical shift an it represents the average of the principal values of the anisotropic chemical shift:

$$\delta^{iso} = \frac{1}{3} * (\delta_{xx} + \delta_{yy} + \delta_{zz})$$

In solution, the chemical shift anisotropy cannot be observed due to molecular tumbling; however, the anisotropy is still present [122] .

The chemical shift can be used in structure determination of proteins. In particular the analysis of the chemical shift of $^1\text{H}^\alpha$, and of ^{13}CO , $^{13}\text{C}^\alpha$, and of $^{13}\text{C}^\beta$ of the peptide backbone can be used to determine the secondary structure of a given peptide segment. For such analyses, chemical shifts

need to be assigned to the respective atoms in the protein. In solution, assignment is mostly accomplished using well established 3D heteronuclear correlation experiments. These correlate amide ^1H and amide ^{15}N with a ^{13}C dimension.[123]

2.2 RELAXATION

For a better interpretation of NMR spectra it is important to understand the relaxation processes, in which the bulk magnetization M_z is perturbed from its equilibrium state (along the z-axis, parallel to the permanent magnetic field), and the emitted signal is observed as the sample returns to equilibrium.

As previously described, in the presence of the applied magnetic field (B_0) spin polarization occurs and results in a net alignment of spin states in the direction of the external applied magnetic field (z-axis). A pulse with exactly the Larmor frequency can interact with the spins and transfer the magnetization to the transversal plane, generating the detectable transverse magnetization (M_{xy}). Then, the signal starts to relax back to equilibrium (M_{z0}), by a process called relaxation and defined by the relaxation time constants T1 and T2 (described in more details in paragraph 2.4.1) in the Bloch equations.

$$M_z(t) = M_{z0} \left(1 - e^{-\frac{t}{T1}} \right)$$
$$M_{xy}(t) = M_{xy0} \left(e^{-\frac{t}{T2}} \right)$$

where $M_z(t)$ is the magnetization as a function of time t, M_{z0} is the equilibrium magnetization, $M_{xy}(t)$ is the transverse magnetization as a function of time t and M_{xy0} is the initial transverse magnetization.

2.3 $\{^1\text{H}\}$ - ^{15}N HETERONUCLEAR NOE

Structure determination by high resolution NMR has traditionally relied on the use of Nuclear Overhauser Effect (NOE) derived distance restraints. The NOE is the phenomenon where the relaxation of the spin effect relaxation of the nearby spins too, due to dipole-dipole interactions. This cross relaxation involves double quantum and zero quantum transitions giving rise to positive or negative NOEs respectively and the gyromagnetic ratio of the involved nuclei. The NOE effect is

the change in population of spin state when another magnetic nucleus close in space is saturated by irradiation or by a selective 180 degree pulse.

The type of transition is largely defined by the size of the molecule. Structures of proteins up to 20-30 kDa and protein-small molecule complexes can be determined successfully by NMR. NOEs provide a mechanism for both inter- and intramolecular magnetization transfers. The magnitude of the NOE between two nuclei spins is inversely related to the internuclear distance (r^{-6}) between them. Therefore, NOE related experiments have been widely used for determining three dimensional structures of protein and protein–ligand complexes as well as for deriving dynamic information for the protein-ligand interactions.

2.4 PROTEIN NMR

NMR is well recognized in biochemistry for its ability to deliver the structure and dynamics of large macromolecules, alone or in complexes with drugs or with other biomacromolecules, under nearly physiological conditions [115]. The molecular motions are essential for protein functions including catalysis, binding, regulation, cellular structure and stability. The protein dynamics can be characterized as a continuous exchange between many conformations on time scale ranging from femtoseconds to hours.

NMR spectroscopy yields information on dynamics and can be used to identify specific interactions, based on the analysis of some parameters that influence the observation of signals: chemical shift, the spin-lattice relaxation time T_1 , the spin-spin relaxation time T_2 , the pulse shape and the nuclear overhauser effect (NOE).

The peak intensity can be quantified by the integral of the peak and it is an indication of the number of protons forming each peak.

The nuclei commonly used in structural biology are ^1H , ^{13}C , ^{15}N , ^{31}P . Each of them possess different spin properties. Modern techniques in molecular biology allow the expression of labeled proteins in host cells. For biomolecular NMR spectroscopy, it is possible to uniformly enrich proteins in these nuclei by growing bacteria or other culture media containing ^{15}N ammonium chloride and ^{13}C glucose as sole nitrogen and carbon source respectively.

2.4.1 RELAXATION AND MODEL-FREE ANALYSIS

There are two different relaxation processes: longitudinal and transversal relaxation. The longitudinal relaxation, also called spin-lattice relaxation, T1, arises with the movement of spin populations back to their Boltzmann equilibrium distribution. This relaxation happens along the z-direction.

The transversal relaxation, also called spin-spin relaxation, T2, is the process by which the magnetization in the transverse plane decays to zero at equilibrium via the decay of coherences (loss of phase coherence).

The magnetic interactions that produce local magnetic fields are modulated by the molecular tumbling. As a result, the spins experience fluctuating local magnetic fields that allow the spins to return to equilibrium. T1 and T2 depend on the correlation time τ_c of the molecule, which in turn depends on the molecular size. Small molecules tumble faster and have high T1 and T2 values whereas large molecules such as proteins tumble slowly and have high T1 but low T2 value.

Protein internal motions as well as molecular tumbling which ranges from pico- to microseconds time scale can be deciphered using T1 relaxation whereas T2 measurement is further sensitive to the chemical exchange.

The ratio between T1 and T2 can yield rotational correlation time (τ_c) (time taken by a molecule to rotate by an angle of one radian). Considering globular proteins as spherical molecules the tumbling in solution is described by the rotational correlation time (τ_c) as follows:

$$\tau_c = \frac{4\pi\eta r^3}{3kT}$$

where η is the viscosity of the solvent r is the hydrodynamics radius, k is the Boltzmann constant, T is the temperature.

The relation between the molecular tumbling and the T1, T2 relaxation is described by the spectral density $J(\omega)$, which is the measure of the power to relax the spin at the given angular frequency ω .

$$J(\omega) = \frac{2\tau_c}{1 + (\omega\tau_c)^2}$$

The ^{15}N -relaxation parameters T1, T2 and heteronuclear NOE of backbone amides are, as mentioned above, sensitive to the dynamics of the backbone of a protein. In 1982 Lipari and Szabo published a model-free approach, with which it was possible to calculate further parameters for the relaxation analysis[124].

For two atoms connected by a bond, e.g. N-H, the correlation function describes the rotational motion with a single number which tells us how much has N-H tumbled after a certain time $i + t$.

The molecular correlation time is denoted as τ_m . Obviously, the curve will be more complicated and difficult to represent mathematically in the real systems. For spherical molecules in isotropic solvents, it is possible to approximate the correlation function with an exponential decay:

$$C(t) = e^{\frac{-t}{\tau_m}}$$

$C(t)$ decays from value of one at $t = 0$ to zero at $t = \infty$, and shape of the decay represents different timescales (Figure 2.4 plot on the left).

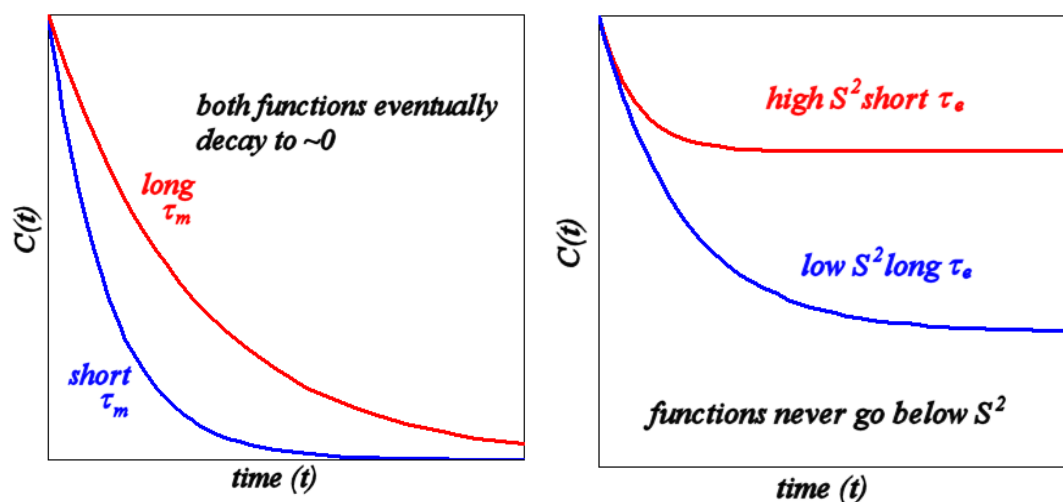


Figure 2.4 : Examples of correlation functions where the red curve represents correlation function for small molecules, and the blue curve represents correlation function for large molecules. In plot on the left, orientation of the N-H bond vector is unrestricted, thus the red and blue functions decay eventually to 0. In plot on the right the N-H bond vector is part of a larger system, thus the correlation function decay to a constant value depending on how constrained is the motion of the bond inside the larger system

The molecular correlation time τ_m expresses the speed at which N-H vector tumbles, and it is the time which takes the molecule to rotate about one radian. Now, imagine the N-H bond vector to be part of a larger system (e.g. protein). Then the correlation function would be that simple only if the protein would be completely rigid. If the N-H bond vector moves with respect to the protein, the correlation function decays to some constant value, which represents spatial restriction of the motion of the N-H bond vector and it is described by the correlation time τ_e (Figure 2.4 plot on the right).

When the correlation function of the internal motion approaches unity, the correlation function is given only by the overall rotational motion (completely rigid molecule), while when the internal

correlation function approaches zero, the relaxation is given only by internal motions (completely flexible molecule). The parameter which describes spatial restriction of the motion, the rigidity of the bond, is called as generalized order parameter S^2 ($0 \leq S^2 \leq 1$). The correlation time describing the internal motion is the effective correlation time (τ_e) and the correlation function becomes:

$$C(t) = S^2 + (1 - S^2)e^{-\frac{t}{\tau_e}}$$

However, ^{15}N the relaxation parameters provide informations about the spectral density function, which can then be used to derive τ_m and τ_e .

Those quantities are values of the spectral density function $J(\omega)$, which is a Fourier transformation of the correlation function $C(t)$.

The model-free spectral density function presented in Lipari and Szabo model-free analysis is:

$$J(\omega) = \frac{2}{5} \frac{\tau_m S^2}{1 + \omega^2 \tau_m^2} + \frac{(1 - S^2)\tau_e}{1 + \omega^2 \tau_e^2}$$

Model-free formalism introduced by Lipari and Szabo in 1982[124] naturally separates isotropic or axially symmetric rotational diffusion and internal motions of the molecule. In comparison with the spectral density functions, the model-free formalism tells us whether the oscillations of the bond vector are associated with the overall molecular rotation or with internal dynamics. The model-free approach assumes that the overall rotation of the molecule is isotropic, the internal motions are independent of, and much faster than the overall molecular rotation, and the protein does not aggregate during the analysis. The name "model-free" comes from the fact that no specific structural model is used to describe the motions. The variations of the model-free incorporate axially symmetric or fully anisotropic overall molecular tumbling, or divide between two separable timescales of internal motions.

The internal dynamics is quantified by three types of parameter: the square of the Lipari and Szabo generalized order parameter S^2 which characterizes the amplitude of the motion; the effective internal correlation time τ_e , which links the amplitude to a timescale; and the chemical exchange relaxation parameter R_{ex} which is an indicator of slower microsecond to millisecond timescale dynamics.

An analysis of ^{15}N -relaxation data according to the described model free approach can, i.e. be done with the Programm TENSOR2 [125]. In TENSOR2 different models are iteratively tested, starting with the simplest one (model 1 or m1, which consider only the overall motion). A model appears to describe the relaxation behaviour appropriately if the proposed model could give rise to the

measured relaxation rates within 95 % confidence limits [125]. In model 2 (m2) internal motion relaxations are considered active and models 3 (m3) and 4 (m4) represent same models as m1 and m2 with addition of a conformational exchange broadening parameter (R_{ex}). Model 5 (m5) and model 6 (m6) represent formalism with two time scales (S^2_{fast} and S^2_{slow}) of internal motion, and is usually referred as "extended model". In model free the spatial restriction of motion of the internal bond vector is described by generalized order parameter S^2 . In the following all used models are listed:

- $m1 = \{S^2\}$
- $m2 = \{S^2, \tau_e\}$
- $m3 = \{S^2, R_{ex}\}$
- $m4 = \{S^2, \tau_e, R_{ex}\}$
- $m5 = \{S^2, S^2_f, \tau_s\}$
- $m6 = \{S^2, \tau_f, S^2_f, \tau_s\}$.

2.4.2 CHEMICAL EXCHANGE

The structural investigation of protein-protein interactions provide useful information for understanding biological events. NMR is a powerful technique to study these interactions in solution. Protein interactions are often monitored based on 2D 1H - ^{15}N HSQC.

Chemical exchange occurs when a molecule exists in at least two conformational states, in a time-dependent manner. The chemical shift of a nucleus is extremely sensitive to the surrounding chemical environment. Hence the chemical shift of a nucleus changes when the chemical environment around it changes and alters three NMR observables: frequency, intensity and linewidth.

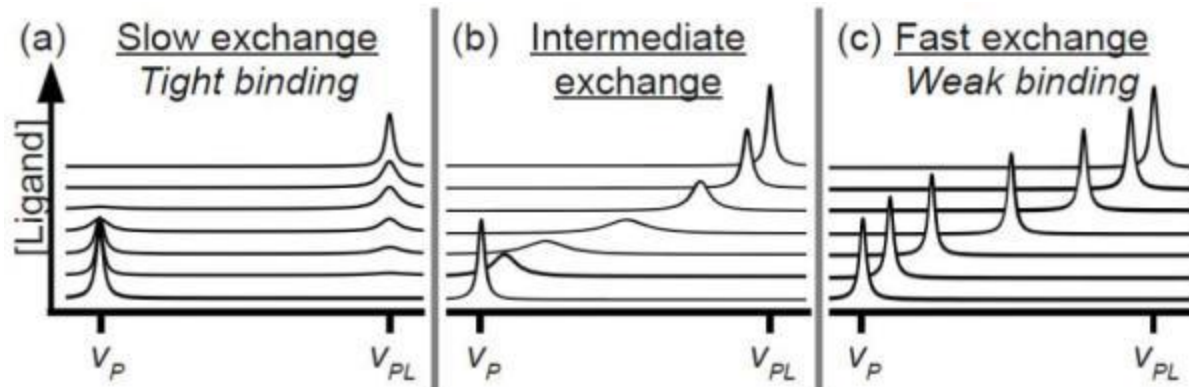


Figure 2.5: Schematic overview of exchange regimes. ν correspond to free (P) and bound (PL) resonances. a) In slow exchange regime upon increasing concentration of ligand the signal which corresponds to the free state gradually decreases while the bound frequency signal increases. c) In contrast, weak binding is usually in fast exchange regime resulting in a shift of frequency observed as more ligand is present. b) Interactions in the intermediate exchange exhibit frequency shift and change in line shape and thus signal intensity upon addition of ligand. Adapted from [126].

Depending on the time scale of the exchange with respect on the time scale of the chemical shift, the spectral appearance changes (Figure 2.5), resulting in different states or conformations visible in the NMR with an own frequency ν : for two states A and B, the appearance of the NMR spectra depends on ν_A and ν_B and population P_A and P_B and the exchange rate, k_{ex} , the sum $k_{ex}=k_A+k_B$.

Overall, three exchange regimes can be identified: slow, intermediate and fast exchange. In the intermediate regime, peaks may be so broad, that they are not observed in an NMR spectrum.

As long as the exchange rate between two sites (k_{ex}) is smaller than the difference in resonance frequencies ($\Delta\nu$), the exchange process is slow on the chemical shift time scale and two resonance frequencies are observed in the spectrum. When the exchange is fast on the chemical shift time scale ($k_{ex} \gg \Delta\nu$) a single resonance is observed.

It is also worth noting that if there is a large difference in the populations between the two conformations, then despite slow exchange, only the large peak may be observable (though it may be somewhat broader than normally expected). However in the slow exchange regime signals from both states are observed reflecting their distinct chemical shifts, intensities and linewidths and the intensity of each peak directly reports on the population of that species.

The formation of protein-ligand complex is a special case of exchange. When the chemical shift differences associated with ligand binding are fast on the NMR chemical shift time scale, binding

sites can be mapped easily by following the chemical shift changes upon adding increasing amounts of the ligand. In this case the dissociation constant can be derived from the data.

2.4.3 REAL TIME NMR

By looking either at NMR signals of the protein or the substrate, we can determine affinities of interactions and even follow enzymatic activity in real time.

In this powerful yet simple approach, dynamic processes on the ~ s or slower timescale are directly detected by quantifying the time-dependence of NMR signal intensities[127].

The real-time (RT) NMR experiment is performed by initiating the physical process of interest then rapidly acquiring a sequence of NMR spectra. The sequence of NMR spectra often demonstrate a progressive weakening of an initial set of signals and a progressive strengthening of a new set of signals resulting from time-dependent changes in the populations of different species and/or local structures (i.e., revealing the kinetics of interconversion).

The resulting function depends on the signal intensities over the time and can be plotted as an exponential conversion from A→B.

Since each time point requires a single NMR spectrum, RT-NMR had historically been limited to 1D spectroscopy and/or relatively slow kinetic processes ($\tau_{ex} = 1/k_{ex}$ ~minutes)

Recent advanced progress in hardware and methodology have reduced these limitations, indicating an exciting trajectory for current and future applications. Nowadays it is possible to record 2D RT-NMR by reducing the experimental time from ~10 min to as low as seconds per 2D spectrum, like the SO-FAST experiment.

2.5 FINGERPRINT SPECTRA AND BIOMOLECULAR RESONANCE ASSIGNMENT.

The most basic NMR experiment to be recorded for protein studies is the one-dimensional (1D) ^1H -spectrum. This spectrum provides a fast evaluation of the state of the protein, i.e. if it is folded or stable in the buffer. Although the 1D spectrum is unique for each protein, it is too complex to analyze since most of the signals overlap. In the 1D spectrum of folded proteins the proton signals are spread from around -0.5 to 12 ppm.

The fingerprint spectrum of the protein is given by the two dimensional (2D) experiment ^1H - ^{15}N HSQC (heteronuclear single quantum coherence). This spectrum is unique for each protein. During

the experiment the only protons visible are the ones bound to the observed heteronuclear atom, in this case ^{15}N . This spectrum has now two dimensions, one presents the frequencies of the ^1H attached to the ^{15}N and the other one shows the frequencies of the ^{15}N attached to the proton respectively as cross-peaks. Since there is one ^{15}N - ^1H bond per amino acid in the backbone, each cross-peak in a HSQC experiment represents a specific residue. Proline residues are not visible, due to the lack of the amide proton. This spectrum contains the signals of the protein backbone amides and usually additional peaks for the side chains of Asn, Gln, Trp, Lys and Arg residues. The sequential assignment of the observed signals is necessary to correlate NMR signals to the amino acids residues of the protein, for this assignment a set of three dimensional (3D) experiments are required [123].

The chemical shifts of the nitrogen and proton are very sensitive to changes in their chemical environment. For this reason ^1H - ^{15}N HSQC experiments are largely used in protein-ligand interaction studies, specifically by doing titration series of the protein in presence of increasing ligand concentrations. In this case the protein is ^{15}N labeled and the ligand is unlabeled, the ligand can be another protein, DNA, RNA, compounds or anything else that might interact with the labeled protein.

While ^{15}N -labelled proteins are sufficient to record ^1H - ^{15}N HSQC, ^{15}N -, as well as, ^{13}C -labelled proteins are required to record triple resonance experiments (e.g. HNCA and C(CO)NH). Because HNCA spectra show not only information about the C_α of the residue (i), but also about the C_α of the previous residue (i-1) (Figure 2.6), they can be used for the sequential assignment. C(CO)NH-spectra correlate the amide proton and nitrogen with the side chain carbon atoms of the previous residue (i-1), but not with aromatic carbons. Thus the C(CO)NH enables the identification of the residue type at the position i-1 [128].

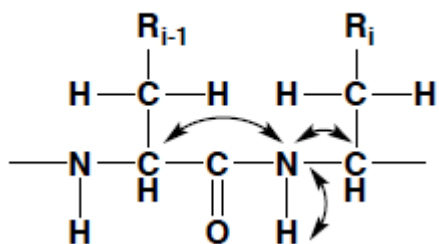


Figure 2.6: Visualization of the HNCA triple-resonance experiment The arrows show the way and direction of the magnetization transfer. The backbone hydrogen and nitrogen of a residue are in this experiment linked to the C_α -carbon or residue (i) as well as of the previous residue (i-1).

2.6 CIRCULAR DICHOISM.

Circular dichroism involves the interaction of polarized light with chiral molecules.

The underlying physical principle is the varying wavelength dependent absorption of left and right circularly polarized light by chromophores in chiral molecules. Besides glycine, which is not optically active, peptides and proteins exclusively consist of enantiomeric amino acids and are therefore highly suitable for characterization by CD spectroscopy. Moreover, all amino acids are connected by peptide bonds, which represent the most ubiquitous chromophore in peptides and proteins. This yields two characteristic absorption bands in the far UV region ($\lambda = 190\text{-}250\text{nm}$): a $\pi\text{-}\pi^*$ transition at 190nm and a weaker and broader $n\text{-}\pi^*$ transition at 210 nm. Different types of secondary structure arrange the peptide bonds in a specific asymmetric, non-random fashion, giving rise to characteristic CD spectra in this wavelength range.

Although modern instruments directly measure the difference in absorption, for historical reasons the circular dichroism is usually expressed in degrees of ellipticity [θ].

CD spectra are often normalized to show the mean residue ellipticity θ_{MRW} :

$$\theta_{\text{MRW}} = \frac{(\theta_m - \theta_{\text{ref}}) * 100}{c * d * Na}$$

where θ_m is the ellipticity of the peptide sample [mdeg], θ_{ref} is the ellipticity of the reference sample (usually the used buffer) [mdeg], c denotes the peptide concentration [mol/l], d corresponds to the path length of the cuvette [cm], and Na equals the number of amino acids in the peptide-sequence

Far-UV spectra of peptides and proteins can be used to predict characteristics of their secondary structure. This is based on the fact that isolated α -helices, β -sheets, and random coils possess characteristic, distinctly different signatures.

The α -helix content of a protein might be estimated by the magnitude of the negative band around 222 nm. The CD spectrum for a β -strand is represented by a negative band at around 210 - 225 nm and a positive band with a maximum at 190 - 200 nm. A typical random coil spectrum points out a negative band around 200 nm (Figure 2.7).

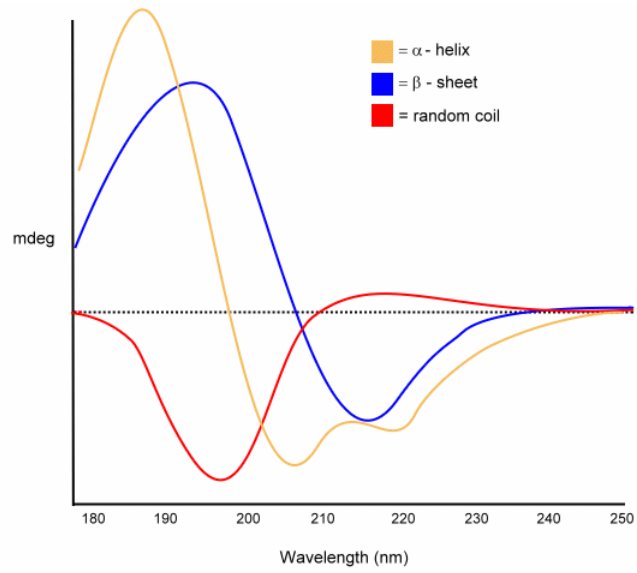


Figure 2.7: CD spectra of representative secondary structure: α -helix, β -sheet, and random coil

CHAPTER 3

3.1 MATERIALS

If not indicated otherwise, chemicals and supplementary materials were purchased from Roth (Germany), Serva (Germany), Sigma-Aldrich (Germany), and VWR (Germany). The isotopes, $^{15}\text{NH}_4\text{Cl}$ and ^{13}C glucose, and D_2O were bought from Eurisotop (Germany) and Sigma Aldrich (Germany).

3.1.1 BACTERIAL STRAINS AND PLASMIDS.

Escherichia coli BL21 (DE3) cells were supplied by Novagen (Merck, Darmstadt, Germany). *E. coli* XL1-Blue cells were purchased from Stratagene (Agilent Technologies Deutschland GmbH, Waldbronn, Germany).

The expression plasmid for Rheb Δ CT was provided by the group of Prof. Dr. Alfred Wittinghofer from the Max-Planck Institute for Molecular Physiology in Dortmund, Germany.

The expression plasmid for FKPB38-BD was provided by the group of Prof. Dr. Ho Sup Yoon from the Nanyang Technological University, Singapore.

3.1.2 CELL GROWTH MEDIA

Lysogeny Broth (LB), containing 10 g tryptone, 10 g NaCl, 5 g yeast extract in 1L water, was used for expression of unlabeled proteins, minipreps or precultures. LB medium was autoclaved prior to use.

For the expression of labeled proteins M9 minimal medium was used, which was composed of 200 mL 5xM9 salts (34 g/L Na_2HPO_4 , 15 g/L K_2HPO_4 , 2.5 g/L NaCl, H_2O), 2 mL 1 M MgSO_4 , 0.1 mL 1 M CaCl_2 , 10 mL 100xBME vitamins (Sigma), 1 g NH_4Cl , 2 g glucose, 100 mg/L ampicillin, adjusted to 1 L H_2O . Each single component was either autoclaved or sterile filtrated. Uniformly ^{15}N -labeled protein was prepared in M9 minimal medium containing $^{15}\text{NH}_4\text{Cl}$ as the sole nitrogen source. Uniformly ^{15}N - ^{13}C -labeled protein was prepared in M9 minimal medium containing $^{15}\text{NH}_4\text{Cl}$ and ^{13}C glucose as the sole nitrogen and carbon sources, respectively

3.2 METHODS

3.2.1 PROTEIN EXPRESSION AND PURIFICATION

All the proteins were expressed *Escherichia coli* BL21 (DE3) in LB or ¹⁵N or both ¹³C and ¹⁵N M9 minimal medium, containing ¹⁵NH₄Cl and ¹³C₆-glucose.

3.2.2 RHEBΔCT EXPRESSION PURIFICATION

A C-terminal truncated version of human Rheb (Uniprot-ID Q15382) lacking the CaaX box needed for farnesylation (1-170 = RhebΔCT) was expressed as a glutathione-S-transferase (GST) fusion protein from pGEX-4T. Cells were grown at 37 °C. At an OD₆₀₀ of 0.6-0.8 cells were induced with 0.1 mM isopropyl-B-D-thiogalactopyranoside and incubated at 15 °C overnight. Cells were disrupted in 50 ml 20 mM Tris, 100 mM NaCl, 5 mM MgCl₂, and 2 mM benzamidine, pH 7.5, by sonication (Sonoplus Bandelin, UV 3200) for 15 minutes on ice with a power level of 35 % and a pulse length of 5 s. The cells were centrifuged and the supernatant was loaded on a Glutathione Sepharose® 4B (GE Healthcare) column. The target protein was purified according to the manufacturer's manual, except for the fact that the used buffers contained no Triton X-100.

The fusion protein was eluted using 20 mM of reduced glutathione in 20 mM Tris, 150 mM NaCl and 5 mM MgCl₂, pH 7.5. The GST tag was removed from RhebΔCT with thrombin (5U per mg fusion protein), which recognises the consensus sequence Leu-Val-Pro-Arg-Gly-Ser and cleaves the peptide bond between Arg and Gly.

In order to separate the GST tag from the pure RhebΔCT protein a size exclusion chromatography was performed with a 75 µg Superdex™ HiLoad™ 16/600 column (GE Healthcare) coupled to an ÄKTA Prime FPLC system (GE Healthcare). The resulting fractions were collected and concentrated using centrifugal filter devices (Amicon® Ultra Centrifugal Filter Units MWCO 3000, 15 ml, Merck Millipore) at 3500xg and 4 °C.

3.2.3 FKBP38-(BD) EXPRESSION AND PURIFICATION

FKBP38-BD (Uniprot-ID 14318, residues 88-206 of human FKBP38 isoform 2) was expressed as His-tagged protein from a pET-16b (Novagen) expression vector. Cells were grown at 37 °C. At an OD₆₀₀ of 0.8, cells were induced with 0.5 mM isopropyl-B-D-thiogalactopyranoside and incubated

at 37 °C overnight. The cell pellet was resuspended in 50 ml 50 mM Tris, 2 mM EDTA, 2 mM benzamidine, 2 mM DTT, pH 8, and the cell suspension sonicated as described for Rheb Δ CT. The resulting cell lysate was centrifuged for 30 min at 23000 xg at 4 °C.

The fusion protein was extracted from inclusion bodies. First the pellet was washed with 50 mM Tris, pH 8, 1 M urea 1 mM TCEP, and then the target protein was extracted by incubation of the pellet in 50 mM Tris, pH 8, 6 M guanidinium chloride (GdmCl), 1 mM TCEP for 1h at 4 °C on a rocking device.

After centrifugation, the supernatant was loaded on a column filled with Ni-NTA resin (Qiagen) (5 ml bed volume) that had been equilibrated in 50 mM Tris, 6 M GdmCl, 1 mM TCEP, 30 mM imidazole, pH 8. The protein that bound to the column was refolded by a step-wise decrease of the GdmCl concentration from 6 to 0 M in 1 M steps. The refolded protein was eluted with 40 ml 50 mM Tris, 350 mM NaCl, 1 mM TCEP, 500 mM imidazole, pH 8. The eluted fractions containing the target protein (based on an analysis by SDS-PAGE) were pooled and concentrated to 2.5 ml using centrifugal filter devices (Amicon® Ultra Centrifugal Filter Units MWCO 3000, 15 ml, Merck Millipore) at 3500 x g and 4 °C. Following exchange of the buffer to 20 mM Tris, 100 mM NaCl, 1 mM CaCl₂, pH 8, using a PD-10 column (GE Healthcare), factor Xa (New England Biolabs, 1 U per 50 μ g substrate protein) was added to cleave off the His-tag at 25 °C overnight. FKBP38-BD was separated from the His-tag by size exclusion chromatography and concentrated as described for Rheb Δ CT.

3.2.4 FKBP38-FATC

3.2.4.1 PLASMID CLONING.

The region encoding residues 88-206 of human FKBP38 isoform 2 (= FKBP38-BD, Uniprot-ID: Q14318) was amplified by PCR using as template the expression plasmid pET16::FKBP38-BD. The sequence of the forward primer that included a NdeI site (bold) was 5'-GCGC CATATG CCG GCC CCA GAA GAG TG-3' and that of the reverse primer that included a BamHI site (bold) 5'-CCG GGATCC GTC CAC AGC CGT CTT CAG-3'. The Taq Polymerase, the nucleotide mix and the restriction enzymes used in this work had been obtained from New England Biolabs. The purified PCR product was inserted into the TA cloning® vector pCR2.1 (Invitrogen) and transformed into TOP10 cloning cells (Invitrogen) and used to inoculate a culture in LB medium

for a small scale plasmid preparation using a Wizard® Plus SV Miniprep Kit (Promega). The purified plasmid pCR2.1::FKBP38-BD and a plasmid encoding for a GB1-tagged version of the FATC domain of yeast TOR1 (residues 2438-2470 = y1fatc, Uniprot-ID P35169) 29, were both separately digested with NdeI and BamHI. The digested FKBP38-BD coding fragment and pGEV2 plasmid were ligated using the Quick Ligation™ Kit (New England Biolabs). The authenticity of the obtained DNA construct was confirmed by DNA sequencing. An N-terminal six residues long histidine-tag (MHHHHHMK-FKBP38-BD-y1fatc Fig. 1A) was introduced by site-directed mutagenesis following the QuickChange site directed mutagenesis protocol (Stratagene) using as forward PCR primer 5'-TTT GTT TAA CTT TAA GAA GGA GAT ATA ATG CAT CAT CAT CAT CAT CAT ATG CCG GCC CCA GAA GAG TGG CTG GAC ATT CTG-3' and as backward one 5'-CAG AAT GTC CAG CCA CTC TTC TGG GGC CGG CAT ATG ATG ATG ATG ATG ATG CAT TAT ATC TCC TTC TTA AAG TTA AAC AAA-3' and Phusion® High-Fidelity DNA Polymerase and DpnI from New England Biolabs. The success of the mutagenesis was verified by DNA sequencing. The final sequence of the His-tagged FKBP38-BD-y1fatc chimera that has a factor Xa site (IEGR) in-between is:

MHHHHHMPAPEEWLDILGNLLRKKTLVPGPPGSSRPVKGQVVTVHLQTSLENGTRVQ
 EEPFLVFTLGDCDVIQALDLSVPLMDVGETAMVTADSKYCYGPQGSRSPIPPHAALCLEV
 TLKTAVD-GSIEGR-NELDVPEQVDKLIQQATSIERLCQHYIGWCPFW.

3.2.4.2 PROTEIN EXPRESSION AND PURIFICATION.

The His-tagged FKBP38-y1fatc chimeric protein was expressed in *Escherichia coli* BL21 (DE3) cells in M9 minimal medium containing as sole nitrogen source ¹⁵N-NH₄Cl. At an OD₆₀₀ of ~0.7–0.9 cells were induced with 1 mM IPTG and grown for another 3 h at 37 °C in a shaking flask incubator. The cells were harvested by centrifugation (6'000 x g, 30 min, 4 °C). The supernatant was discarded and the pellet was resuspended in 40 ml nanopure water, centrifuged again (6'000 x g, 30 min, 4 °C) and the pellet stored at -20 °C. The next day this pellet was resuspended in 50 ml 50 mM Tris, pH 7.8, 2 mM EDTA, 2 mM benzamidine, 2 mM DTT per 1 l culture. The resuspension was vortexed and the cells were lysed by sonication (Sonoplus Bandelin, UV 3200) for 15 minutes on ice with a power level of 35 % and a pulse length of 5 s and then centrifuged (23'000 x g, 20 min, 4 °C). Since the majority of the expressed His-tagged FKBP38-y1fatc chimeric protein was insoluble and expressed into inclusion bodies, the supernatant was discarded.

The pellet was washed with 20 ml 50 mM Tris, 1 M urea, 1 mM TCEP, pH 7.8, centrifuged again and the resulting pellet was treated with 15 ml 50 mM Tris pH 7.8, 8 M urea, manual disruption and incubation on a rocking device at 4 °C for 1 h in order to extract the target protein. Following centrifugation, the supernatant was dialyzed to decrease the urea concentration in several steps (4, 2, 1, 0 M) using a membrane with a molecular weight cut-off (MWCO) of 3.5 kDa. The resulting protein solution was loaded on a column filled with Ni-NTA resin (Qiagen) (5 ml bed volume) that had been equilibrated with 50 mM Tris pH 7.8, 150 mM NaCl. The protein was eluted in 5 fractions of 5 ml using buffer containing 20, 50, 100, 200, 500 mM imidazole. The eluted fractions containing the target protein (based on an analysis by SDS-PAGE), were pooled, washed with 20 mM Tris, 150 mM NaCl, 5 mM MgCl₂, pH 7.8 and concentrated with centrifugal filter devices (Amicon® Ultra Centrifugal Filter Units MWCO 3000, 15 ml, Merck Millipore) at 3500 x g and 4 °C. The protein was further purified by a size exclusion chromatography step using a 75 µg Superdex™ HiLoad™ 16/600 column (GE Healthcare) coupled to an ÄKTA Prime FPLC system (GE Healthcare) equilibrated in 20 mM Tris, 150 mM NaCl, 5 mM MgCl₂, pH 7.8, which was also used as running and elution buffer, at a flow rate of 1 ml/min. Protein concentrations were determined by UV spectroscopy using the extinction coefficient at 280 nm calculated based on the amino acid sequence and assuming that all cysteines are oxidized (FKBP38-BD-y1fatc $\epsilon(280 \text{ nm}) = 22710 \text{ M}^{-1} \text{ cm}^{-1}$).

3.2.5 PREPARATION OF THE RHEB SWITCH-1 PEPTIDE

A chemically synthesized peptide (HPLC purified, purity >90%) corresponding to the switch1 region of human Rheb (residues 33 to 45 referred to as hRheb_sw1 = Acetyl-NH-DSYDPTIENTFTK-CONH₂) was bought from Thermo Scientific. 2.2 mg were diluted in 900 µL of buffer (20 mM Tris, pH 7.5, 150 mM NaCl, 5 mM MgCl₂), in order to obtain 1.6 mM stock solution.

3.2.6 SYNTHESIS OF Y1FATC-PEPTIDES

The following peptides corresponding to different length fragments of the yeast TOR FATC domain have been synthesized by the group of Dr. L.G. Milroy from University of Eindhoven, Netherlands.

The Peptides y1fatc-pep1 (2460-2470), y1fatc-pep2 (2457-2470), y1fatc-pep3 (2454-2470) and y1fatc-pep3mutant (2454-2470. Y2463E/W2466) were synthesized by Fmoc SPPS using an automated solid-phase peptide synthesizer (Intavis MultiPep RSi, INTAVIS Bioanalytical Instruments AG) on a preloaded Fmoc Trp(Boc) Tentagel R PHB resin (Rapp Polymere, 0.19 mmolg⁻¹ loading). Reactions were performed on a 50 μmole scale using NMP (Biosolve) as reaction solvent, 4 eq. *N*-Fmoc protected amino acids (Novabiochem), 20 % piperidine (Biosolve, v/v) in NMP for Fmoc deprotection, 4 eq. *O*-benzotriazole-*N,N,N',N'*- tetramethyluronium-hexafluoro-phosphate (HBTU, Biosolve), and 8 eq. of *N,N*-diisopropylethylamine (DIPEA, Biosolve) as base. Amino acid coupling (30 min incubation) and Fmoc-deprotection (8 min) steps were each performed twice Peptide resin cleavage and side-chain deprotection was achieved using a 92.5/2.5/2.5/2.5 (v/v) mixture of trifluoroacetic acid (TFA)/H₂O/triisopropylsilane (TIS)/ethanedithiol (EDT), and then precipitated through drop wise addition into ice-cold diethyl ether, followed by centrifugation (2000 rpm, 10 min), washing with ice-cold ether and a second centrifugation to isolate the crude pellet. All four peptides were purified by mass-triggered reverse-phase preparative HPLC fitted with fraction collector, which was programmed to collect on detection of *m/z* value corresponding to [M+2H]²⁺ molecular ion. Separation was performed on an Alltima HP C18 column (5 μm, length 125 mm, ID: 20 mm) and 0.1% trifluoroacetic acid (TFA) in H₂O/MeCN was used as mobile phase. Combined H₂O/MeCN fractions were dried by lyophilization to afford the peptide as a white amorphous powder. The isolated peptides were analyzed for molecular integrity and purity by analytical LC-MS using a Shimadzu LC Controller V2.0, LCQ Deca XP Mass Spectrometer V2.0, Alltima C18- column 125 x 2.0 mm, Surveyor AS and PDA with solvent eluent conditions: CH₃CN/H₂O/1% TFA. Alternatively, the peptides were analyzed by LC-MS using a LCQ Fleet from Thermo Scientific on a C18 column, Surveyor AS and PDA with solvent eluent conditions: MeCN/H₂O/0.1% formic acid.

3.2.7 PREPARATION OF MEMBRANE MIMETICS

Bicelles were prepared by first drying an appropriate amount of the long chain phospholipid in organic solvent (DMPC stock in chloroform) under a stream of nitrogen gas in a glass vial. The dried lipid was then resuspended in a small amount of buffer, followed by the addition of the short chain lipid (DihepPC) in buffer. After thorough vortexing of the bicelle mixture, the protein solution was added.

Liposomes of the small unilamellar vesicle (SUV) type were prepared by drying an appropriate amount of DMPC stock in chloroform under a stream of nitrogen gas. To dissolve the pellet in an amount of buffer needed to obtain a 100 mM solution, it was exposed to seven cycles of freezing in liquid nitrogen, thawing by incubation in a water bath at 40 °C and thorough vortexing. The DMPC suspension was incubated in an ultra sonication bath for 20 minutes, in order to induce the formation of small unilamellar vesicles (SUVs) from large uni- and multilamellar vesicles. To remove the remaining large vesicles, the milky suspension was centrifuged in a tabletop centrifuge for 5 minutes at 14.8 K rpm. This resulted in a clear supernatant and a rather big flocculent white precipitate. For the preparation of a protein sample in the presence of liposomes, only the clear supernatant containing small unilamellar vesicles was used.

3.3 NMR SAMPLE PREPARATION

3.3.1 RHEB Δ CT AND FKBP38-BD

Samples contained 80-200 μ M protein for the NMR monitored interaction studies and 310-380 μ M protein to record 3D HNCA and 3D CCONH-TOCSY, and 15 N-relaxation data in 20 mM Tris, 150 mM NaCl, 5 mM MgCl₂, pH 7.5 supplemented with 5 % D₂O. The Rheb protein purified from *E. coli* exists primarily in the GDP-bound form. The GTP analogue- (guanosine 5'-[β,γ -imido]triphosphate, trisodium salt = GppNHp, also known as GMPPNP, and guanosine-5'-[(β,γ -methylene]triphosphate, sodium salt = GppCp-, also known as GMPPCP and GppCH₂p, used as 50 mM stocks in buffer, Jena Bioscience) bound forms were obtained by adding a 10-fold excess of the respective nucleotide to the GDP form in 20 mM Tris, 150 mM NaCl, 5 mM MgCl₂, pH 7.5, in the presence of 10 mM EDTA to decrease the affinity for GDP and a catalytic amount of Antarctic phosphatase (5 U = 1 μ l for each NMR sample of 0.25 ml, New England Biolabs) to degrade GDP [129]. To record 3D assignment and 15 N-relaxation data the samples were incubated for 7 days at 4 °C to achieve a complete exchange from GDP to GppNHp or GppCp form.

All the samples that were used to determine the influence of FKBP38-BD on the GDP to GppNHp exchange rates (see also table 1) contained about 0.1 mM 15 N-Rheb Δ CT-GDP in the usual buffer supplemented with 0.5 mM GppNHp, 1 (series A-C) or 10 (series F-H) mM EDTA, 5 units Antarctic phosphatase (= PPase, New England Biolabs, 1 μ l with 5000 units/ml for each 0.25 ml sample) in the first and second subseries (A1 to H1 and A2 to H2), and either no FKBP38-BD in

the first subseries of each series (A1 to H1) or at the following molar ratios of ^{15}N -Rheb Δ CT-GDP to FKBP38-BD: 102:1 (A2/3-C2/3), or 96:1 (F2/3) or 29:1 (G2/3) or 15:1 (H2/3).

3.3.2 FKBP38-Y1FATC

NMR samples contained $\sim 100\ \mu\text{M}$ ^{15}N -labeled FKBP38-BD-y1fatc fusion protein in 20 mM Tris buffer (pH 7.8 or 6.5, 95 % H_2O / 5 % D_2O) with 150 mM NaCl, 5 mM MgCl_2 (not in case of the pH 6.5 samples) and 0.02 % NaN_3 . For the natural abundance experiments, the NMR sample contained $\sim 665\ \mu\text{M}$ peptide in 50 mM Tris, 100 mM NaCl, pH 6.5, (95% H_2O /5% D_2O). Dodecylphosphocholine (DPC) and 1,2-diheptanoyl-sn-glycero-3-phosphocholine (DihepPC) and 1,2-dimyristoyl-sn-glycero-3-phosphocholine (DMPC) were obtained from Avanti Polar Lipids and deuterated DPC (d_{38} -DPC) from Cambridge Isotopes. Generally, DPC stock solutions for the titrations were prepared as follows. A defined amount of DPC from a concentrated stock (usually 0.5 M) in chloroform was placed in a glass vial and dried under a stream of nitrogen gas. The dried lipid was then dissolved in buffer or a protein sample. DPC micelles form above the critical micelle concentration (CMC), which is 1.1 mM for DPC [130].

3.3.3 Y1FATC DERIVED PEPTIDES

Peptides were dissolved in 50 mM Tris, 100 mM NaCl, pH 6.5. The peptides y1fatc-pep1-3 (Figure 4.22A) were dissolved stepwise in an amount of buffer necessary to result in a clear solution. To obtain a higher concentrated sample of y1fatc-pep3mutant (Figure 4.22A) it was dissolved in an excess of buffer (20 ml) and then concentrated using a centrifugal filter device (Amicon® Ultra Centrifugal Filter Units MWCO 3000, 15 ml, Merck Millipore) at 3500 x g and 4 °C. However, due to the small size of the peptide and the rather large MWCO more than half of the peptide went into the flow-through. The final concentrations in the used NMR samples were 40 μM for y1fatc-pep1, 25 μM for -pep2, 12.5 μM for -pep3, and 47 μM for -pep3mutant. For y1fatc-pep2 an additional higher concentrated sample of $\sim 0.46\ \text{mM}$ and for -pep3mutant one of $\sim 0.65\ \text{mM}$ had been prepared. Peptide concentrations were determined by UV spectroscopy using the extinction coefficient at 280 nm calculated based on the amino acid sequence and assuming that all cysteines are oxidized (y1fatc-pep1-3 $\epsilon_{(280\ \text{nm})} = 12615\ \text{M}^{-1}\ \text{cm}^{-1}$ and y1fatc-pep3-mutant $\epsilon_{(280\ \text{nm})} = 5625\ \text{M}^{-1}\ \text{cm}^{-1}$).

3.4 NMR SPECTROSCOPY

NMR spectra were acquired at 298 K on Bruker Avance 500 and 600 MHz spectrometers, the 500 MHz and one 600 MHz equipped with a cryogenic probe. The data were processed with NMRPipe [131] and analyzed using NMRView [132]. Chemical shift assignments for rat and mouse Rheb in the GDP- and/or GppNHp-bound forms have been published [133-135]. Since we used human Rheb and a slightly different fragment and/or buffer conditions, we assigned the backbone ^1H , ^{15}N , and $^{13}\text{C}^\alpha$ nuclei based on newly recorded 3D HNCA and CCONH-TOCSY data in combination with the published assignments. The ^1H and ^{15}N resonances of Rheb-GppCp were assigned based on the similarity of its ^1H - ^{15}N HSQC spectrum to that of Rheb-GppNHp. The assigned ^1H - ^{15}N HSQC spectra for Rheb Δ CT-GDP, -GppNHp, -GppCp are displayed in Figures 4.1-4.3, respectively. Information about the backbone dynamics was derived from ^{15}N -relaxation experiments including T_1 , T_2 and $\{^1\text{H}\}$ - ^{15}N NOE. The relaxation times were sampled at the following time points: for T_1 : 10.8, 216, 432, 648, 864 ms; for T_2 : 25.6, 51.2, 76.8, 102.4, 128 ms. Relaxation times were determined based on a fit to the equation $y = A \exp(-t/B)$, where B corresponds to T_1 or T_2 and A to the signal intensity at time 0, using the relaxation analysis tool provided in NMRView. ^{15}N - T_1 , ^{15}N - T_2 and $\{^1\text{H}\}$ - ^{15}N - NOE values of well-resolved peaks of different nucleotide-binding states of Rheb Δ CT were analyzed based on a model-free approach [124, 136] using the program TENSOR2 [125] and the solution structure of rat Rheb-GDP (PDB-ID 2L0X) and the crystal structure of mouse Rheb-GppNHp (PDB ID 4O25). For the determination of the rotational correlation time, τ_c , residues for which T_1/T_2 was within one standard deviation from the average value were considered (for Rheb Δ CT-GDP: 6-12, 14-16, 18-22, 24-29, 31-36, 38-48, 51-66, 68, 69, 74-79, 83-99, 105-112, 118-125, 127-152, 154-161, 163-170; for Rheb Δ CT-GppNHp: 6-14, 16-18, 20-23, 26-29, 43-49, 51-59, 63, 65-68, 77, 79-88, 90, 92-102, 107-112, 114-124, 126-152, 154-160, 162, 164-170).

To monitor the exchange times of bound GDP to GppNHp in ^{15}N -Rheb Δ CT in absence and presence of FKBP38-BD and/or Antarctic phosphatase (= PPase) by NMR (table 1 in appendix), the samples were brought to the NMR machine right after mixing. The times given in the spectra figures (see Results Figures 4.13-4.15) refer to the time the respective ^1H - ^{15}N HSQC experiment was started after mixing of the sample. To determine the exchange times only backbone amide resonances for residues sensitive to the nucleotide exchange and thus showing a significant change

in the ^1H and ^{15}N chemical shifts between the GDP- and the GppNHp-bound states were analyzed (see Results Figure 4.15-4.16).

Table 1 Overview of the analysis of the GDP to GppNHp exchange of Rheb Δ CT in the absence and presence of FKBP38-BD and/or Antarctic phosphatase (= PPase) by real time NMR spectroscopy					
Series name	[Rheb Δ CT]: [FKBP38-BD] [§]	Addition of PPase	[EDTA] (mM)	Analyzed residues	Average exchange time τ_{ex} (min) \pm standard deviation*
A1	1:0	yes	1	A10, G13, K19, S20,	132 \pm 55
A2	102:1	yes	1	V32, Y35, E40, D60,	297 \pm 77
A3	102:1	no	1	G63, Q64	52 \pm 30
B1	1:0	yes	1	I9, A10, G13, S20, V32,	128 \pm 35
B2	102:1	yes	1	Y35, E40, G63	163 \pm 62
B3	102:1	no	1		133 \pm 46
C1	1:0	yes	1	A10, S20, Y35, E40,	329 \pm 108
C2	102:1	yes	1	D60, G63, Q64	239 \pm 108
C3	102:1	no	1		267 \pm 120
F1	1:0	yes	10	I9, A10, G13, S16, K19,	108 \pm 19
F2	96:1	yes	10	S20, V32, Y35, E40,	101 \pm 17
F3	96:1	no	10	D60, G63, Q64, E66	74 \pm 38
G2	29:1	yes	10	None, because of too fast exchange	--
G3	29:1	no	10		--
H2	15:1	yes	10		--
H3	15:1	no	10		--
					--

[§] The Rheb Δ CT concentration in the samples was always $\approx 100 \mu\text{M}$ (A series: 98, B series: 114, C series: 106 μM). The concentration of GppNHp was always 0.5 mM.
* The average was taken over all residues analyzed for a particular series (see column labeled 'analyzed residues').

Usually, I9, A10, S16, K19, S20, V32, Y35, E40, G63, Q64, and E66 were considered. Exchange times ($\tau_{\text{ex}} = 1/k_{\text{ex}}$) were obtained by fitting the signal intensity for the recorded time points to an exponential decay function $y = A \exp(-t/B) + C$, where B corresponds to τ_{ex} and A to the signal intensity in the ^1H - ^{15}N HSQC spectrum corresponding to the first time point, and C to the offset along the y-axis), using the rate analysis tool provided in NMRView. In some series the error of the fitted exchange times were very high (> 30 min) because of too low signal intensity in most of the spectra of the respective time series. Accordingly the corresponding values were not used to calculate average exchange times ($\tau_{\text{ex}}(\text{average})$, Table 1). As a control, the ^1H - ^{15}N peak intensity of

I90 have been considered, which is not affected by the GDP to GppNHp exchange and which thus should not show an exponential decay of its signal intensity.

3.5 CD SPECTROSCOPY

All CD spectra were recorded at room temperature on a Jasco J715 spectropolarimeter using a cuvette of a path length of 0.1 cm. All spectra were recorded with an acquisition time of 50 nm per minute (8 s response time) and five scans if not otherwise mentioned.

CHAPTER 4

4. RESULTS

4.1 BACKBONE ASSIGNMENT OF RHEB Δ CT-GDP

Chemical shift assignments for rat Rheb in the GPD and GppNHp bound forms have been published by Schwarten et al. [134] and by Berghaus et al. [133].

Since in this work human Rheb and slightly different fragments as well as buffer conditions have been used, the backbone ^1H , ^{15}N , and $^{13}\text{C}_\alpha$ nuclei has been assigned based on newly recorded 3D HNCA and CCONH-TOCSY data in combination with the published assignments. The ^1H and ^{15}N resonances of Rheb-GppCp were assigned based on the similarity of its ^1H - ^{15}N HSQC spectrum to that of Rheb-GppNHp. The assigned ^1H - ^{15}N HSQC spectra for Rheb Δ CT-GDP, GppNHp, GppCp are displayed in figures 4.1, 4.2 and 4.3 respectively. These assignments are the basis for the analysis of the ^{15}N -relaxation and the rate analysis data presented in the next sections.

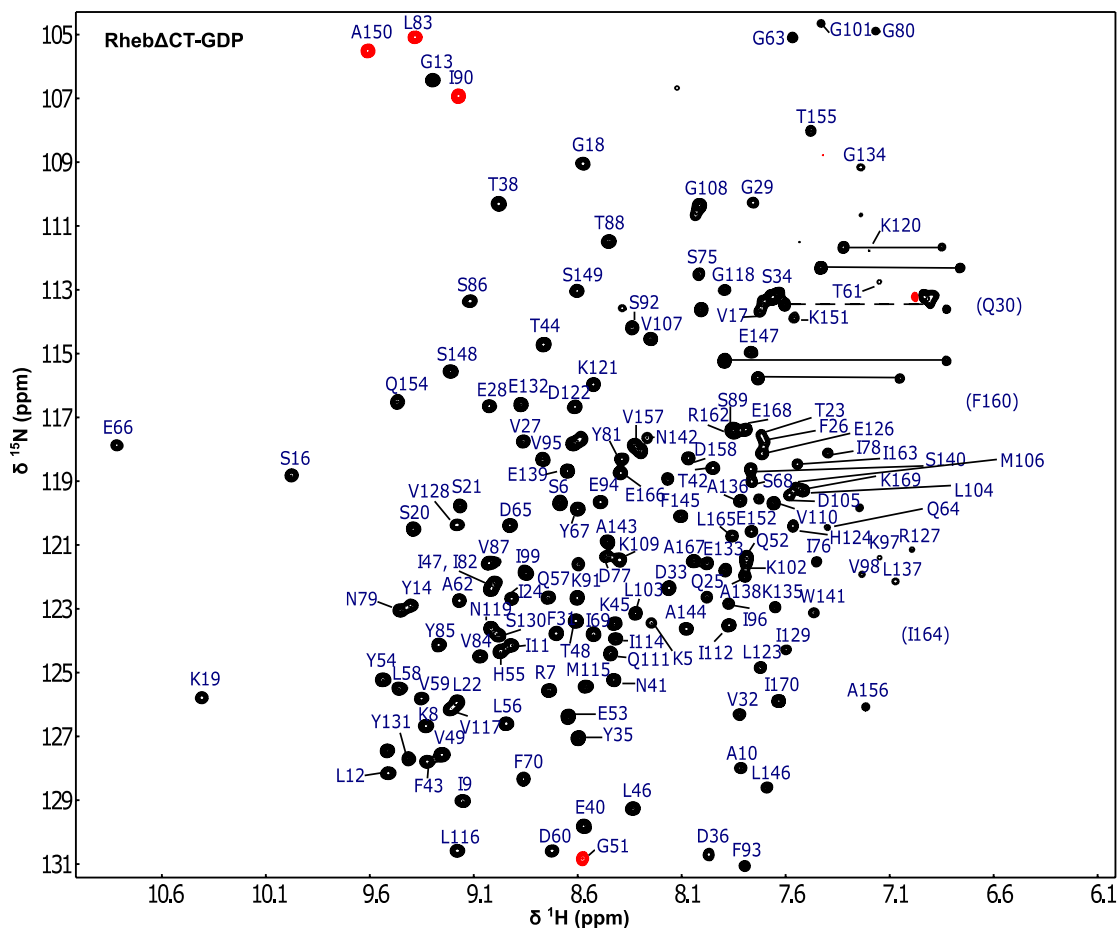


Figure 4.1: ^1H - ^{15}N HSQC spectrum of Rheb ΔCT in the GDP-bound state. The assignments are indicated by the one letter amino acid code and the sequence position. Side chain amide proton resonances of glutamine and asparagine residues are connected by black lines. The resonances of some residues (assignment labels in brackets) are only visible at lower contour level. Negative peaks (red) correspond to residues that are spectrally folded. Adapted from [70]

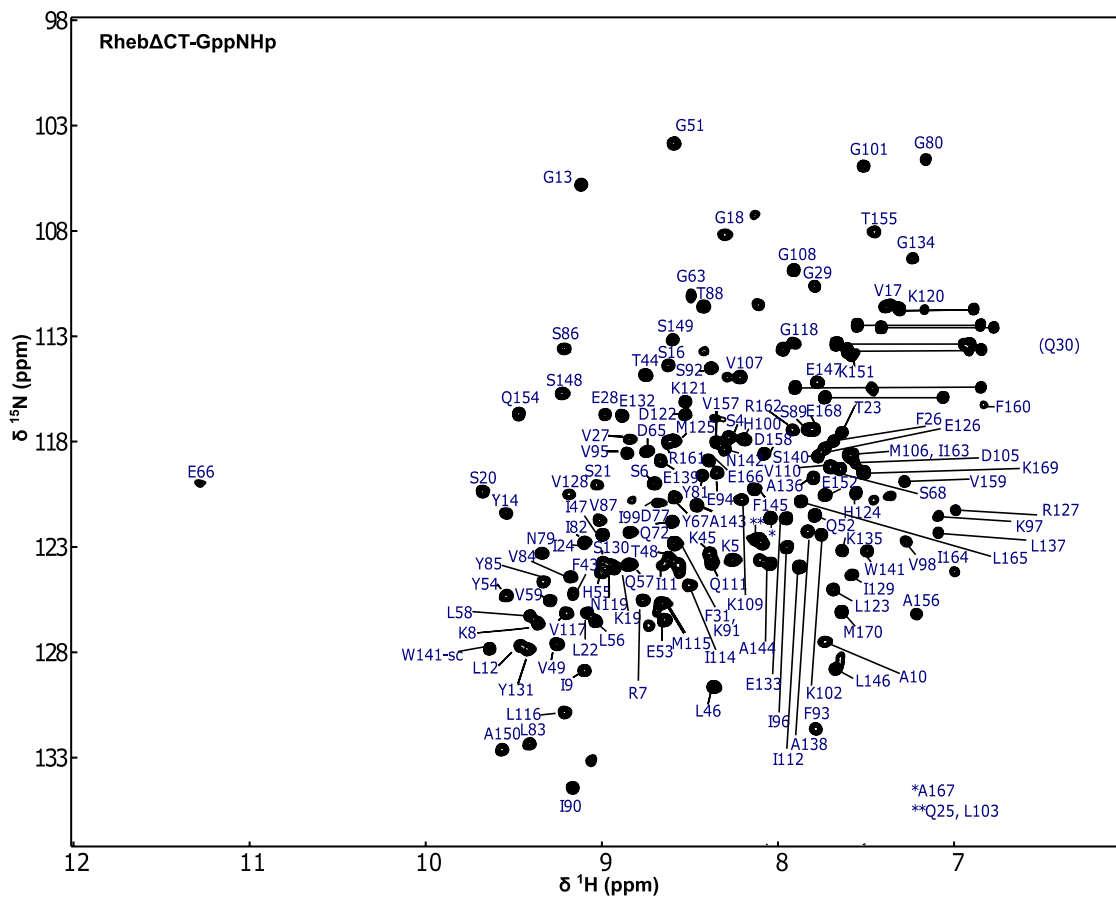


Figure 4.2: ^1H - ^{15}N HSQC spectrum of Rheb Δ CT in the GppNHp-bound state. The assignments are indicated by the one letter amino acid code and the sequence position. Side chain amide proton resonances of glutamine and asparagine residues are connected by black lines. The resonances of some residues (assignment labels in brackets) are only visible at lower contour level. Negative peaks (red) correspond to residues that are spectrally folded. Adapted from [70]

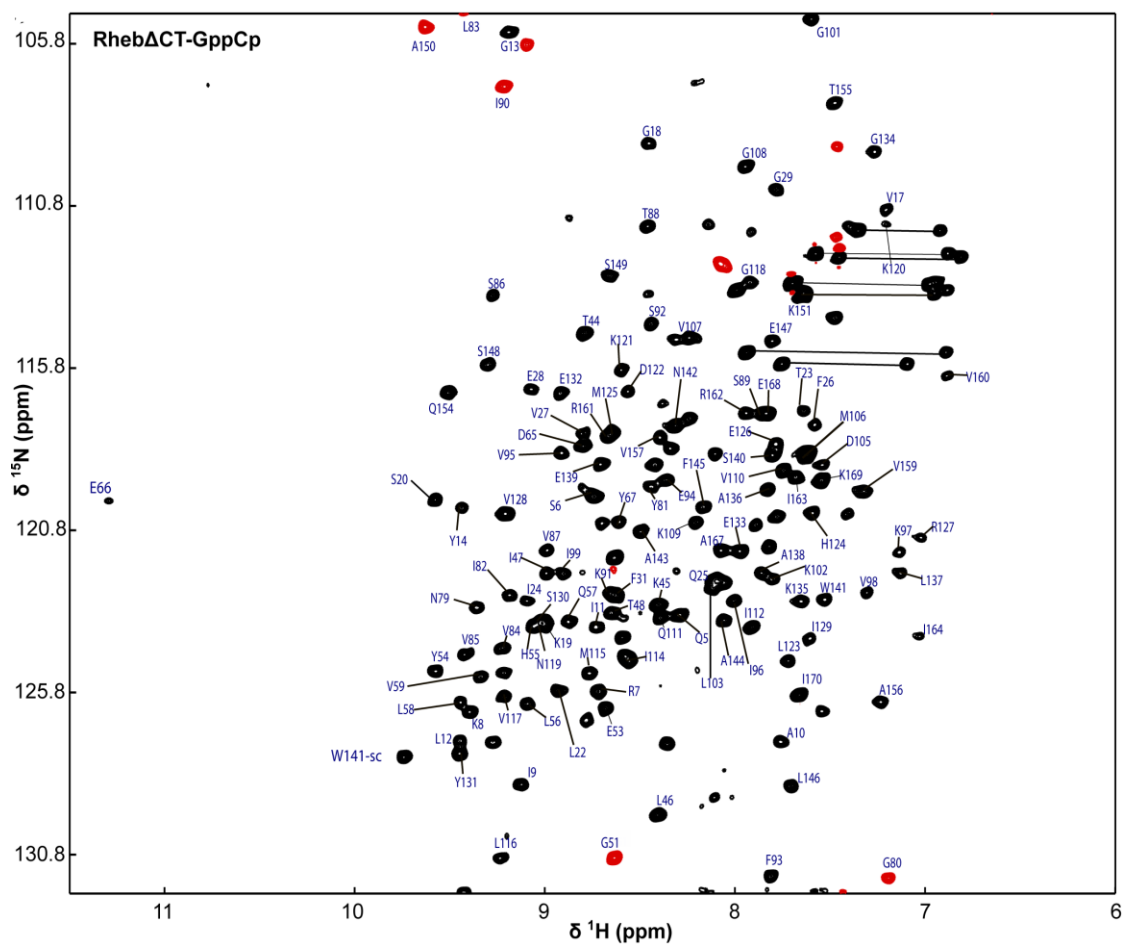


Figure 4.3: ^1H - ^{15}N HSQC spectrum of Rheb Δ CT in the GppCp-bound state. The assignments are indicated by the one letter amino acid code and the sequence position. Side chain amide proton resonances of glutamine and asparagine residues are connected by black lines. The resonances of some residues (assignment labels in brackets) are only visible at lower contour level. Negative peaks (red) correspond to residues that are spectrally folded. Adapted from [70]

4.2 ANALYSIS OF ^{15}N RELAXATION DATA

In line with published crystal structure data [4], the superposition of the ^1H - ^{15}N HSQC spectra of Rheb Δ CT-GDP and -GppNHp indicates that GDP-GTP cycling results in significant conformational changes (Figure 4.4).

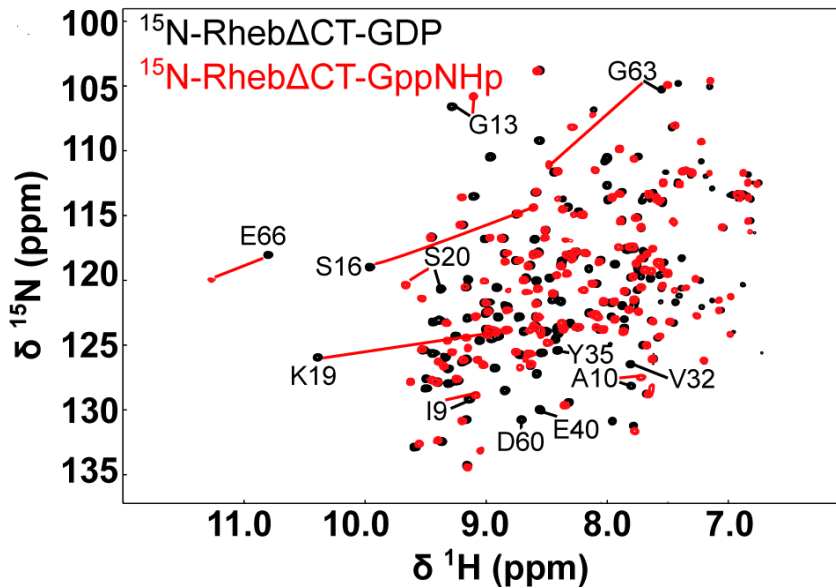


Figure 4.4: Superposition of the ^1H - ^{15}N HSQC spectra of ^{15}N -Rheb Δ CT in the GDP- (black) and GTP-analogue (= GppNHp, red) bound form. Some residues showing large chemical shift changes between the two states are labeled with the one letter amino acid code and the residue number and in the same color as used for the respective spectrum. The fully assigned spectra for each state as well as that of Rheb Δ CT bound to another GTP-analogue, referred to as GppCp, are displayed in Figure 4.1, 4.2, 4.3, respectively. Adapted from [70]

In order to determine if the inactive GDP- and the active GTP-bound state of Rheb show differences in the backbone dynamics that may play a functional role, the backbone dynamics were studied based on ^{15}N -relaxation experiments for Rheb Δ CT in the GDP- and two GTP analogue-bound states, namely Rheb Δ CT-GppNHp and -GppCp.

The $\{^1\text{H}\}^{15}\text{N}$ -NOE values for the GDP- and the GppNHp-bound forms of human Rheb (1-170) were compared to those reported for rat Rheb (1-184) that differs within 1-170 only at positions 1 and 170 (M1 and M170 in human and S1 instead of the native M1 and I170 in rat Rheb). [77, 133] The values are overall similar, however, it was possible to get some more data points within the switch II region of the GppNHp-bound state and in addition ^{15}N -T1 and -T2 values for the GDP and GTP-analogue bound states had been measured.

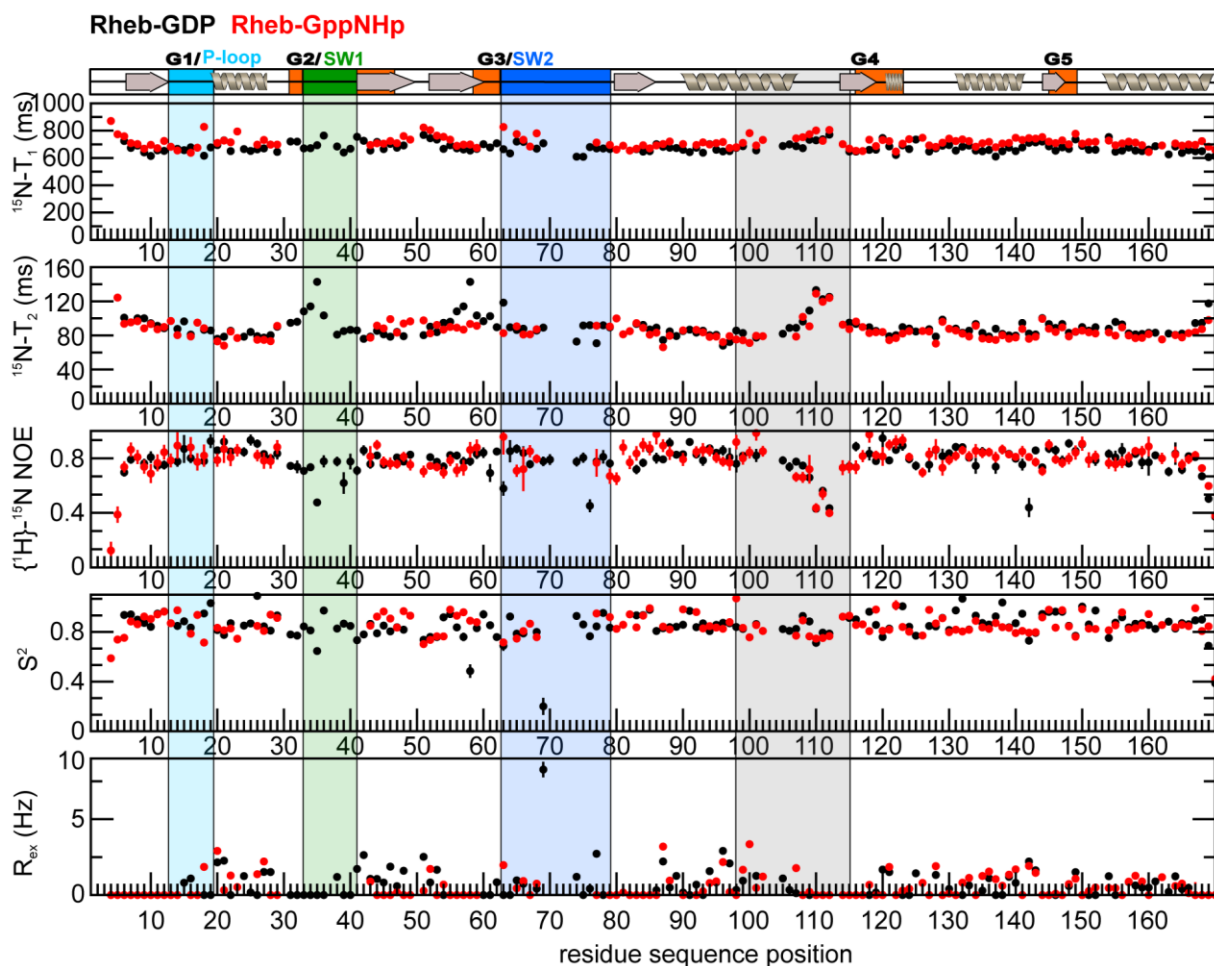


Figure 4.5: Plots of the ^{15}N -relaxation data of Rheb ΔCT in the GDP- (black) and GppNHp- (red) bound states including ^{15}N - T_1 (top panel), $-T_2$ (second panel), and $\{^1\text{H}\}$ - ^{15}N NOE (third panel) values and uncertainties and results of the Lipari-Szabo model-free analysis including the order parameter S^2 (fourth panel) and the contribution of chemical exchange R_{ex} to the observed transverse relaxation rate $1/T_2$ (fifth panel). The model-free analysis of the ^{15}N relaxation data was performed using the program TENSOR2 [125] and an isotropic tumbling model. The location of the G-boxes and the switch 1 and 2 (SW1 & 2) regions [65, 67] and the secondary structure elements are indicated at the top. Filled grey arrows represent β -sheet conformation and grey spirals helical conformation. The secondary structure content was derived from the solution structure of C-terminal truncated rat Rheb-GDP (PDB-ID 2L0X) [77]. That of C-terminal truncated mouse Rheb-GppNHp is almost identical (PDB- ID 4O25) [137]. Adapted from [70]

The average ^{15}N - T_1 values for Rheb ΔCT -GDP are 676 ± 34 ms and 716 ± 41 ms for the GppNHp-bound state at 500 MHz field strength and 298 K. The average ^{15}N - T_2 values are 90 ± 15 ms and 87 ± 17 ms and the average $\{^1\text{H}\}$ - ^{15}N NOE values are 0.78 ± 0.10 and 0.79 ± 0.11 for the GDP- and GppNHp-bound states, respectively. The ^{15}N -relaxation parameters are in the range expected for an about 19.3 kDa molecule (GS-human Rheb 1-170). The analysis of the ^{15}N -relaxation data based on

a model-free approach using the program TENSOR2 [125] and an isotropic diffusion tumbling model provides overall rotational correlation times τ_c of 9.9 ns for Rheb Δ CT-GDP and of 10.4 ns for Rheb Δ CT-GppNHp at 298 K as well as the subnanosecond order parameter S^2 and the parameter R_{ex} , which contains information about the contribution of conformational exchange to the relaxation process. The fitted τ_c values are 1-2 ns lower than estimated based on the number of residues and the molecular weight (\approx 11-12 ns). This can be explained with the well-defined and compact folds observed for C-terminally truncated rat Rheb-GDP (PDB-ID 2L0X) and mouse Rheb-GppNHp (PDB-ID 4O25) [77, 137]. In agreement with this, the S^2 order parameter values (Figure 4.5, Tables 5-6 in appendix) are on average 0.84 ± 0.15 and 0.89 ± 0.09 for Rheb Δ CT-GDP and -GppNHp, respectively.

The G2/switch 1 and G3/switch 2 regions (Figure 4.5) of the inactive GDP and the active GTP form of Rheb Δ CT show most differences in the backbone dynamics.

In the GDP state, Y35 in the switch 1 regions provides higher $^{15}\text{N-T}_1$ and $^{-T}_2$ and lower $\{^1\text{H}\}$ - ^{15}N -NOE values (Figure 4.5, Tables 1 in appendix), indicating increased backbone dynamics on the ns- μ s time scale for this region. For residues 30-42 of the GppNHp state no ^{15}N -relaxation data could be measured since the respective peaks were broadened beyond detection (Figure 4.5, Tables 2 in appendix). This suggests that the switch1 region in this state shows also increased backbone dynamics however only a slightly slower time scale as the GDP state.

The same is true for several residues of the G3 box/switch 2 region (63-75) in both states, since residues 70-73 in the GDP and residues 69-76 in the GppNHp could also not be detected. For both, Rheb Δ CT-GDP and -GppNHp, residues G109 to Q112 show higher $^{15}\text{N-T}_1$ and $^{-T}_2$ and lower $\{^1\text{H}\}$ - ^{15}N -NOE values. Thus the loop around residues 108-114, which is spatially close to the C-terminal half of the switch 2 region, shows also increased backbone dynamics on the subnanosecond timescale.

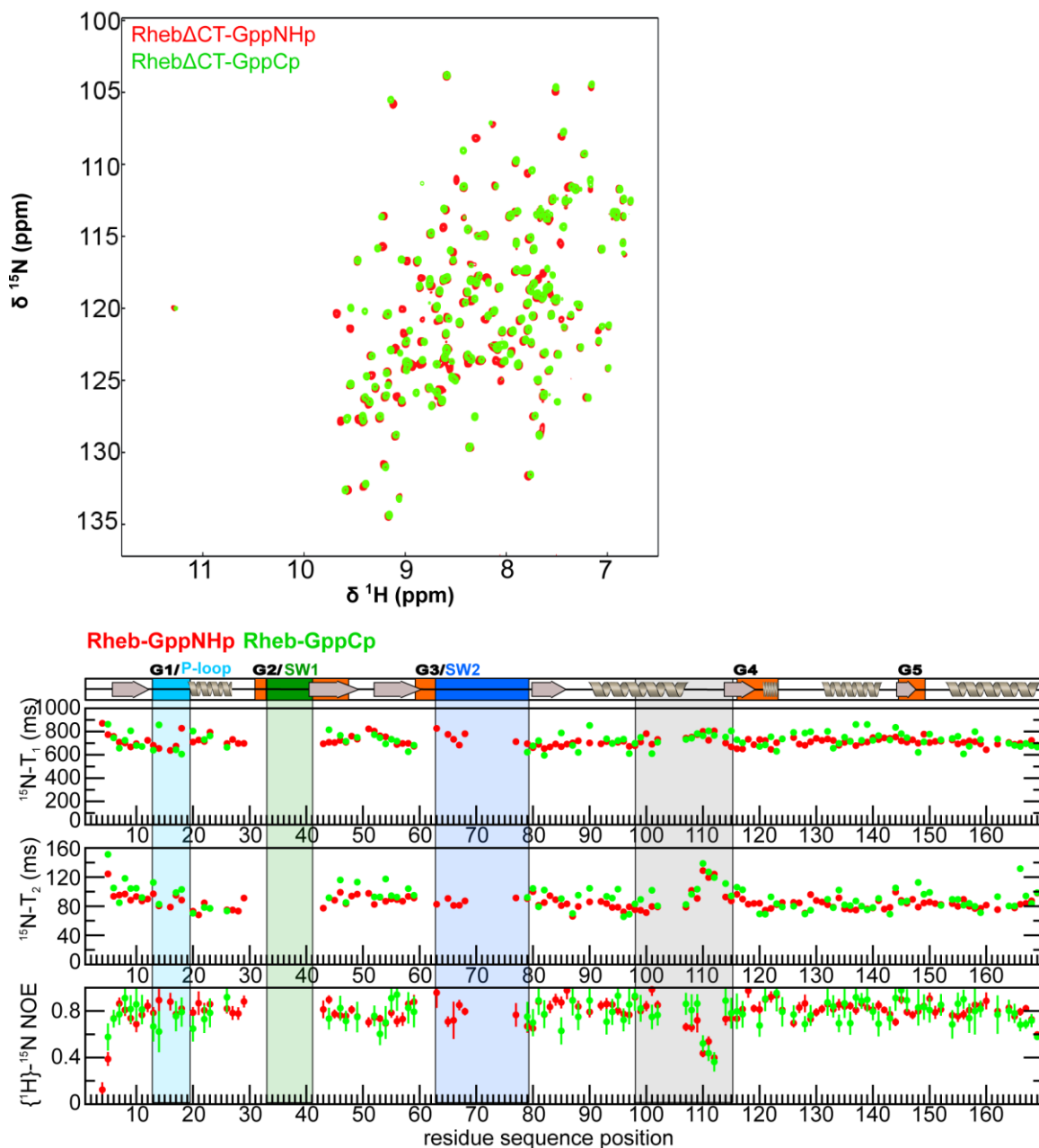


Figure 4.6: On the top superposition of the ^1H - ^{15}N HSQC spectra of Rheb Δ CT in the GppNHp (red) and GppCp (green) bound states. On the bottom comparison of the backbone dynamics of Rheb Δ CT in the GppNHp- (red) and GppCp- (green) bound states. Plots of the ^{15}N -relaxation data including ^{15}N -T₁ (top panel), -T₂ (second panel), and $\{^1\text{H}\}$ - ^{15}N NOE (third panel) values are shown. The location of the G-boxes and the switch 1 and 2 (SW1 & 2) regions [65, 67] and the secondary structure elements are indicated on the top. Filled grey arrows represent β -sheet conformation and grey spirals helical conformation. The secondary structure content was derived from the solution structure of rat Rheb-GDP (PDB-ID 2L0X) [77]. That of mouse Rheb-GppNHp is almost identical (PDB-ID 4O25) [137]. Adapted from [70]

Figure 4.6 shows the comparison of the backbone dynamics of Rheb Δ CT in both GTP-analogue bound states (Rheb Δ CT-GppNHp and -GppCp) and as expected the dynamic behavior is overall rather similar (Figure 4.6). The average ^{15}N -T₁, -T₂, and $\{^1\text{H}\}$ - ^{15}N -NOE values for Rheb Δ CT-GppCp are 725 ± 77 ms and 94 ± 21 ms, and 0.77 ± 0.14 , respectively. The values for all analyzable residues are listed Table 3 in appendix.

For some residues in the P-loop such as K19 and S20 and residues in the loop formed by residues 85-90 and around the small 3¹⁰ helix formed by residues 121-123 small differences were observed. These residues are in the vicinity of the nucleotide binding site, especially near the β and γ phosphate group of the nucleotide.

In addition, the conformational differences due to the different chemical bond between the β and γ phosphate group of the nucleotide appear to slightly modulate the dynamics of the residues in the two β -strands following the switch 1 region (\approx residues 45-55).

4.3 NMR INTERACTION STUDIES OF RHEB IN GDP AND GPPNHP BOUND STATES WITH FKBP38

NMR monitored interaction studies have been performed in order to elucidate the disagreeing previous studies about the interaction between Rheb and FKBP38 and to better understand whether there is a dependence on the nucleotide binding state.

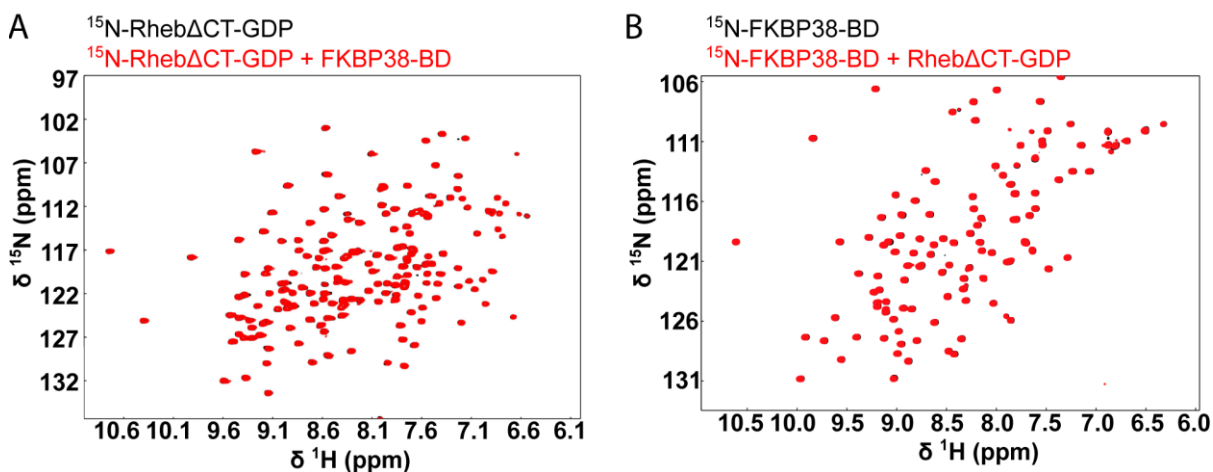


Figure 4.7: Rheb Δ CT-GDP does not interact with FKBP38-BD. Superposition of the ^1H - ^{15}N HSQC spectra of ^{15}N -Rheb Δ CT in the GDP-bound states in the presence of unlabeled FKBP38-BD (A) and vice versa (B). The color coding is indicated at the top of each plot. Adapted from [70]

Figure 4.7A shows the superposition of the ^1H - ^{15}N HSQC spectra of GDP-bound ^{15}N -Rheb ΔCT in absence (black) and presence (red) of unlabeled FKBP38-BD and in the plot B that of ^{15}N -FKBP38-BD in the presence of unlabeled Rheb ΔCT -GDP. In both cases, no significant spectral changes can be observed, indicating that Rheb ΔCT -GDP does not interact with FKBP38-BD.

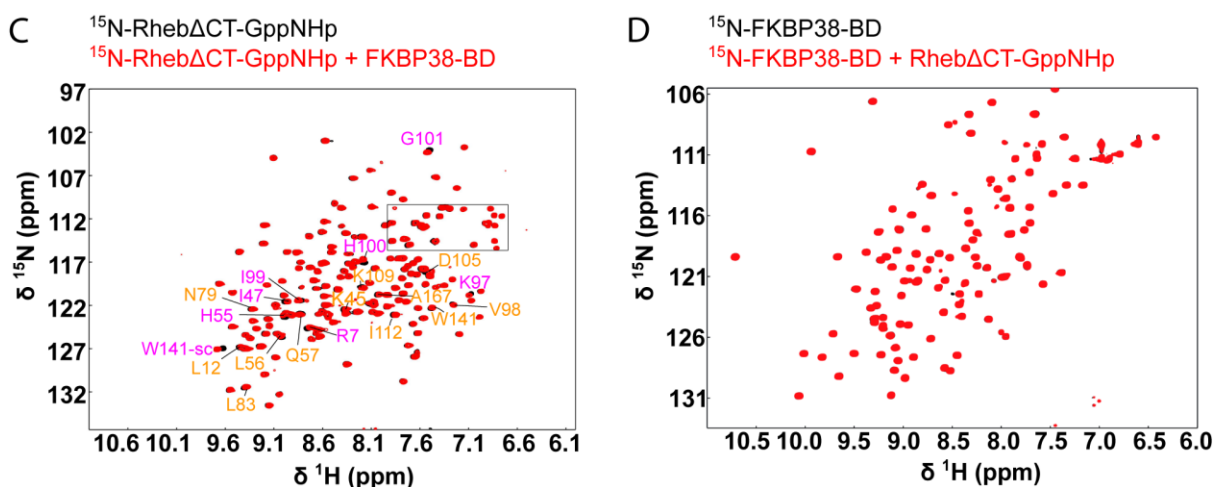


Figure 4.8: Rheb ΔCT interacts only weakly and/or transiently with FKBP38-BD in the active GTP-bound state. Superposition of the ^1H - ^{15}N HSQC spectra of ^{15}N -Rheb ΔCT in the GppNHp-bound states in the presence of unlabeled FKBP38-BD (C) and vice versa (D). Adapted from [70]

Figure 4.8C shows the superpositions of the ^1H - ^{15}N HSQC spectra of GTP-analogue bound ^{15}N -Rheb ΔCT in the absence (black) and presence (red) of unlabeled FKBP38-BD and in D that of ^{15}N -FKBP38-BD in the presence of unlabeled Rheb ΔCT -GppNHp.

^{15}N -FKBP38-BD in the presence of unlabeled Rheb ΔCT -GppNHp does not show significant spectral changes. In line with the studies of Bai et al.[45] Rheb-GppNHp showed spectral changes indicating a GTP-dependent interaction.

Mapping the spectral changes residues onto the crystal structure of mouse Rheb-GTP (PDB-ID 4O25) (Figure 4.9) [137] is evident that the presence of FKBP38-BD affects the long helix, formed by residues K97-D105, the nearby W141 and the subsequent loop encompassing residues 108-114, which are spatially close to the switch 2 region and show, based on the ^{15}N -relaxation data, increased backbone dynamics (Figure 4.5 and Tables 1-2) .

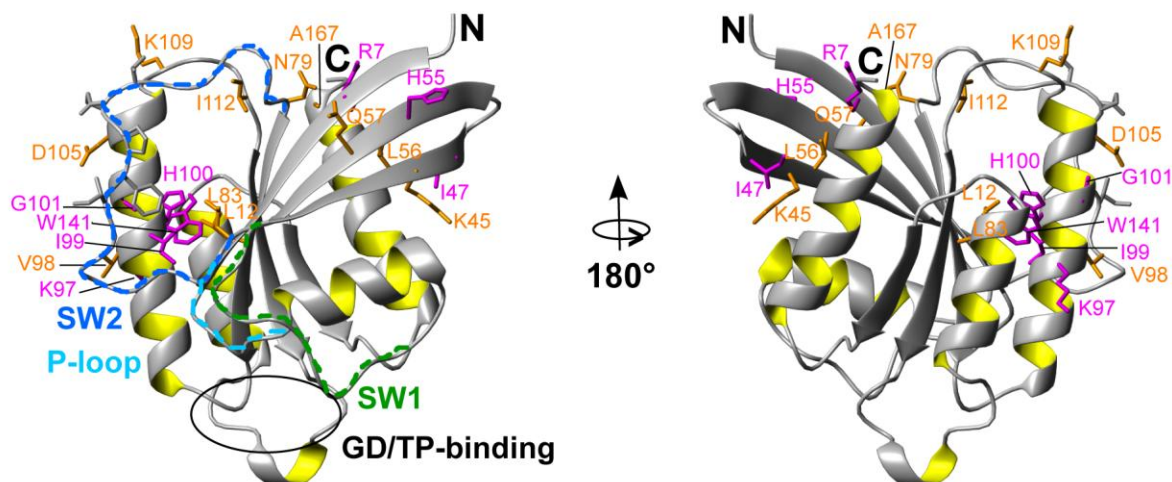


Figure 4.9: Ribbon representation of the crystal structure of C-terminal truncated mouse Rheb-GppNHp (PDB-ID 4O25) [137]. The P-loop (light blue) and the switch 1 and 2 (SW1 green, SW2 blue) are highlighted by dashed colored lines. The side chains of the residues showing medium or weak shifts in Figure 4.8(C) are shown in stick representation in the same colors as the labels there. Adapted from [70]

Furthermore, several residues in the β -sheet region on the other side of the switch 2 region show weak to very weak shifts (e.g. R7, K45, I47, and H55-Q57, respectively). For the part of switch 2 region that is localized between the mapped regions, chemical shift changes could mostly not be observed since the backbone amide resonances for residues 69 to 73 are broadened beyond detection.

These studies were performed at molar ratio of about 1:1 between Rheb and FKBP38 and were confirmed in the titration of ^{15}N -Rheb Δ CT-GppNHp with unlabeled FKBP38-BD up to a molar ratio of about 1:2 (Figure 4.10B).

Figure 4.10 shows more NMR data that has been recorded in order to characterize the interaction between Rheb Δ CT in the three nucleotide binding states (-GDP, -GppNHp and -GppCp) and FKBP38-BD.

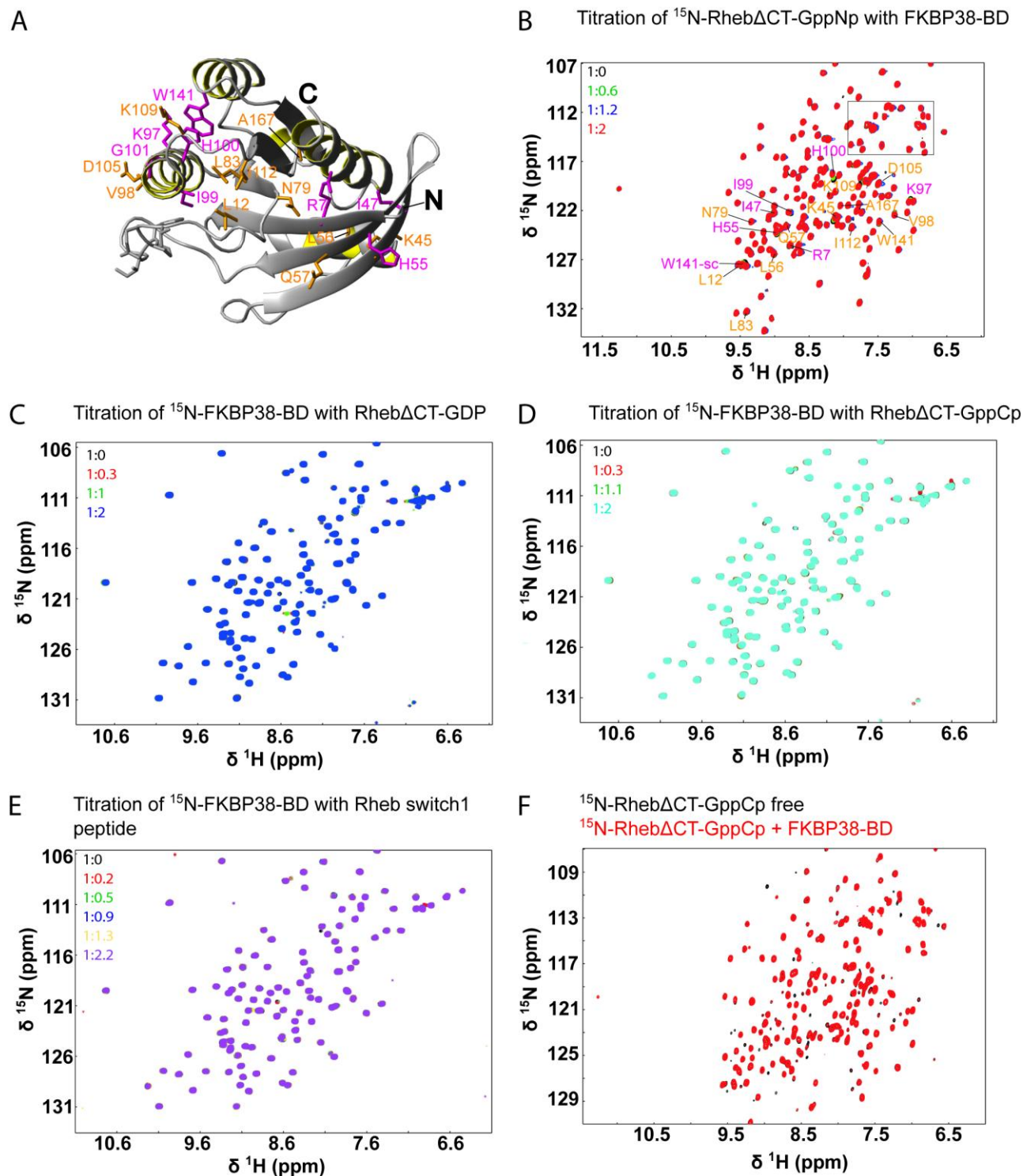


Figure 4.10: More NMR data recorded to characterize the interaction between Rheb Δ CT and FKBP38-BD. **(A)** View of the structure of mouse Rheb-GppNHp with the spectral changes observed in Figure 4.8C mapped onto it (magenta – medium and orange – weak chemical shift changes). The representation corresponds to a view from the top on the structure as shown left side in Figure 4.9 (90° rotation around a horizontal axis). **(B)** Superposition of the ^1H - ^{15}N HSQC spectra of ^{15}N -Rheb Δ CT-GppNHp in the presence of increasing concentrations of unlabeled FKBP38-BD. The color

coding and the molar ratios of the two proteins are indicated in the upper left. The residues that showed medium (magenta) or weak (orange) shifts comparing ^{15}N -Rheb Δ CT-GppNHp in the absence (black) and presence of unlabeled FKBP38-BD (red) in Figure 4.8C are labeled in the same color coding. The boxed region contains peaks for the side chain $-\text{NH}_2$ groups of glutamines and asparagines. (C-E) Superposition of the ^1H - ^{15}N HSQC spectra of ^{15}N - FKBP38-BD in the presence of increasing concentrations of unlabeled Rheb Δ CT-GDP or $-\text{GppNHp}$ or a 13mer peptide corresponding to the switch 1 region of Rheb, respectively. The color coding and the molar ratios of the two components are indicated in the upper left. (F) Superposition of the ^1H - ^{15}N HSQC spectra of ^{15}N -Rheb Δ CT-GppCp in the absence (black) and presence of unlabeled FKBP38-BD (red). Adapted from [70]

^{15}N -Rheb Δ CT-GppCp in presence of unlabeled FKBP38-BD resulted only in a decrease of the GDP state signals that were still present due to a yet incomplete exchange (Figure 4.10F)

The fact that ^{15}N -Rheb Δ CT-GppCp did not show the same shifts as the GppNHp state may be explained by the presence of few remaining peaks of the GDP state (most black peaks with no red peaks on top); the protein was not fully exchanged. Since the latter disappeared upon addition of FKBP38-BD, its presence appeared to have stimulated the further exchange from the GDP to the GppCp state of Rheb Δ CT. Note that the exchange of GDP to the GTP-analogue GppNHp occurred generally faster during the sample preparation for the NMR studies (see Chapter 3 Methods) than to GppCp using otherwise the same conditions.

More interaction studies have been performed with different molar ratio ^{15}N FKBP38-BD and Rheb Δ CT in-GDP and GppCp bound states. (Figure 4.10C-D)

Published studies proposed that the switch1 region of Rheb plays an important role for the interaction with FKBP38 [46]. The tration of ^{15}N -FKBP38-BD with a 13mer peptide encompassing the switch 1 region (Figure 4.10E) have been recorded. This in agreement with the data for Rheb Δ CT-GDP and $-\text{GppNHp}$, resulted in no significant spectral changes. The fact that FKBP38-BD shows no significant spectral changes in the presence of Rheb-GppNHp (Figure 4.8D) or Rheb Δ CT-GppCp (Figure 4.10D) may be explained by the interaction being only weak or transient and by the fact that the regions of the FKBP38-BD mediating it do not significantly alter their conformation.

FKBP38 has been shown to contain a low affinity Ca^{2+} -binding site around residues L90-I96 corresponding to residues L147-I153 in the full-length sequence, which modulates the interaction with Bcl-2 [76].

For this reason it has been additionally analyzed if the FKBP38-BD in the presence of CaCl_2 interacts stronger with Rheb-GppNHp (Figure 4.11).

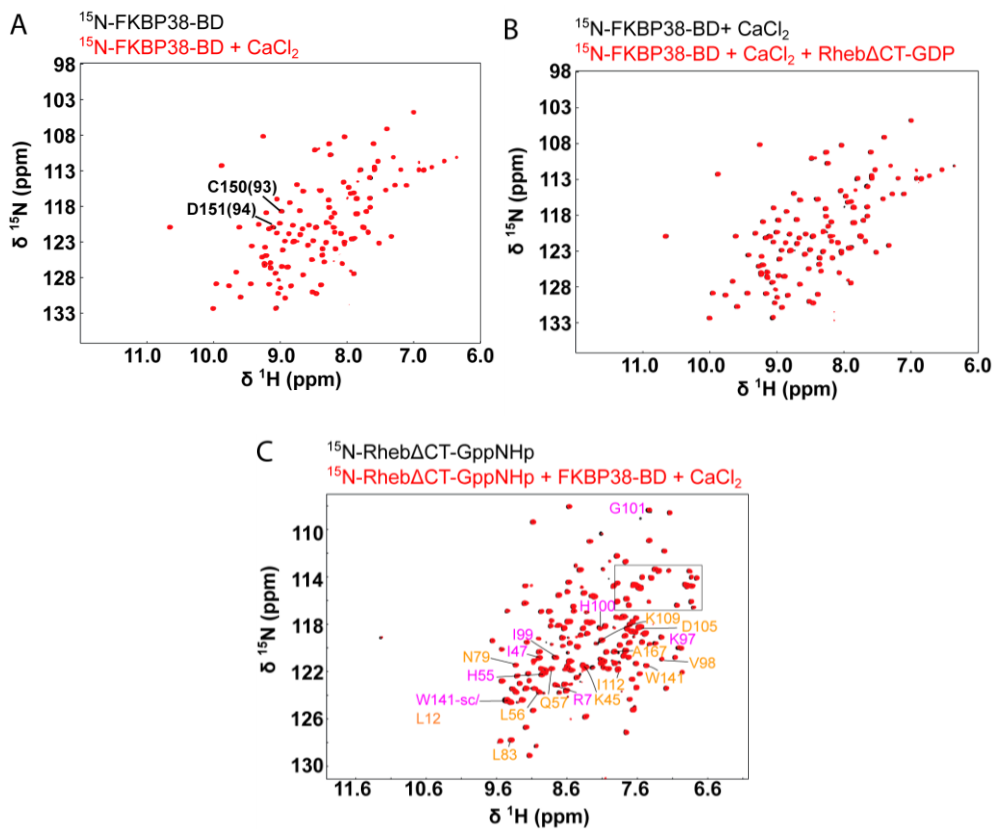


Figure 4.11: NMR data recorded to characterize a potential influence of the addition of CaCl_2 on the interaction between FKBP38-BD and Rheb Δ CT. (A) Superposition of the ^1H - ^{15}N HSQC spectra of ^{15}N - FKBP38-BD in the absence (black) and presence of 2 mM CaCl_2 (red) in the buffer. Two of the residues of FKBP38-BD that have been suggested to weakly interact with Ca^{2+} [76] are labeled with the one letter amino acid code and the sequence position in the full-length protein and in brackets in the protein used in the published study [76]. (B) Superposition of the ^1H - ^{15}N HSQC spectra of ^{15}N - FKBP38-BD in the presence of only 2 mM CaCl_2 in the buffer in the absence (black) and presence of unlabeled Rheb Δ CT-GppNHp (red). (C) Superposition of the ^1H - ^{15}N HSQC spectra of ^{15}N -Rheb Δ CT-GppNHp in the absence (black) and presence of unlabeled FKBP38-BD and 2 mM CaCl_2 (red). The residues that showed medium (magenta) or weak (orange) shifts comparing ^{15}N -Rheb Δ CT-GppNHp in the absence (black) and presence of unlabeled FKBP38-BD (red) in Figure 4.8C are labeled in the same color coding. The boxed region contains peaks for the side chain -NH₂ groups of glutamines and asparagines. Most of the medium shifting ones such as G101, H100, K97 or I99 show also shifts here. However R7 and I47 did not show significant shifts. The peak of the side chain amide proton of W141 has presumably a slightly different peak position as in Figure 4.8C and overlaps here with L12. Most of the residues showing weak shifts in the Figure 4.8C (orange labels) do not show a significant shift

here. Presumably because of the slightly different buffer conditions (+/- 2 mM CaCl₂) and slight differences in the used protein concentrations and corresponding molar ratios. Adapted from [70]

Although addition of Ca²⁺ results in some weak shifts for C93 and D94 of FKBP38, corresponding to C150 and D151 in the full-length sequence, upon addition of CaCl₂ (Figure 4.11A), Ca²⁺ binding appears not to have a significant effect on the affinity for Rheb-GppNHp or vice versa (Figures 4.11B -C).

In comparison with the observed chemical shift changes of Rheb-GppNHp with FKBP38-BD in the absence of CaCl₂ (Figure 4.8C), the chemical shift changes of W141 and the nearby helical residues K97-G101 are well detectable. However most of the others, mostly weak ones were not clearly visible. Maybe the fact that the molar ratio of Rheb Δ CT to FKBP38-BD was a bit lower (only 1:0.82 compared to 1:0 in the absence of CaCl₂) and that the presence of CaCl₂ may rather weaken the interaction with the β -sheet region, can explain this difference. Since in three independent binding studies (Figure 4.8, Figures 4.10 & 4.11) between Rheb-GppNHp and FKBP38-BD, residues K97 to G101 of the helix next to switch 2 and of the nearby W141 (Figure 4.9, Figure 4.10A) were consistently showing well visible chemical shift changes, this region of Rheb appears the major interaction side for the GTP-dependent interaction with FKBP38-BD.

4.4 ANALYSIS OF RELAXATION DATA OF ¹⁵N- RHEB Δ CT-GPPNHp IN PRESENCE OF FKBP38

This weak or transient interaction of Rheb Δ CT-GppNHp in presence of FKBP3-BD is in line with the respective ¹⁵N- relaxation data. Infact the presence of FKBP38-BD lowered the average ¹⁵N-T₂ values of ¹⁵N-Rheb Δ CT-GppNHp only slightly from 87 \pm 17 ms to 81 \pm 24 ms and also modulated the average ¹⁵N- T₁ and {¹H}-¹⁵N-NOE only weakly from 716 \pm 41 ms, and 0.79 \pm 0.12, respectively, in the absence to 704 \pm 52 ms and 0.79 \pm 0.11, respectively, in the presence of FKBP38-BD (Figure 4.12, Tables 4 in appendix).

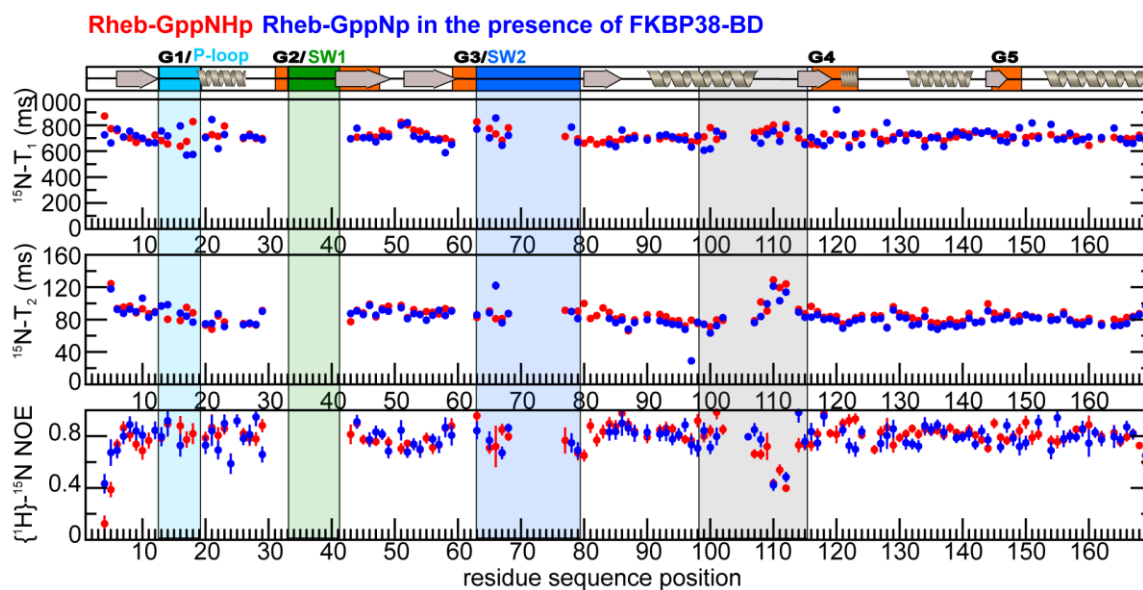


Figure 4.12: Comparison of the backbone dynamics of Rheb Δ CT in the GppNHp-bound state in the absence (red) and presence (blue) of unlabeled FKBP38-BD. Shown are plots of the ^{15}N relaxation data including $^{15}\text{N-T}_1$ (top panel), $^{-T}_2$ (second panel), and $\{^1\text{H}\}\text{-}^{15}\text{N}$ NOE (third panel) values. The location of the G-boxes and the switch 1 and 2 (SW1 & 2) regions is indicated at the top. Filled grey arrows represent β -sheet conformation and grey spirals helical conformation. The secondary structure content was derived from the solution structure of rat Rheb-GDP (PDB-ID 2L0X) [77]. That of mouse Rheb-GppNHp is almost identical (PDB- ID 4O25) [137]. Adapted from [70]

K97 that shows consistently rather strong chemical shift changes in ^{15}N -Rheb Δ CT-GppNHp in the presence of FKBP38-BD (Figure 4.8C, Figures 4.10, 4.11) shows also a very strong decrease in its $^{15}\text{N-T}_2$ time from 79 to 30 ms (Table 2,4 in appendix).

4.5 ROLE OF FKBP38-BD IN THE RHEB –GDP/GTP CYCLE.

GEFs (Figure 1.5) typically form ternary complexes with the GDP-bound state in which the GEF is bound loosely and shows the highest affinity for the nucleotide-free state. The affinity for the GTP-bound state is in principle similarly low to that for the GDP-bound one [78, 138]. Because the interaction between Rheb Δ CT-GppNHp and FKBP38-BD is only weak and may be even weaker and thus not detectable for Rheb-GDP, a real-time NMR study was performed (Figure 4.13-4.16 and table 1 in Chapter 3) to evaluate if FKBP38 may stimulate the exchange of GDP bound to Rheb Δ CT for GppNHp.

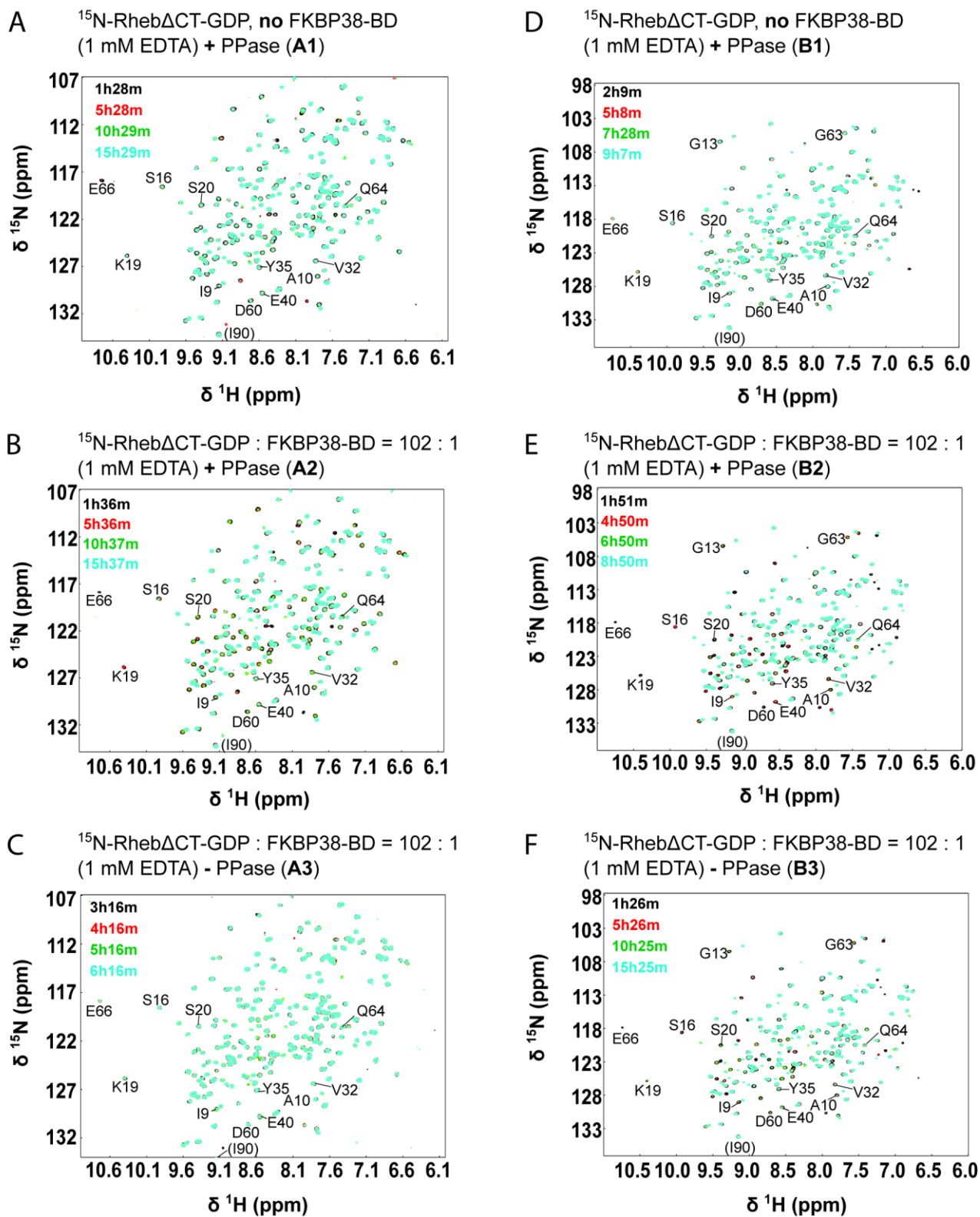


Figure 4.13: NMR data regarding the effect of FKBP38-BD on the GDP to GppNHp exchange of Rheb Δ CT. (**A-F**) Superpositions of the ^1H - ^{15}N HSQC spectra of ^{15}N -Rheb Δ CT-GDP in the presence of GppNHp and if indicated at the top of unlabeled FKBP38-BD at a molar rate of 1:102 and/or catalytic amounts of Antarctic phosphatase (= PPase) after

different incubation times. The color coding is indicated in upper left of each plot. The ^1H - ^{15}N crosspeaks of the residues of Rheb Δ CT-GDP showing strong chemical shift changes to the GppNHp-bound state and that have been considered for the rate analysis are labeled with the one letter amino acid code and the sequence position. The corresponding analysis for the shown series **A** and **B** (**A1/B1** - only FKBP38-BD present, **A2/B2** - FKBP38-BD and PPase present, **A3/B3** only PPase present) are displayed as a function of the residue sequence position in Figure 4.15 (**C**) and (**D**), respectively. Adapted from [70]

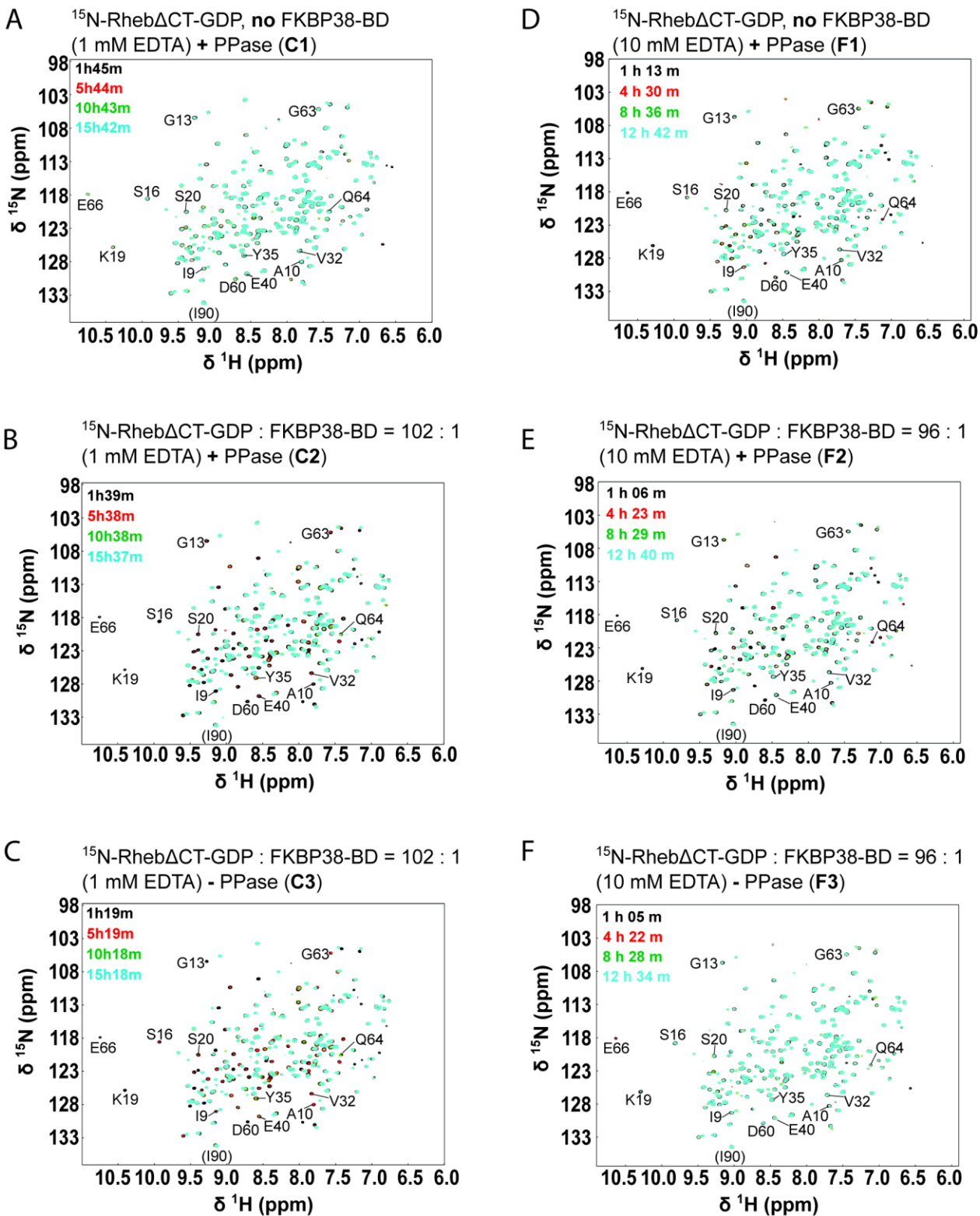


Figure 4.14: More NMR data regarding the effect of FKBP38-BD on the GDP to GppNHp exchange of Rheb Δ CT. (A-F) Superpositions of the ^1H - ^{15}N HSQC spectra of ^{15}N -Rheb Δ CT-GDP in the presence of GppNHp and if indicated at the top of unlabeled FKBP38-BD at a molar rate of 1:102 (series C) or 1:96 (series F) and or catalytic amounts of

Antarctic phosphatase (= PPase) after different incubation times. The color coding is indicated in the upper left of each plot. The ^1H - ^{15}N crosspeaks of the residues of Rheb Δ CT-GDP showing strong chemical shift changes to the GppNHp-bound state and that have been considered for the rate analysis are labeled with the one letter amino acid code and the residue number. The corresponding analysis for the shown series C and F (C1/F1, only FKBP38-BD present, C2/F2 - FKBP38-BD and PPase present, C/F3 only PPase present) are displayed as a function of the residue sequence position in Figure 4.15 E and F, respectively. Adapted from [70]

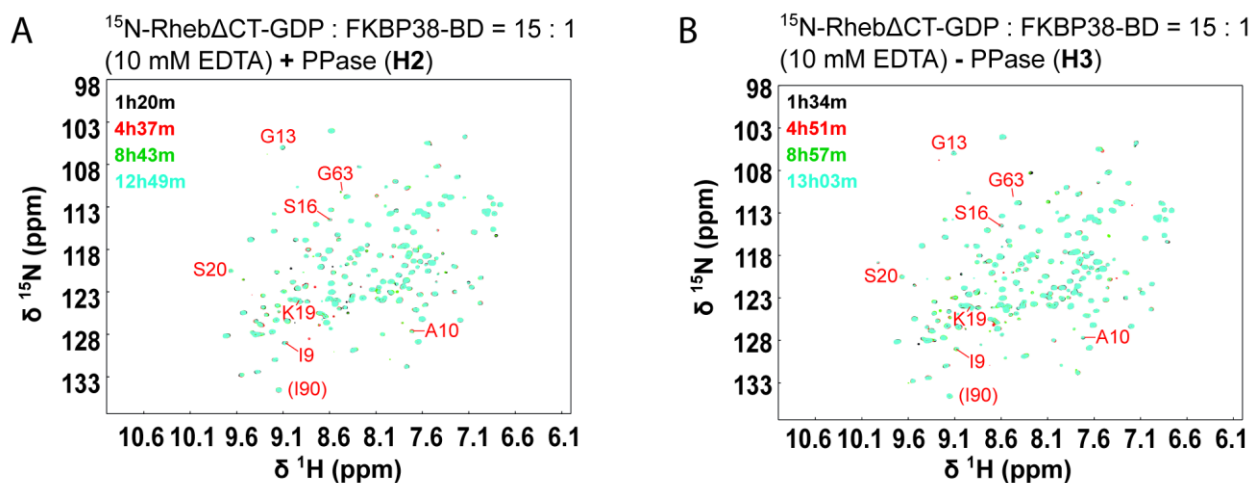


Figure 4.15: Superposition of the ^1H - ^{15}N HSQC spectra of ^{15}N -Rheb Δ CT-GDP in the presence of GppNHp and unlabeled FKBP38-BD at a molar ratio of 1:15 (series H) and either catalytic amounts of Antarctic phosphatase (= PPase) (**A**) or no Antarctic phosphatase (**B**) after different incubation times. The color coding is indicated in upper left of each plot. If FKBP38-BD is present at such large amounts the exchange is so fast that the peaks of the starting GDP state are mostly not visible anymore. Thus the peaks of the target GppNHp and not of the starting GDP state have been labeled with the one letter amino acid code and the residue number. Adapted from [70]

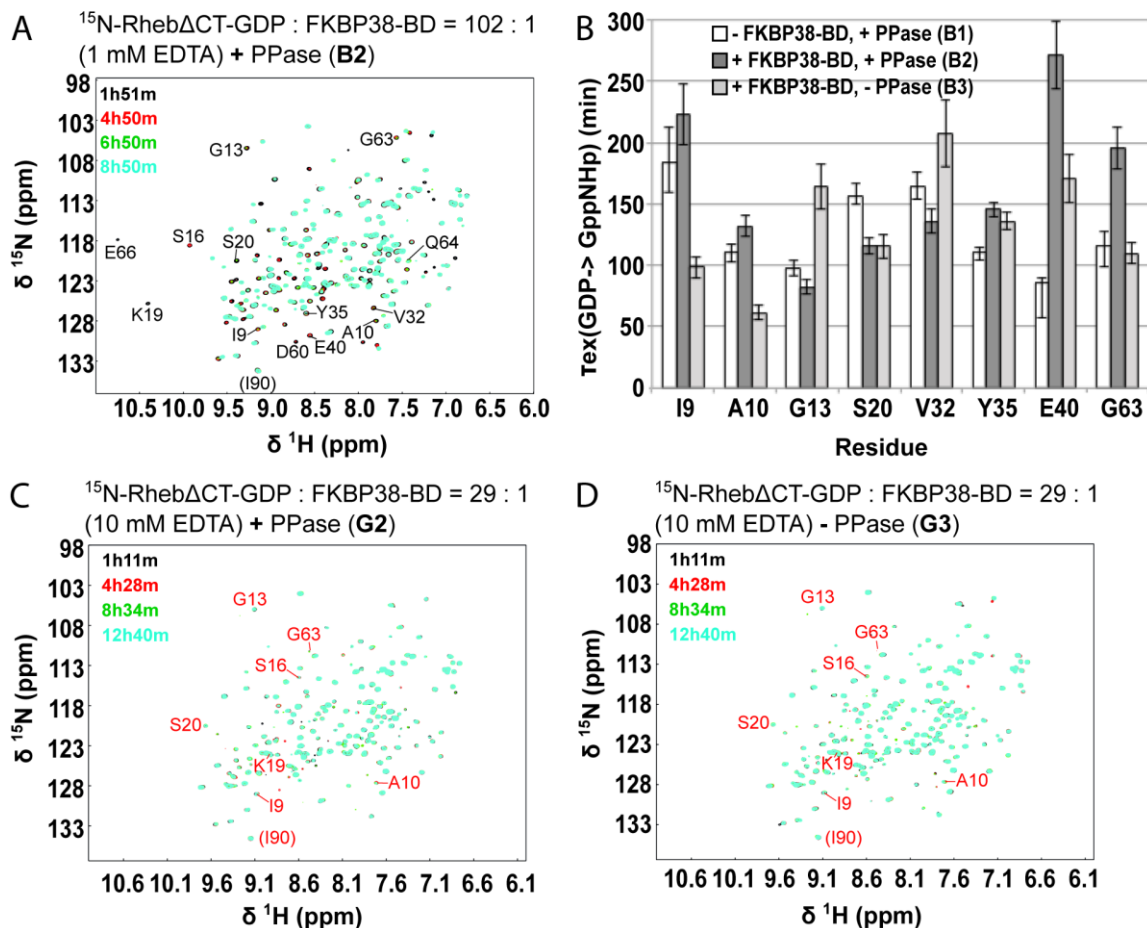


Figure 4.16: The presence of the FKBP38-BD stimulates the GDP to GppNHp exchange of Rheb Δ CT only weakly if present at low concentrations but significantly if present at higher concentrations. (A) Superposition of the ^1H - ^{15}N HSQC spectra of ^{15}N -Rheb Δ CT-GDP in the presence of GppNHp and unlabeled FKBP38-BD at a molar rate of 1:102 as well as catalytic amounts of Antarctic phosphatase (= PPase) after different incubation times. The color coding is indicated in the upper left of the plot. The ^1H - ^{15}N crosspeaks of the residues of Rheb Δ CT-GDP showing strong chemical shift changes to the GppNHp bound state and that have been considered for the rate analysis are labeled with the one letter amino acid code and the residue number. The corresponding analysis for this subseries (B2 - FKBP38-BD and PPase present) together with that for the two other subseries of this series (B1 – only PPase, and B3 – only FKBP38-BD present) are displayed as a function of the residue in (B). Please, see also table 1, which lists the conditions used for each series together with the average values of the exchange times. (C-D) Superposition of the ^1H - ^{15}N HSQC spectra of ^{15}N -Rheb Δ CT-GDP in the presence of GppNHp and unlabeled FKBP38-BD at a molar rate of 1:29 and either catalytic amounts of PPase (C) or no PPase (D) after different incubation times (see upper left of the plot). If FKBP38-BD is present at larger amounts the exchange is so fast that the peaks of the starting GDP state are mostly not visible anymore. Thus the peaks of the target GppNHp and not of the starting GDP state have been labeled with the one letter amino acid code and the residue number. Adapted from [70]

Figures 4.13, 4.14, 4.15 show superpositions of the ^1H - ^{15}N HSQC spectra of ^{15}N -Rheb Δ CT at different time points after adding GppNHp in the absence and presence of unlabeled FKBP38-BD at different molar ratios and/or Antarctic phosphatase (= PPase) and with 1 or 10 mM EDTA in the buffer. If FKBP38-BD would be a GEF (guanine nucleotide exchange factor), the rates for the exchange from GDP to GppNHp should be significantly increased in the presence of only catalytic amounts. For ratios of ^{15}N -Rheb Δ CT to FKBP38-BD of 1:102 (series A3-C3, Figure 4.13, 4.14A-C) or 1:96 (series F3, Figure 4.14D-F), the fitted exchange times τ_{ex} (Table 1 in Chapter 3, Figure 4.16B) were overall similar or sometimes slightly higher than that in the presence of only Antarctic phosphatase (series A1-C1 and F1, Figure 4.13A, D and 4.14A) or the additional presence of it (series A2-C2 and F2, Figure 4.13B, E and 4.14B). At molar ratios of 1:29 (series G2-G3, Figure 4.16 C-D) or 1:15 (series H2-H3, Figure 4.15A-B) of ^{15}N -Rheb Δ CT to FKBP38-BD, the exchange of GDP to GppNHp was significantly faster and the spectrum of the first time point looked already almost like that of the final fully GppNHp-bound state of Rheb Δ CT. Because GEFs usually have the highest affinity for the nucleotide-free state [78, 138], we further prepared a mutant of Rheb Δ CT (D60K) that cannot interact with nucleotides by site-directed mutagenesis [88]. Presumably due to the high expression rates in *E. coli* all the protein was present in inclusion bodies and we did not succeed refolding it and thus were not able to test its interaction with FKBP38-BD (data not shown).

4.6 ANALYSIS OF THE INTERACTIONS BETWEEN THE FKBP38-BD-Y1FATC CHIMERIC PROTEIN AND MEMBRANE MIMETICS.

The ability of the fusion protein His-tagged FKBP38-BD-y1fatc, to interact with membranes was probed by recording ^1H - ^{15}N -HSQC spectra in the presence and absence of different membrane-mimetics (structure shown in Figure 4.17 right side on the bottom).

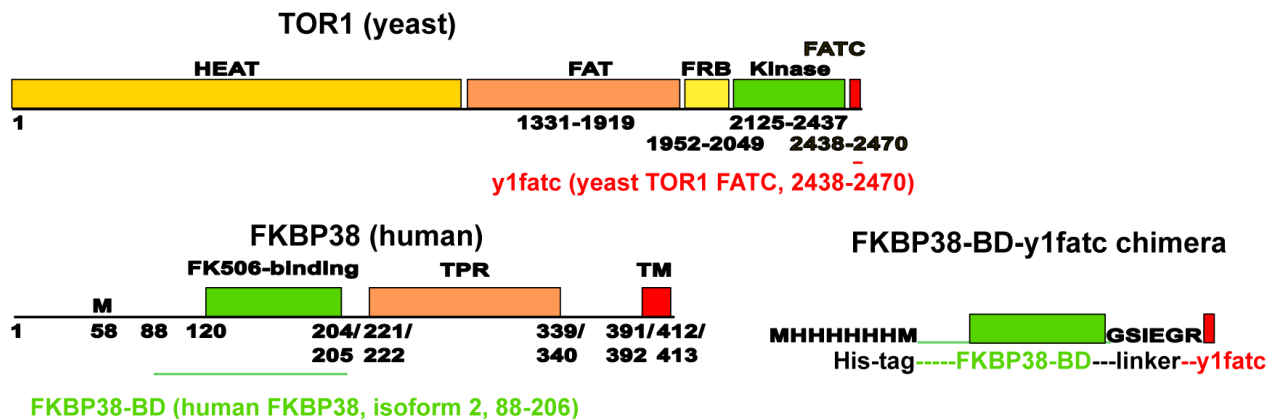


Figure 4.17: Domain organization of yeast TOR1 and human FKBP38 and built-up of the used FKBP38-BD-y1fatc fusion protein that contains an N-terminal His tag and factor Xa cleavage site (IEGR). The residue numbering corresponds to that in full-length yeast TOR1 (Uniprot-ID P35169) and human FKBP38 (Uniprot-ID Q14318). Adapted from [139]

To evaluate if y1fatc can be used as membrane anchoring unit for the interaction of the fusion protein FKBP38(BD)-y1fatc in presence and absence of DPC micelles, DMPC/DihpPC bicelles and DMPC as small uni- and multilamellar vesicles (schematic representation in Figure 4.18) have been analysed.

The domain organization of FKBP38-BD-y1fatc the chimera and how it differs from the natural proteins FKBP38 and TOR is shown in Figure 4.19A with the superposition of the ^1H - ^{15}N HSQC spectra of the newly prepared His-tagged FKBP38-BD-y1fatc fusion protein and of FKBP38-BD and y1fatc. The spectra of the latter two are additive overall to result in that of the fusion protein. Additionally visible peaks arise from the His-tag (MH6M, Figure 4.17) and the linker between the FKBP38-BD and y1fatc (GSIEGR) as well as from different chemical environments of the C- and N-terminal residues in the isolated fragments compared to the equivalent residues in the fusion protein (FKBP38-BD D206 and y1fatc N2438, the residue numbering corresponds to that in the respective full-length proteins).

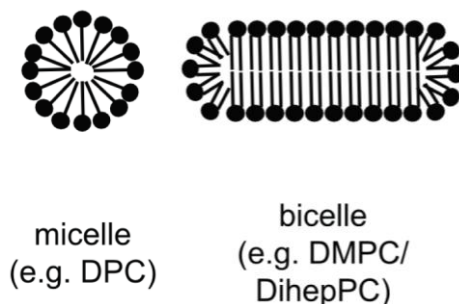


Figure 4.18: Schematic representations of membrane mimetics typically used for interaction and structural studies, including micelles and bicelles. DPC—dodecylphosphocholine, DihepPC/DMPC—diheptanoyl/dimyristoyl phosphocholine.

Figure 4.19B shows the titration with DPC micelles. No significant spectral changes could be observed up to 0.5 mM DPC. However, at a DPC concentration of 2 mM, which is above the CMC of 1.1 mM, the intensity of several γ fatc peaks was observed to decrease and in some cases disappear, e.g. the easily identifiable backbone and side chain indole N ϵ 1-H ϵ 1 crosspeaks of W2470 and W2466 and the backbone amide cross peaks of E2457, R2458, Q2461, Y2463 and F2469.[106] Overall the behavior of the γ fatc fraction in the presence of DPC is very similar to that of the isolated [110, 140] or GB1-tagged [112, 113] γ fatc protein. The peaks of the micelle immersed states of γ fatc become only visible at higher DPC concentrations (circa < 100 mM) and for the oxidized state additionally measuring at higher temperatures (45 °C).[110] DPC micelles are rather small spherical particles with high curvature (Figure 4.18, left representation) that do not contain a bilayer structure [130, 141]. Because of this the interaction of the FKBP38-BD- γ fatc chimera with bicelles in which the planar lipid bilayer core is formed by neutral DMPC and the rim by also neutral DihepPC (Figure 4.18, central picture) and with liposomes of the small unilamellar vesicle (SUV) type composed of neutral DMPC (Figure 4.18, right side), which even better resemble natural membranes has also been analyzed.[142] The superposition of the ^1H - ^{15}N HSQC in the presence and absence of bicelles (Figure 4.19C) and SUVs (Figure 4.19D) indicates again significant spectral changes for the γ fatc part and thus its interaction with DihepPC/DMPC bicelles and DMPC SUVs. Coherently with previously published data, [110, 112, 113] the association with the large bicelles and the even larger SUVs broadens many or almost all, respectively, of the γ fatc NMR signals beyond detection.

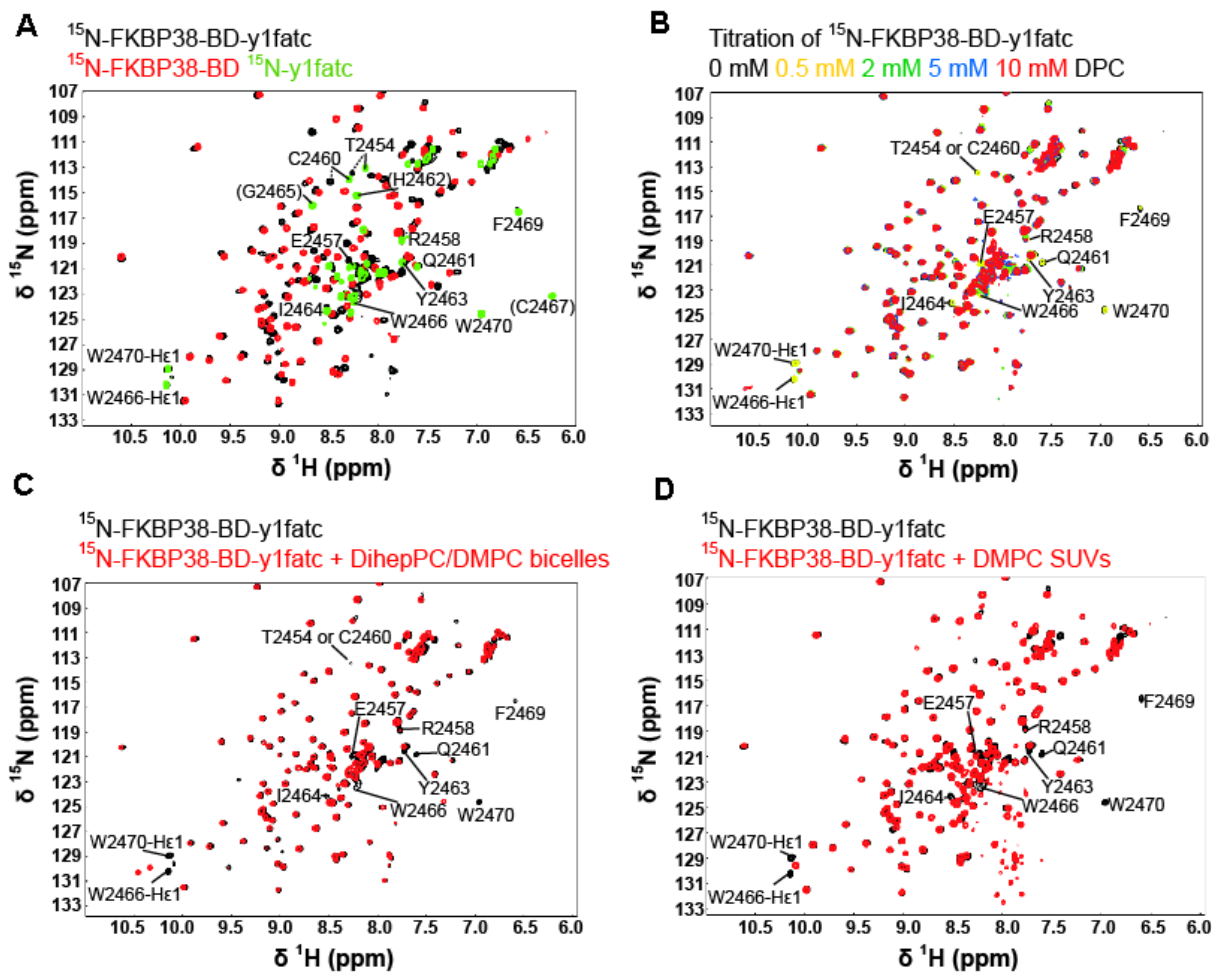


Figure 4.19: (A) Superposition of the ^1H - ^{15}N HSQC spectra of FKBP38-BD-y1fatc in black, FKBP38-BD in red, and y1fatc in green. The y1fatc part is present in the oxidized state with a disulfide bond between C2460 and C2467. Assignments for easily identifiable peaks of y1fatc are labeled by the one letter amino acid code and the residue sequence position in full-length yeast TOR1.[106] The indicated assignments for well-resolved peaks for free y1fatc were adapted from the published values (BMRB accession code 6228).[106] The labels for backbone amide crosspeaks only visible in y1fatc at pH 6.5 but not in FKBP38-BD-y1fatc at pH 7.8 are shown in brackets. (B)–(D) Superposition of the ^1H - ^{15}N HSQC spectra of FKBP38-BD-y1fatc in the absence and presence of increasing DPC concentrations or DihepPC/DMPC bicelles ($q = 0.2$, $cL = 15\%$, ~ 43 mM DMPC and ~ 215 mM DihepPC), or SUVs (< 50 mM DMPC). ^1H - ^{15}N crosspeaks of the y1fatc part that can be easily assigned based on the superposition of the FKBP38-BD-y1fatc fusion and y1fatc shown and labeled in Figure 4.17. Adapted from [139]

Interestingly, the FKBP38-BD part showed also spectral changes in the presence of higher concentrations of DPC. In the titration of FKBP38-BD-y1fatc with DPC (Figure 4.20A) basically all peaks of the FKBP38-part showed a reduction of their peak intensity at 40 mM. Because of this

the effect of the presence of membrane mimetic DPC micelles, DihepPC/DMPC bicelles and DMPC SUVs on the isolated FKBP-BD (Figure 4.20B-D) has been further analyzed. In the presence of 40 mM DPC many peaks almost or completely disappeared. Thus the spectral changes are stronger than observed for the FKBP38-BD-y1fatc fusion protein (Figure 4.20A). Since FKBP38-BD alone does not show significant spectral changes in the presence of neutral bicelles and SUVs (Figure 4.20C-D), it appears not to interact with these membrane mimetics.

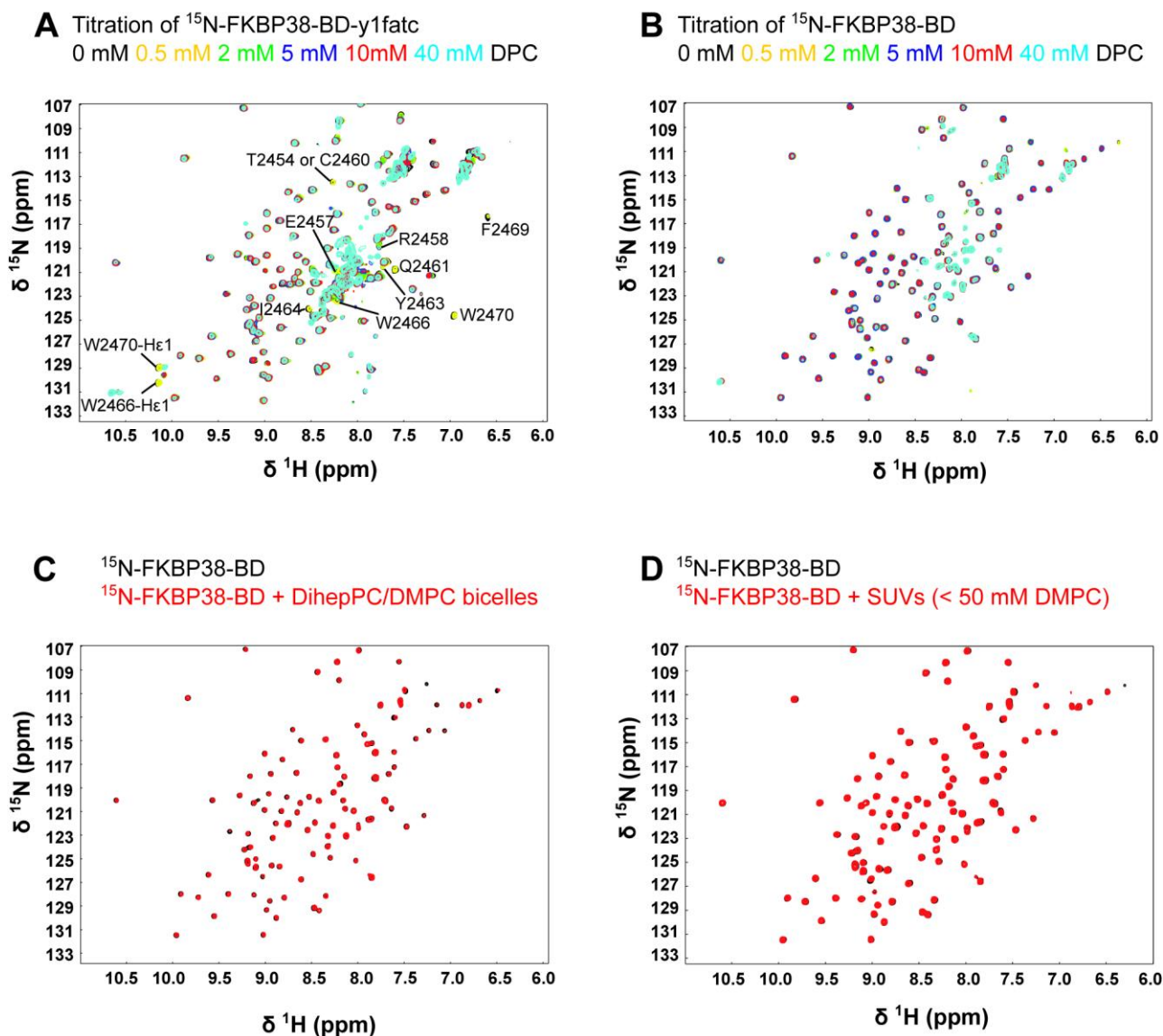


Figure 4.20: (A-B) Superposition of the ^1H - ^{15}N -HSQC spectra of ^{15}N -FKBP38-BD-y1fatc (A) and ^{15}N FKBP38-BD (B) in the presence of increasing concentrations of DPC. The color coding and the molar concentrations of used DPC are indicated at the top of each plot. In (A) Assignments for easily identifiable peaks of y1fatc are labeled by the one letter amino acid code and the residue sequence position in full-length yeast TOR1 [106]. The indicated assignments for

well-resolved peaks for the free y1fatc were adapted from the published values (BMRB accession code 6228 [106]). (C-D) Superposition of the ^1H - ^{15}N -HSQC spectra of ^{15}N -FKBP38-BD in the absence (black) and presence (red) of DihepPC/DMPC bicelles ($q = 0.2$, $c_L = 15\%$, ~ 43 mM DMPC and ~ 215 mM DihepPC) and SUVs (< 50 mM DMPC), respectively. Adapted from [139]

The FKBP-BD-y1fatc chimera shall be used for other interaction studies with another membrane associating protein at pH 7.8 and all the data shown in Figure 4.19-4.20 was recorded at this pH. However, the published membrane mimetic interaction studies of y1fatc had been done at pH 6.5. Thus we additionally recorded data at this pH (Figure 4.21).

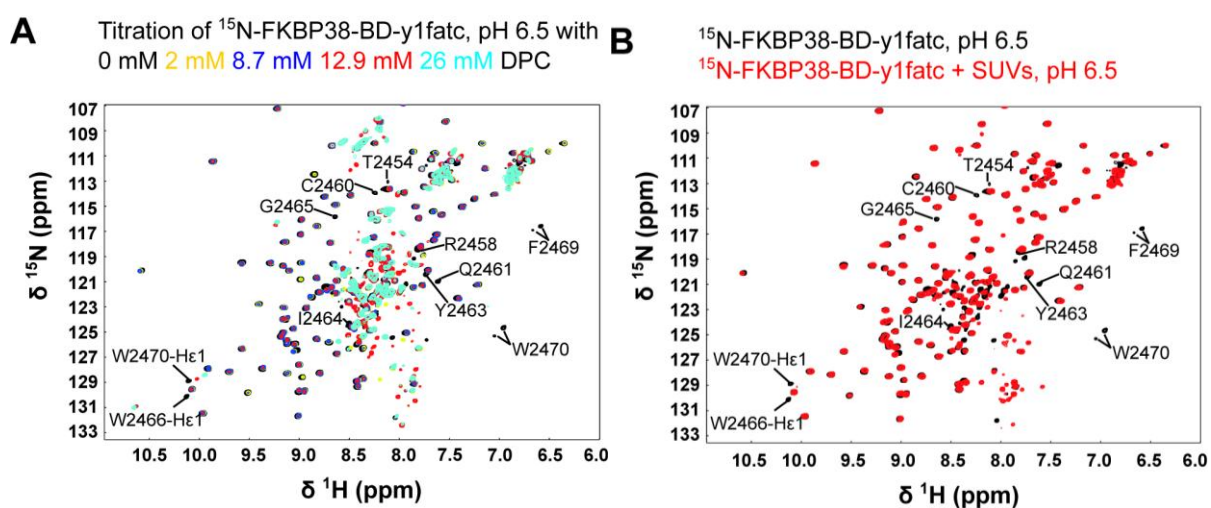


Figure 4.21: Interaction data for FKBP38-BD-y1fatc with membrane mimetics at pH 6.5. These data were recorded because previous interaction studies of y1fatc with different membrane mimetics had been done at this pH [110, 112, 113, 140]. (A-B) Superposition of the ^1H - ^{15}N HSQC spectra of FKBP38-BD-y1fatc in the absence and presence of increasing concentrations of DPC or SUVs (< 50 mM DMPC), respectively. The sample buffer was the same as the one of the samples used to record the spectra shown in Figures 4.19-4.20, except that the pH was 6.5 instead of 7.8 and that it contained no MgCl_2 . The color coding is indicated at the top of each plot. Assignments for easily identifiable peaks of y1fatc are labeled by the one letter amino acid code and the residue sequence position in full-length yeast TOR1 [106]. The indicated assignments for well-resolved peaks for the free y1fatc were adapted from the published values (BMRB accession code 6228 [106]). Adapted from [139]

The FKBP38-BD part of the FKBP38-BD-y1fatc chimeric protein shows a stronger reduction of the signal intensity at DPC concentrations in the range of 10 to 40 mM, presumably due to a lower stability at pH 6.5 than at 7.8. However, the y1fatc part shows similar spectral changes in the

presence of DPC micelles and DMPC SUVs at pH 6.5 (Figure 4.21) and pH 7.8 (Figure 4.19 and 4.20). The observed spectral changes at pH 6.5 are in line with previously recorded data for y1fatc and GB1 tagged y1fatc at pH 6.5.[110, 112, 113, 140]

Overall the data indicate that the y1fatc part fused to FKBP38-BD interacts with all tested membrane mimetics at both pH conditions and thus may generally be used as membrane anchoring unit for attached proteins in a pH range from circa 6 to 8.5.

4.7 MEMBRANE INTERACTION STUDIES WITH 11 TO 17 RESIDUE LONG Y1FATC PEPTIDES.

Based on molecular dynamics simulations and experiments with spin labeled micelles, the C-terminal half of the FATC domain is crucial for the interaction with micelles. Thus fragments corresponding only to the C-terminal 10 to 20 residues may suffice to mediate membrane mimetic interactions. To test this, three different peptides called y1fatc-pep1 to 3 have been synthesized (Figure 4.22A).

A

y1fatc (2438-2470)	NELDVPEQVDKLIQQATSIERLCQHYIGWCPFW
y1fatc-pep1 (2460-2470)	CQHYIGWCPFW
y1fatc-pep2 (2457-2470)	ERLCQHYIGWCPFW
y1fatc-pep3 (2454-2470)	TSIERLCQHYIGWCPFW
y1fatc-pep3mutant (2454-2470, Y2463E/W2466E)	TSIERLCQHEIG E CFW

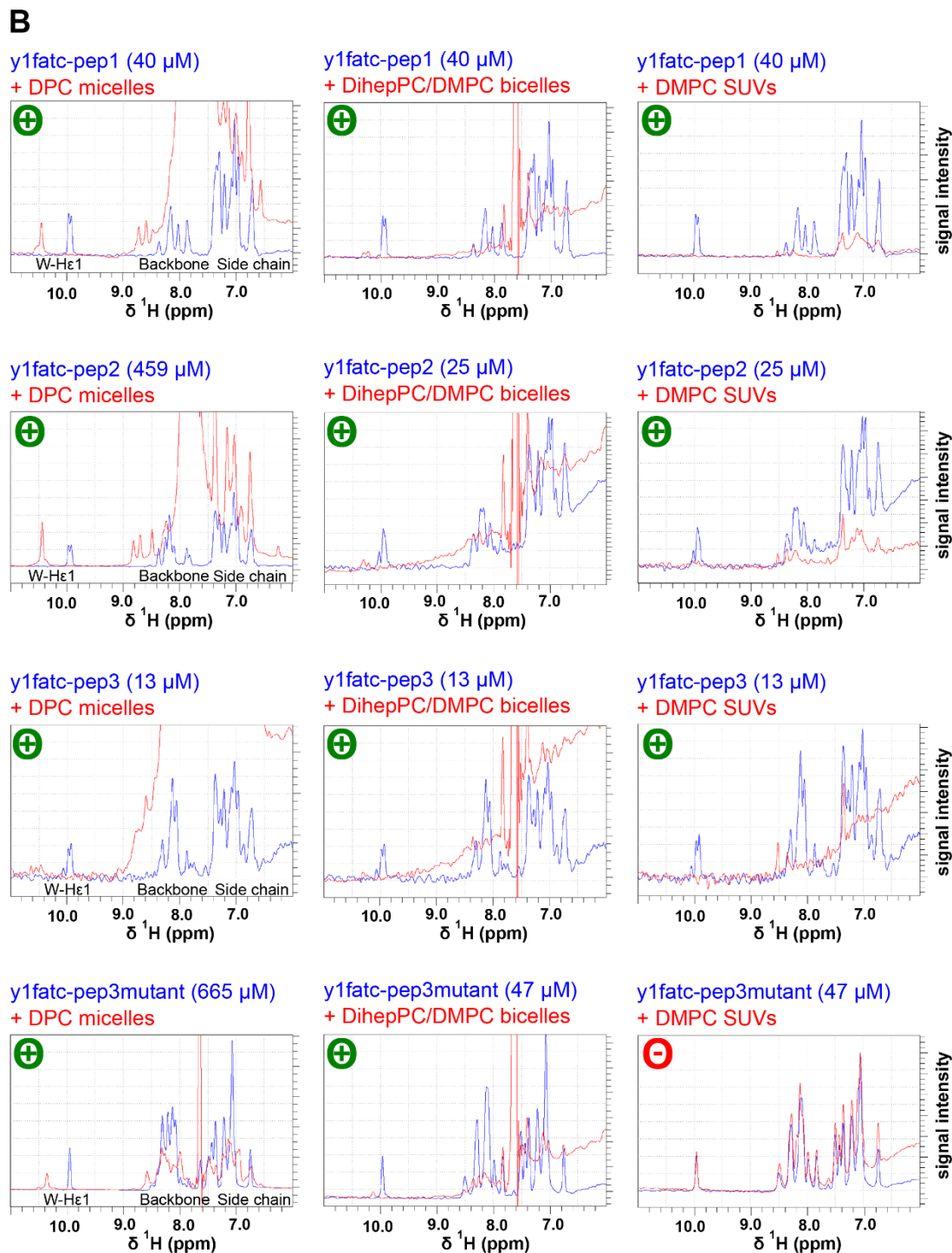


Figure 4.22: Peptides corresponding to the C-terminal 17 to 11 residues of the 33 residue long $y1fatc$ membrane anchor can still interact with membrane mimetics. **A)** Amino acid sequence of $y1fatc$ and of the chemically synthesized peptides $y1fatc\text{-}pep1$ (11 residues), $y1fatc\text{-}pep2$ (14 residues), $y1fatc\text{-}pep3$ (17 residues). Since $y1fatc$ harboring the mutations Y2463E and W2466E does not anymore interact with SUVs, it has been further prepared a variant of $y1fatc\text{-}pep3$ containing the same mutations called $y1fatc\text{-}pep3\text{mutant}$. **B)** Monitoring of the interaction of the unlabeled $y1fatc$ peptides with membrane mimetics by 1D ^1H NMR spectroscopy. The spectra picture in **B)** show the spectral region

containing the backbone and side chain amide as well as the aromatic proton resonances (6 to 11 ppm). Figure 2 in appendix shows the full spectra including the aliphatic region for the interaction studies with DPC micelles and DMPC SUVs. In the presence of bicelles the aliphatic region is completely dominated by the lipid signals and thus not shown. The spectra of the peptides in buffer are shown in blue and those in the additional presence of micelles (100 mM d₃₈-DPC), DihepPC/DMPC bicelles (q = 0.2, cL = 12 %, ~35 mM DMPC and ~173 mM DihepPC), or SUVs (<42 mM DMPC), respectively, in red. If the spectral changes indicate an interaction with the respective membrane mimetic a circled green plus sign is shown in the upper left. If there are no significant spectral changes and thus interactions, a circled red minus sign is shown instead. The peptide concentrations are indicated at the top of each spectrum. Since y1fatc-pep3mutant showed a higher solubility in aqueous buffer than the other peptides, a second sample with a concentration of 0.665 mM was used to record ¹H-¹⁵N HSQC spectra at natural abundance of the peptide in buffer and in the additional presence of DPC and SUVs (only half peptide concentration due to sample preparation method, Figure 4.23). Adapted from [139]

Y1fatc-pep1 is the shortest and encompasses only the C-terminal 11 residues (2460-2470 in full-length yeast TOR1). Y1fatc-pep2 encompasses the C-terminal 14 (2457-2470) and y1fatc-pep3 the C-terminal 17 (2454-2470) residues. Since wild type y1fatc with the mutations Y2463E and W2466E does not anymore interact with DMPC SUVs,[113] it has been further prepared a mutant version of y1fatc-pep3 containing the same amino acid replacements. The peptides were not ¹⁵N labeled and their ability to interact with micelles composed of deuterated DPC (d₃₈-DPC), DihepPC/DMPC bicelles and DMPC SUVs has been tested based on 1D ¹H NMR experiments (Figure 4.21 – only amide/aromatic region, Figure 2 in appendix – full 1D ¹H ppm range). Usually the peptide concentration ranged between 10 and 50 μM. For y1fatc-pep2 and –pep3mutant it was further possible to prepare a higher concentrated sample (circa 0.46 and 0.67 mM, respectively). Indicated by the overall spectral changes of the region showing the amide and aromatic protons and/or the clearly visible shift or disappearance of the indole ring Hε1 signals (Figure 4.21B), all peptides can interact with all tested membrane mimetics, except y1fatc-pep3mutant that as y1fatc-Y2463E/W2466E does not significantly interact with SUVs. Especially in the low concentrated samples, the amide region shows in the presence of DPC and DihepPC/DMPC bicelles some signal distortions presumably arising from remaining traces of chloroform and imperfect water suppression and baseline correction. Since deuterated DPC results only in small signals in the aliphatic regions, spectral changes due to micelle interactions can also be observed in the chemical shift range from -1 to 5 ppm. In the presence of DMPC SUVs this is only partially possible,

because the protonated DMPC produces signals in the aliphatic range (Figure 2 in appendix, spectra plots on the right side). The signals originating from the lipids of bicelles are so strong that those of the peptides cannot be detected anymore.

The y1fatc-pep3mutant was the peptide with the highest solubility and it was possible to prepare a sample with a concentration of 0.65 mM. For this reason it has been further recorded ^1H - ^{15}N HSQC spectra of the peptide in buffer and in the presence of d_{38} -DPC micelles and DMPC SUVs (Figure 4.23). The natural abundance spectrum of the peptide in buffer looks overall like a typical ^1H - ^{15}N HSQC spectrum of a peptide. The presence of DPC micelles (100 mM d_{38} -DPC) results in large spectral changes that indicate an interaction. The presence of DMPC SUVs results in no significant spectral changes for most strong backbone crosspeaks as well as the $\text{H}\epsilon_1$ - $\text{N}\epsilon_1$ crosspeak at circa 10 ppm on the ^1H axis and the side chain $-\text{NH}_2$ signals of Q2461 at circa 7.6 and 6.8 ppm on ^1H and 112.5 ppm on the ^{15}N axis. The disappearance of some weaker peaks may be explained by the fact that the peptide concentration in the SUV sample was only half (0.325 mM) of that in the reference and the DPC sample because SUVs are added as stock and cannot be added as dried film of lipid or detergent. In line with the 1D ^1H data, the natural abundance ^1H - ^{15}N HSQC data confirms that y1fatc-pep3mutant interacts with DPC micelles but shows no significant interaction with DMPC SUVs.

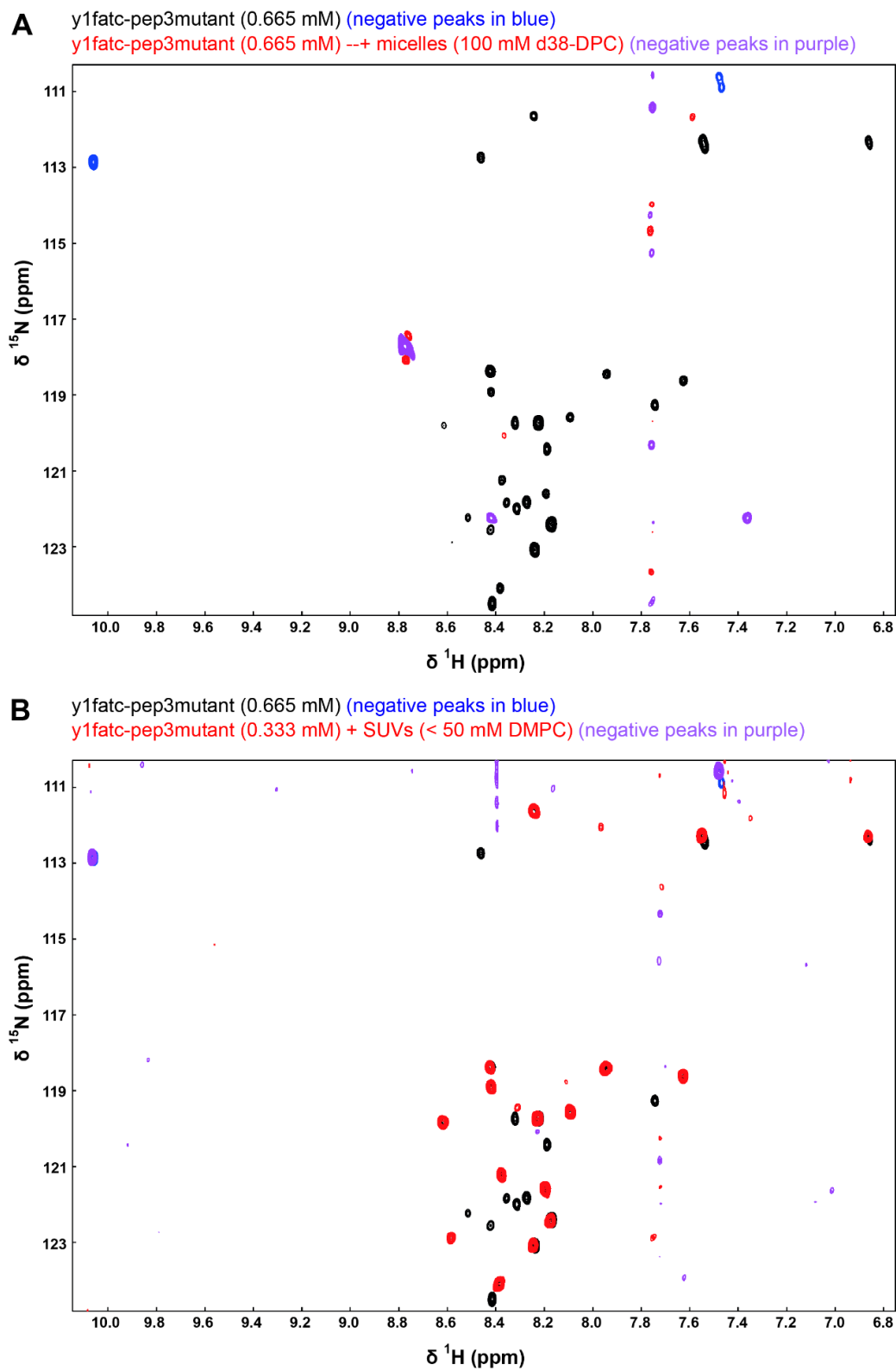


Figure 4.23: Superposition of the natural abundance ^1H - ^{15}N HSQC spectra of the well soluble y1fatc-pep3mutant in the absence (positive peaks in black, negative ones in blue) and presence (positive peaks in red, negative ones in purple) of

100 mM d38-DPC (A) and SUVs (<50 mM DMPC) (B). The color coding and the used concentrations are indicated at the top of each plot. Negative signals represent spectrally folded ones. Thus the true ^{15}N chemical shift is the shown values plus one times the sweep width in ppm. Note that the sample in the presence of SUVs contained only half the concentration of peptide as the reference sample and that in the presence of DPC micelles, because of the difference in the sample preparation method (see Chapter 3-Methods section in main text). To compensate for this partially the contour level was set to half the value used for the other spectra. The presence of DPC results in the disappearance of most peaks due to interactions with the micelles. In contrast, the presence of SUVs results in no significant spectral changes for the stronger backbone signals and the side chain N-H signal of W2470 (≈ 112.8 ppm – corresponding to an unfolded value of $128.8\text{ppm}/10.1$ ppm) and the side chain N-H2 signals of Q2461 (≈ 112.5 ppm/ 7.6 and 6.8 ppm). Thus in line with 1D ^1H data suggesting that y1fatc-pep3mutant does not significantly interact with SUVs. The lower concentration of the SUV sample may explain why some of the weaker peaks are not visible in their presence. Since more peaks are visible than estimated based on the number of residues in the peptide, the weaker ones presumably correspond to an additional populated minor conformation. Adapted from [139]

The solution structure of oxidized y1fatc in buffer (PDB-ID 1W1N) contains an α -helix from residue E2444 to C2460 and that of micelle immersed y1fatc one from residue E2444 to H2462 in the oxidized (PDB-ID 2KIO) and E2444 to Y2463 in the reduced (PDB-ID 2KIT) state.[106, 110] The used y1fatc peptides start within the helical region. To qualitatively estimate the helical content of the y1fatc peptides in the free and the DMPC micelle immersed states, CD spectra in the absence and presence of micelles were recorded (Figure 4.24). Indicated by α -helix typical minima at circa 208 and 222 nm, the longest peptide, y1fatc-pep3, contains a helical stretch in the free state. The shorter peptides y1fatc-pep1 and -2 and y1fatc-pep3mutant show rather a spectrum typical for an unfolded protein. The addition of DPC micelles increases the α -helical content of all peptides. Again it is the lowest for the 11-residues peptide y1fatc-pep1. These data confirm the NMR monitored interaction with micelles and indicate that the α -helical secondary content of the micelle immersed states correlates as expected based on the structural data for y1fatc[110, 140] with their length.

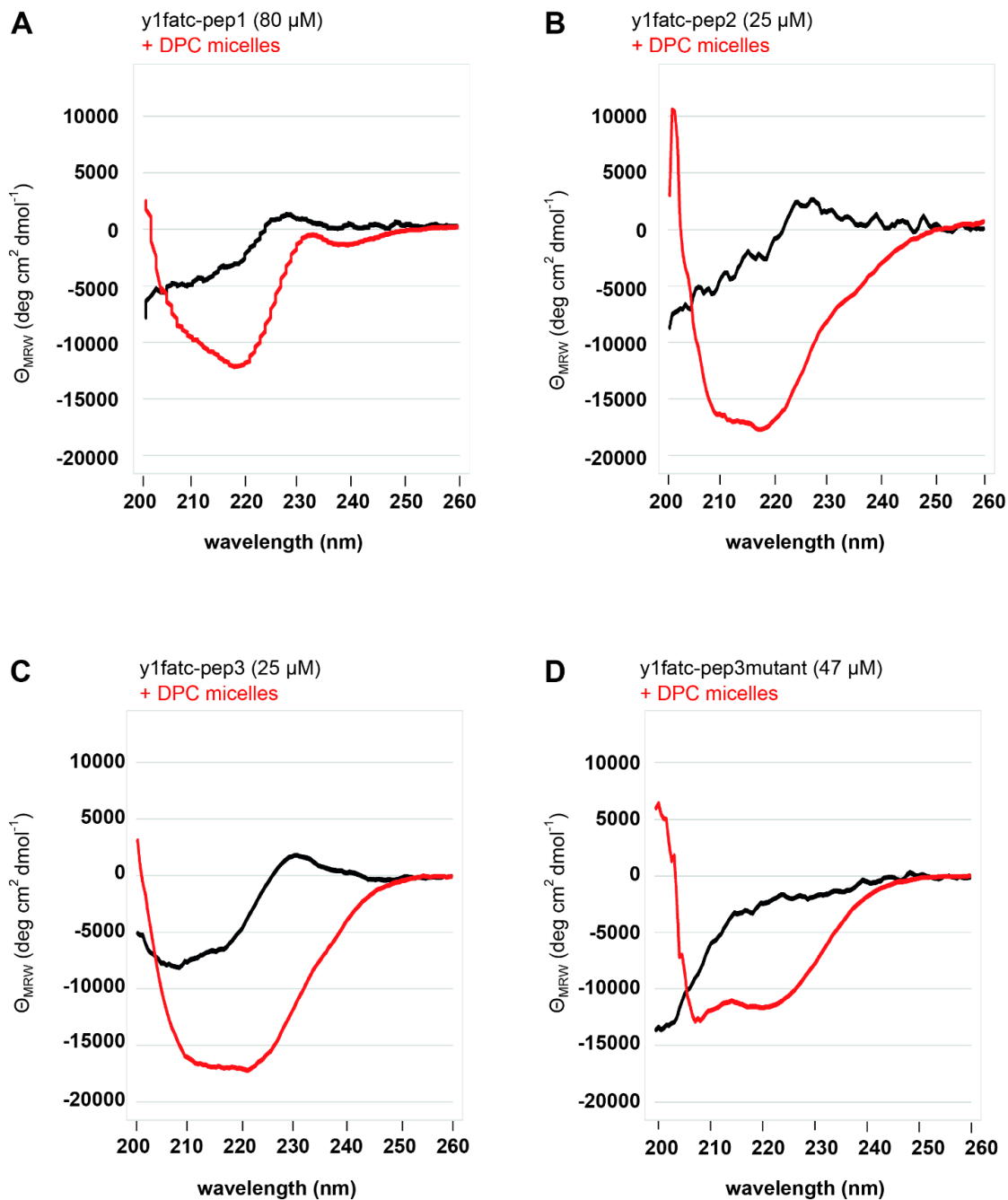


Figure 4.24: Superposition of the CD spectra of y1fatc-pep1, y1fatc-pep2, y1fatc-pep3, y1fatc-pep3mutant in the absence (black) and presence of 100 mM DPC. Adapted from [139]

CHAPTER 5

5.1 SUMMARY AND DISCUSSION

The role of increased backbone dynamics in the two switch regions and around residues 98-115 in the inactive GDP- and the active-like GppNHp-bound state of Rheb for the interaction with regulators and effectors.

The switch 1 region has generally a critical role in the on- and off-switching cycle of GTPases and for the interaction with other proteins [67, 69]. In line with this, the switch 1 region and especially Y35 showed increased backbone dynamics on the ps-ns time scale in Rheb-GDP and the broadening of the peaks for Y35 and the surrounding residues in the GppNHp-bound state indicates also increased backbone dynamics in this state (Figure 4.5). Increased mobility around Y32 of Ras (p21^{ras}), corresponding to Y35 of Rheb (Figure 1 in appendix), was first indicated by ³¹P-NMR and EPR data of wild type and mutant proteins and assigned to an interplay with the terminal phosphate groups (β , γ) of the bound nucleotide [143]. This observation led to the detection of at least two conformational states of GTP- and GTP analogue-bound Ras [143-146]. For the small GTPase Cdc42 it has been shown, that replacement of T35, corresponding to T38 in Rheb (Figure 1 in appendix), to alanine reduces the conformational freedom and thereby the affinity for a regulatory protein inhibiting GTP hydrolysis [147]. With respect to Rheb, it has been suggested that the switch 1 region plays an important role for the interaction with FKBP38 [148]. However based on the interaction data performed (Figures 4.7-4.11) the switch 1 region may only indirectly influence the interaction with FKBP38-BD, which is discussed in more detail below. Whereas the switch 1 region shows higher B-factors in the crystal structures of Rheb-GDP and -GppNHp (55 versus 28.1 and 50 versus 31.1 Å² for the whole protein), the switch 2 region shows only somewhat higher B-factors in the GDP- and GppNHp-bound states compared to the whole protein (38.8 versus 28.1 and 35.0 versus 31.1 Å²) [68]. Since a few residues of the G3 box/switch 2 region (63-75, Figure 4.1) could not be detected in the GDP- (70-73) and a larger number in the GppNHp-bound (69-76) state (Figure 4.2), the switch 2 region shows as the switch 1 region increased backbone dynamics in both nucleotide-binding states (Figure 4.5). However, the type of bound nucleotide modulates the dynamic behavior (Figure 4.4, 4.5, 4.9 Tables 1-6 in appendix). A similar broadening of NMR signals of the switch 1 and 2 regions in the GppNHp- compared to the GDP-bound state has also been observed for Ras [149]. Regarding this and the overall dynamic properties, ¹⁵N-relaxation data analyzed in this work, including besides {¹H}-¹⁵N NOE further T₁ and T₂, are in agreement with

earlier published $\{^1\text{H}\}$ - ^{15}N NOE data for rat Rheb (1-184)-GDP and -GppNHp that differs within 1-170 only at positions 1 and 170 (S1 and I170 compared to M1 and M170 in human Rheb) [77]. The importance of increased backbone dynamics around G63 in the G3 box may explain the finding that replacement of glycine 63 to alanine makes Rheb a more potent mTORC1 activator [137]. In addition, it had already earlier been suggested that the switch 2 region of Rheb is critical for signaling to mTORC1 [87]. Besides G2 box/switch 1 and the G3 box/switch 2 regions, the region around residues 97-115, which is overall spatially close to the G3/switch 2 region (Figure 4.9) shows similarly increased backbone dynamics in all states of Rheb. A functional role of the region around residues 97-115 is in line with the interaction data for ^{15}N -Rheb Δ CT-GppNHp and FKBP38-BD. This suggests that residues 97-101 together with W141 represent the major interaction side (Figures 4.7-4.11C) and has been confirmed by the ^{15}N -relaxation data of Rheb Δ CT-GppNHp in the presence of FKBP38-BD (Figure 4.12). Moreover, showed Rheb-GDP and -GppNHp tethered to protein-lipid nanodiscs increased backbone dynamics for residues in and around the switch regions and around residues 90-115 [150]. The increased dynamics of the switch but also the other mentioned regions are expected to facilitate or even enable the interaction with various regulatory proteins [69]. The Rheb effector FKBP38 accelerates the GDP to GTP exchange by interacting weakly with the active but apparently not the inactive state and may further play a role for membrane targeting.

In line with the suggestion that the interaction between Rheb and FKBP38 is GTP-dependent [45], chemical shifts changes for several residues in regions spatially close to the in part undetectable switch 2 region of ^{15}N -Rheb Δ CT in the GppNHp- (Figure 4.8C, 4.9, 4.10A-B and 4.11) but not the GDP-bound state (Figure 4.7A) have been observed. Since the spectrum of ^{15}N -FKBP38-BD in the presence of Rheb-GppNHp (Figure 4.8D) showed however no significant spectral changes, the interaction appears to be only weak or transient and has only an effect on the structure and dynamics of Rheb Δ CT but not FKBP38-BD. Moreover, the chemical shifts changes of Rheb Δ CT-GppNHp in the presence of FKBP38-BD become only clearly visible once the GDP- to GTP-analogue exchange is complete (Figures 4.7, 4.8, 4.10B, 4.11). These two observations and the only weak spectral changes of Rheb Δ CT-GppNHp in the presence of FKBP38-BD, which nevertheless have been largely reproduced using three different samples (Figures 4.8C, 4.9, 4.10A, B and 4.11C), may also explain why one group could not verify this interaction [47], which however had been observed by other groups albeit Wang *et al.* mentioned that it must not necessarily be direct

[45, 46, 48]. Discrepancies between the different interaction studies may further be accounted for by differences in the used protein preparation and experimental protocols [45, 47, 48] and regarding the fact whether Rheb is present in farnesylated form and thus able to localize to membranes or not (see also below) and if other cellular proteins may stabilize the interaction in the pull-downs. It has been proposed that the switch 1 region of Rheb is critical for the interaction with FKBP38 [46]. The presented interaction data between Rheb Δ CT and FKBP38-BD (Figures 4.7-4.11) including a titration of ^{15}N -FKBP38-BD with a 13mer Rheb switch 1 peptide (Figure 4.10E) indicated no chemical shift changes for the switch 1 region if looking at ^{15}N -Rheb or of ^{15}N -FKBP38 in the presence of Rheb Δ CT or only the respective switch 1 peptide. Thus this may be an indirect effect, which reflects the role of the switch I region for the nucleotide-binding.

There are three main small GTPase-interacting and -regulatory proteins: the GTPase activating proteins (GAPs) that stimulate GTP hydrolysis and thus deactivation, the guanine nucleotide exchange factors (GEFs) that facilitate GDP dissociation and thus activation, and the nucleotide dissociation inhibitors (GDI) that regulate the membrane/cytosol alternation [69, 78, 138]. A GAP for Rheb has been described, namely the TSC complex [83, 89]. Since the function of translationally controlled tumor protein (TCTP) as a Rheb GEF [85] has been questioned [86], proteins acting as GEF or GDI for Rheb have still to be found. Because it has already been shown that FKBP38 acts not as GDI for Rheb [47], another aim of the present study was to evaluate if FKBP38 might have a GEF-like or another effector effect on Rheb. The presented real time NMR rate analysis data indicated that the presence of FKBP38-BD in a range more typical for a catalytically acting protein ($[\text{Rheb}\Delta\text{CT}]:[\text{FKBP38-BD}] = \approx 100:1$) only weakly accelerated the exchange of GDP to GppNHp (Figure 4.16, table 1 in Chapter 3-Methods, 4.13, 4.14, 4.1B). However at molar rates of Rheb-GDP to FKBP38-BD of 29:1 or 15:1, FKBP38-BD strongly accelerated the nucleotide exchange (Figures 4.16C-D, 4.15A-B). For the following reasons FKBP38 is however most likely not a GEF. First of all, usually catalytic amounts of GEFs accelerate the GDP to GTP exchange much faster than observed for FKBP38. In a real-time NMR study analyzing the effect of a Rho GEF, it stimulated the exchange about 200-fold if only present at a molar ratio of 1:8000 with respect to Rho [151]. Secondly, GEFs form initially a low-affinity ternary complex with the GDP-bound GTPase, where the nucleotide is still bound tightly. Following a conformational change, the interaction with the nucleotide is weakened and the ternary complex converts into a high affinity nucleotide free binary complex. Following binding of GTP,

the GEF is released [69, 78, 138]. In principle a GEF could also catalyze the reverse reaction, which in the cell does not happen because of the higher concentration of GTP compared to GDP [138]. However, FKBP38-BD appears to have only a weak affinity for the GTP- but no significant affinity for the GDP-bound form of Rheb (Figures 4.7-4.11). Thus FKBP38-BD shows rather properties typical for a GTPase effector [152] and does not act as a classical GEF but only stimulates the GDP to GppNHp exchange by interacting more favourably with the GppNHp- than with the GDP-bound state thereby driving the equilibrium of the exchange reaction towards this state. This happens the faster the more FKBP38-BD is present relative to Rheb-GDP at constant GppNHp concentrations (table 1 in Chapter 3-Methods). Finally, the known GEFs for Ras family members typically contain a Cdc25-homology catalytic domain [69], which is not the case for FKBP38.

Rheb localizes by a C-terminal farnesyl modification to endomembranes and FKBP38 by a transmembrane domain to the outer mitochondrial membrane [72, 100]. Based on NMR studies of Rheb tethered to protein-lipid nanodiscs, it has been shown that the GTPase domain interacts transiently with the bilayer surface with two distinct preferred orientations, which are determined by the bound nucleotide. Moreover, membrane conjugation markedly reduced the rate of intrinsic nucleotide exchange, while GTP hydrolysis was unchanged [150]. Thus membrane association of Rheb but also of FKBP38 may enhance their interaction and maybe also the newly detected accelerating effect of FKBP38 on the Rheb GDP to GTP exchange. This suggestion would also be in line with the observation that the Rheb mutant C181S that cannot be farnesylated and thus not localize to endomembranes does not interact with FKBP38 [48]. Whether FKBP38 is just an effector regulating membrane targeting or shows a more typical GEF-like activity if both Rheb and FKBP38 are membrane bound and present as full-length proteins may be clarified in future studies by a suitable kinetic analysis. In addition, the interaction between Rheb and FKBP38 may be stabilized by the presence of other proteins, which may also be membrane localized, such as components of the mTORC1 complex including TOR itself at the lysosomal membrane or the enzyme phospholipase D1 [31, 153, 154]. The proposed low-affinity Ca^{2+} -binding site in FKBP38-BD [76] had no significant influence on the interaction with Rheb, however to date it has not been analyzed if binding of calmodulin may affect the interaction of FKBP38 with Rheb similarly as that with the apoptosis regulator protein Bcl-2 [93]. Therefore, the role of membrane tethering, other proteins, as well as phosphorylation at S130 of Rheb [155] on the Rheb-FKBP38 interaction, which

plays not only a role for mTORC1 signaling [31, 153, 154] but also for the regulation of apoptosis [51], should be targeted in more detail within future studies.

The y1fatc part of FKBP38-BD-y1fatc chimeric protein interacts with all tested membrane mimetics and thus can be used as membrane anchoring unit for other proteins.

The 33 residue encompassing FATC domain of yeast TOR1 (y1atc) has been shown to interact with all tested membrane mimetics including micelles composed of neutral DPC and DihepPC, negatively charged diacyl phosphatidic acid and phosphoinositide lipids, neutral bicelles composed of DihepPC and DMPC as well as SUVs composed of neutral DMPC and or a 1:1 mixture of DMPC and negatively charged 1,2-dimyristoyl-sn-glycero-3-phospho-(1'-rac-glycerol) (DMPG).[110, 113, 140]

Further it has been shown that the presence of the B1 domain of streptococcal protein G (GB1, 56 residues) as N-terminal fusion tag does not impair the ability of y1fatc to interact with membrane mimetics.[112] In this work, it has been demonstrated that y1fatc can even mediate membrane mimetic interactions if fused to larger proteins such as the protein FKBP38-BD (119 residues plus His tag, Figure 4.17) and it is thus generally applicable as membrane anchoring unit for other proteins. FKBP38-BD had been chosen as test case because it has a transmembrane domain (TM, circa 20 amino acids, Figure 4.17). The preparation of the isolated TMs as fusion to a suitable purification tag is often possible, because the tag increases the solubility and can be cleaved off and the TM alone can further be un- and refolded or dissolved in organic solvent and reconstituted in a membrane mimetic.[156]

Purification of the respective full-length protein containing besides the TM more than one additional domain is not straightforward, because the refolding of a multidomain compared to that of single domain protein is not trivial and thus purification under native conditions is preferred.[157] The presence of the TM may further require the addition of a detergent or a membrane mimetic to improve the solubility similar as for membrane proteins.[158] Depending on the biochemical or biophysical study to be done, one may further have to replace the detergent or membrane mimetic for a membrane mimetic suitable for the respective method (e.g. use large unilamellar vesicles instead of small ones). The use of y1fatc as membrane anchor has many advantages. First of all, y1fatc is only 33 residues long and also well soluble in aqueous buffers (up

to circa 0.5 mM),[106] which facilitates the expression and purification of the target protein-y1fatc fusion protein. The good solubility of y1fatc in aqueous buffer allows further to use the respective target protein-y1fatc fusion protein for titrations. One may for example titrate a target protein1-y1fatc fusion to an already membrane mimetic attached interaction partner of target protein1, e.g. a protein already attached to micelles, bicelles, any type of liposome or lipid nanodiscs. [150, 159].

The y1fatc membrane anchor is also a good alternative for proteins that are posttranslationally prenylated/lipidated to obtain a farnesyl, or gernanylgeranyl modification such as many GTPases [160]. If prenylation shall already occur in *E. coli* cells, coexpression with the modifying enzyme and a suitable precursor is necessary [161]. Moreover, the purification has to involve an additional step to separate prenylated from unprenylated protein [161]. Proteins may also chemically be modified to obtain a lipid membrane anchor. The small GTPase Rheb had for example been coupled to the thiol-reactive lipid 1,2-dioleoyl-sn-glycero-3-phosphoethanolamine-N-[4-(p-maleimidomethyl)cyclohexane-carboxamide] (PE-MCC) embedded in lipid nanodiscs. Using such a procedure also an additional purification step is needed to separate free from lipid nanodisc attached protein [150]. Another advantage of the y1fatc membrane anchor is that it can easily be introduced by a traditional cloning procedure, e.g. as shown here, or by site directed mutagenesis in several steps. This method of preparation allows further to introduce a protease site (see Figure 4.17), which enables removal of the y1fatc part, e.g. to release the target protein from the membrane mimetic. Moreover, it allows to introduce a linker region between the target protein and the y1fact part. The presented measurements at pH 7.8 and 6.5 with 150 mM NaCl and if fused to FKBP38-BD additionally 5 mM MgCl₂ as well as earlier studies and purifications that had been done using buffer with pH values from 6 to 8 and containing 100 to 150 mM NaCl and if needed other buffer components (e.g. 2 mM CaCl₂, oxidized and reduced glutathione, the reducing agent TCEP, PF1 phages) and temperatures ranging from 298 to 318 K for the micelle immersed oxidized state [106, 110, 112, 113, 140] indicate that y1fatc can be used for a wide range of experimental conditions.

The FKBP38-BD part appeared itself to interact with DPC micelles at DPC concentration of circa 10 mM or higher (Figure 4.19B-4.20A-B) but not significantly with DiphePC/DMPC bicelles and DMPC SUVs (Figure 4.19C-D, 4.20C-D, 4.21B). Since larger DPC concentrations were necessary to result in comparable spectral changes for FKBP38-BD fused to y1fatc (Figure 4.20A) compared to the isolated FKBP38-BD (Figure 4.20B), the presence of the y1fatc membrane anchor seemed to

lower the affinity for DPC micelles, presumably because y1fatc has a higher affinity for them than FKBP38-BD. The low chemical shift dispersion of FKBP38-BD in the presence of high DPC concentrations (> circa 10 mM) may be explained by unfolding of the protein or by a conformational change to a more helical micelle immersed state as it has been observed for Bcl-xL,[162] the FKBP12-rapamycin binding (FRB) domain of TOR, and the N-terminal domain of Formin C.[163, 164] If this conformational transition of the FKBP38-BD shall be suppressed, bicelles, SUVs or presumably also lipid nanodiscs can be used as membrane mimetics. Future studies have to evaluate if the spectral changes of the FKBP38-BD in the presence of DPC micelles reflect a biologically relevant affinity for membrane regions with a high curvature or content of lysolipids that as DPC have only one fatty acid tail [165-167].

Membrane interaction studies with 11 to 17 residue long y1fatc peptides indicate that shorter fragments of the TOR FATC domain are sufficient to mediate the interaction with membrane mimetics.

The interaction studies with shorter fragments of y1fatc demonstrated that the C-terminal 17 to 11 residues (2454 to 2470 in full-length yeast TOR1, Figure 4.22) are enough to mediate the interaction with neutral membrane mimetic DPC micelles, DihepPC/DMPC bicelles, and DMPC SUVs (Figure 4.22B, 4.23 and Figure 2 in appendix). This is consistent with information about the immersion properties of oxidized and reduced y1fatc from NMR studies using DPC micelles containing doxyl labeled stearic acid molecules and corresponding molecular dynamics studies. These data indicated that the C-terminal circa 20 residues or even only the C-terminal circa 10 residues that form a looped bulb like structure may be enough to mediate membrane association. This can be explained by the presence of many aromatic (H2462, Y2463, W2466, F2469, W2470) residues (Figure 4.22A) that can mediate interactions with the hydrophobic interior as well as the interface between the polar aqueous environment and the more apolar interior of the membrane, some hydrophobic aliphatic residues (L2459, I2464), and a rim of charged residues (E257, R2458) as well as the charged C-terminus that can mediate interactions with the polar lipid headgroups [168, 169]. Thus if no longer linker region between the target protein that shall be localized at membranes and the y1fatc membrane anchor is needed or if attaching the full y1fatc sequence is not possible or disturbing, one may just attach the C-terminal 11 to 17 residues by site-directed

mutagenesis in circa 3 steps. Alternatively, one can chemically synthesize the corresponding y1fatc peptide similar as demonstrated here (Figure 4.22A) and attach them to the target protein by native ligation [170]. The latter approach would further offer the possibility to differently label the y1fatc part and the target protein, e.g. to attach unlabeled or fluorescently labeled y1fatc peptide to ^{15}N -labeled target protein [171].

The y1fatc membrane anchoring region contains two conserved cysteines (C2460 and C2467) [106]. In isolated y1fatc and fused to a GB1 tag, the two cysteines form a disulfide bond during the purification due to oxygen in the surrounding air [106, 112]. This is also true for most y1fatc mutants [113]. Formation of a C-terminal loop in the free oxidized and the micelle immersed oxidized and reduced states is facilitated by the presence of a glycine (G2465) [106, 110, 140]. Indicated by the peak pattern in the ^1H - ^{15}N HSQC spectra shown in Figure 4.19A, y1fatc forms also a disulfide bond if fused to FKBP38-BD. However, if the stability of the target protein affords the presence of reducing agents in the buffer, this is not a problem because reduced y1fatc interacts also with membrane mimetics. Based on NMR diffusion data, reduced y1fatc has a slightly lower affinity for DPC micelles than the oxidized state [110]. If the presence of reduced or disulfide bonds disturbs, one may replace them for alanine or serine by site-directed mutagenesis. Interaction studies with 15 different y1fatc mutants showed that replacement of 6 to 7 aromatic or aliphatic residues in the membrane anchoring region to alanine or even polar and charged residues was not enough to suppress the interaction with membrane mimetic DPC micelles and DihepPC/DMPC bicelles. However, replacement of only aromatic residues (Y243) was already enough to suppress the interaction with DMPC SUVs [113]. Since the affinity of membrane anchoring protein regions is mostly determined by hydrophobic aromatic and aliphatic residues [168, 169], the replacement of the cysteines is not expected to significantly alter the affinity of the y1fatc membrane anchor. Alternatively, one may consider to chemically modify the cysteines [172] or use the FATC domain of another phosphatidylinositol 3-kinase-related kinase (PIKK) called ataxia telangiectasia mutated (ATM) that has also been shown to interact with DPC micelles, DihepPC/DMPC bicelles and DMPC SUVs [114].

REFERENCES

1. Karnoub, A.E. and R.A. Weinberg, *Ras oncogenes: split personalities*. Nat Rev Mol Cell Biol, 2008. **9**(7): p. 517-31.
2. Cox, A.D. and C.J. Der, *Ras family signaling: therapeutic targeting*. Cancer Biol Ther, 2002. **1**(6): p. 599-606.
3. Winter-Vann, A.M. and P.J. Casey, *Post-prenylation-processing enzymes as new targets in oncogenesis*. Nat Rev Cancer, 2005. **5**(5): p. 405-12.
4. Sebt, S.M. and C.J. Der, *Opinion: Searching for the elusive targets of farnesyltransferase inhibitors*. Nat Rev Cancer, 2003. **3**(12): p. 945-51.
5. Jones, S., et al., *Core signaling pathways in human pancreatic cancers revealed by global genomic analyses*. Science, 2008. **321**(5897): p. 1801-6.
6. Mavrakis, K.J., et al., *Tumorigenic activity and therapeutic inhibition of Rheb GTPase*. Genes Dev, 2008. **22**(16): p. 2178-88.
7. De Cicco, M., M.S. Rahim, and S.A. Dames, *Regulation of the Target of Rapamycin and Other Phosphatidylinositol 3-Kinase-Related Kinases by Membrane Targeting*. Membranes (Basel), 2015. **5**(4): p. 553-75.
8. Vezina, C., A. Kudelski, and S.N. Sehgal, *Rapamycin (AY-22,989), a new antifungal antibiotic. I. Taxonomy of the producing streptomycete and isolation of the active principle*. J Antibiot (Tokyo), 1975. **28**(10): p. 721-6.
9. Heitman, J., N.R. Movva, and M.N. Hall, *Targets for cell cycle arrest by the immunosuppressant rapamycin in yeast*. Science, 1991. **253**(5022): p. 905-9.
10. Loewith, R., et al., *Two TOR complexes, only one of which is rapamycin sensitive, have distinct roles in cell growth control*. Mol Cell, 2002. **10**(3): p. 457-68.
11. Sengupta, S., et al., *mTORC1 controls fasting-induced ketogenesis and its modulation by ageing*. Nature, 2010. **468**(7327): p. 1100-4.
12. Jewell, J.L., R.C. Russell, and K.L. Guan, *Amino acid signalling upstream of mTOR*. Nat Rev Mol Cell Biol, 2013. **14**(3): p. 133-9.
13. Laplante, M. and D.M. Sabatini, *mTOR signaling at a glance*. J Cell Sci, 2009. **122**(Pt 20): p. 3589-94.
14. Fingar, D.C., et al., *Mammalian cell size is controlled by mTOR and its downstream targets S6K1 and 4EBP1/eIF4E*. Genes Dev, 2002. **16**(12): p. 1472-87.
15. Zoncu, R., et al., *mTORC1 senses lysosomal amino acids through an inside-out mechanism that requires the vacuolar H(+)-ATPase*. Science, 2011. **334**(6056): p. 678-83.
16. Jacinto, E., et al., *Mammalian TOR complex 2 controls the actin cytoskeleton and is rapamycin insensitive*. Nat Cell Biol, 2004. **6**(11): p. 1122-8.
17. Won Jun Oh, C.-c.W., Sung Jin Kim, Valeria Facchinetti, Louis -André Julien, Monica Finlan, Philippe P Roux, Bing Su, and Estela Jacinto, *mTORC2 can associate with ribosomes to promote cotranslational phosphorylation and stability of nascent Akt polypeptide*. The Embo Journal, 2010. **29**(23): p. 3939-3951.
18. Sarbassov, D.D., et al., *Rictor, a novel binding partner of mTOR, defines a rapamycin-insensitive and raptor-independent pathway that regulates the cytoskeleton*. Curr Biol, 2004. **14**(14): p. 1296-302.
19. Drenan, R.M., et al., *FKBP12-rapamycin-associated protein or mammalian target of rapamycin (FRAP/mTOR) localization in the endoplasmic reticulum and the Golgi apparatus*. J Biol Chem, 2004. **279**(1): p. 772-8.
20. Kim, E., et al., *Regulation of TORC1 by Rag GTPases in nutrient response*. Nat Cell Biol, 2008. **10**(8): p. 935-45.

21. Kunz, J., et al., *HEAT repeats mediate plasma membrane localization of Tor2p in yeast*. J Biol Chem, 2000. **275**(47): p. 37011-20.
22. Sancak, Y., et al., *The Rag GTPases bind raptor and mediate amino acid signaling to mTORC1*. Science, 2008. **320**(5882): p. 1496-501.
23. Zhang, X., et al., *Predominant nuclear localization of mammalian target of rapamycin in normal and malignant cells in culture*. J Biol Chem, 2002. **277**(31): p. 28127-34.
24. Zinzalla, V., et al., *Activation of mTORC2 by association with the ribosome*. Cell, 2011. **144**(5): p. 757-68.
25. Berchtold, D. and T.C. Walther, *TORC2 plasma membrane localization is essential for cell viability and restricted to a distinct domain*. Mol Biol Cell, 2009. **20**(5): p. 1565-75.
26. Liu, X. and X.F. Zheng, *Endoplasmic reticulum and Golgi localization sequences for mammalian target of rapamycin*. Mol Biol Cell, 2007. **18**(3): p. 1073-82.
27. Oh, W.J., et al., *mTORC2 can associate with ribosomes to promote cotranslational phosphorylation and stability of nascent Akt polypeptide*. EMBO J, 2010. **29**(23): p. 3939-51.
28. Zhang, J., et al., *A tuberous sclerosis complex signalling node at the peroxisome regulates mTORC1 and autophagy in response to ROS*. Nat Cell Biol, 2013. **15**(10): p. 1186-96.
29. Yang, Q., et al., *TSC1/TSC2 and Rheb have different effects on TORC1 and TORC2 activity*. Proc Natl Acad Sci U S A, 2006. **103**(18): p. 6811-6.
30. Laplante, M. and D.M. Sabatini, *mTOR signaling in growth control and disease*. Cell, 2012. **149**(2): p. 274-93.
31. Efeyan, A., R. Zoncu, and D.M. Sabatini, *Amino acids and mTORC1: from lysosomes to disease*. Trends Mol Med, 2012. **18**(9): p. 524-33.
32. Dibble, C.C., et al., *TBC1D7 is a third subunit of the TSC1-TSC2 complex upstream of mTORC1*. Mol Cell, 2012. **47**(4): p. 535-46.
33. Long, X., et al., *Rheb binds and regulates the mTOR kinase*. Curr Biol, 2005. **15**(8): p. 702-13.
34. Sancak, Y., et al., *PRAS40 is an insulin-regulated inhibitor of the mTORC1 protein kinase*. Mol Cell, 2007. **25**(6): p. 903-15.
35. Sancak, Y., et al., *Ragulator-Rag complex targets mTORC1 to the lysosomal surface and is necessary for its activation by amino acids*. Cell, 2010. **141**(2): p. 290-303.
36. Korolchuk, V.I., et al., *Lysosomal positioning coordinates cellular nutrient responses*. Nat Cell Biol, 2011. **13**(4): p. 453-60.
37. Hara, K., et al., *Amino acid sufficiency and mTOR regulate p70 S6 kinase and eIF-4E BP1 through a common effector mechanism*. J Biol Chem, 1998. **273**(23): p. 14484-94.
38. Kim, D.H., et al., *mTOR interacts with raptor to form a nutrient-sensitive complex that signals to the cell growth machinery*. Cell, 2002. **110**(2): p. 163-75.
39. Kim, D.H., et al., *GbetaL, a positive regulator of the rapamycin-sensitive pathway required for the nutrient-sensitive interaction between raptor and mTOR*. Mol Cell, 2003. **11**(4): p. 895-904.
40. Avruch, J., et al., *Activation of mTORC1 in two steps: Rheb-GTP activation of catalytic function and increased binding of substrates to raptor*. Biochem Soc Trans, 2009. **37**(Pt 1): p. 223-6.
41. Sekiguchi, T., et al., *Novel G proteins, Rag C and Rag D, interact with GTP-binding proteins, Rag A and Rag B*. J Biol Chem, 2001. **276**(10): p. 7246-57.
42. Bar-Peled, L., et al., *Ragulator is a GEF for the rag GTPases that signal amino acid levels to mTORC1*. Cell, 2012. **150**(6): p. 1196-208.
43. Bar-Peled, L., et al., *A Tumor suppressor complex with GAP activity for the Rag GTPases that signal amino acid sufficiency to mTORC1*. Science, 2013. **340**(6136): p. 1100-6.
44. Schieke, S.M., et al., *The mammalian target of rapamycin (mTOR) pathway regulates mitochondrial oxygen consumption and oxidative capacity*. J Biol Chem, 2006. **281**(37): p. 27643-52.

45. Bai, X., et al., *Rheb activates mTOR by antagonizing its endogenous inhibitor, FKBP38*. Science, 2007. **318**(5852): p. 977-80.
46. Ma, D., et al., *The switch I region of Rheb is critical for its interaction with FKBP38*. J Biol Chem, 2008. **283**(38): p. 25963-70.
47. Uhlenbrock, K., et al., *Reassessment of the role of FKBP38 in the Rheb/mTORC1 pathway*. FEBS Lett, 2009. **583**(6): p. 965-70.
48. Wang, X., et al., *Re-evaluating the roles of proposed modulators of mammalian target of rapamycin complex 1 (mTORC1) signaling*. J Biol Chem, 2008. **283**(45): p. 30482-92.
49. Sato, T., et al., *Specific activation of mTORC1 by Rheb G-protein in vitro involves enhanced recruitment of its substrate protein*. J Biol Chem, 2009. **284**(19): p. 12783-91.
50. Dunlop, E.A., et al., *Mammalian target of rapamycin complex 1-mediated phosphorylation of eukaryotic initiation factor 4E-binding protein 1 requires multiple protein-protein interactions for substrate recognition*. Cell Signal, 2009. **21**(7): p. 1073-84.
51. Ma, D., et al., *Rheb GTPase controls apoptosis by regulating interaction of FKBP38 with Bcl-2 and Bcl-XL*. J Biol Chem, 2010. **285**(12): p. 8621-7.
52. Sun, H., et al., *The preference of tryptophan for membrane interfaces: insights from N-methylation of tryptophans in gramicidin channels*. J Biol Chem, 2008. **283**(32): p. 22233-43.
53. Ballou, L.M., et al., *Ca(2+)- and phospholipase D-dependent and -independent pathways activate mTOR signaling*. FEBS Lett, 2003. **550**(1-3): p. 51-6.
54. Fang, Y., et al., *PLD1 regulates mTOR signaling and mediates Cdc42 activation of S6K1*. Curr Biol, 2003. **13**(23): p. 2037-44.
55. Fang, Y., et al., *Phosphatidic acid-mediated mitogenic activation of mTOR signaling*. Science, 2001. **294**(5548): p. 1942-5.
56. Inoki, K., et al., *Rheb GTPase is a direct target of TSC2 GAP activity and regulates mTOR signaling*. Genes Dev, 2003. **17**(15): p. 1829-34.
57. Saucedo, L.J., et al., *Rheb promotes cell growth as a component of the insulin/TOR signalling network*. Nat Cell Biol, 2003. **5**(6): p. 566-71.
58. Stocker, H., et al., *Rheb is an essential regulator of S6K in controlling cell growth in Drosophila*. Nat Cell Biol, 2003. **5**(6): p. 559-65.
59. Urano, J., et al., *The Saccharomyces cerevisiae Rheb G-protein is involved in regulating canavanine resistance and arginine uptake*. J Biol Chem, 2000. **275**(15): p. 11198-206.
60. Gromov, P.S., et al., *A novel approach for expression cloning of small GTPases: identification, tissue distribution and chromosome mapping of the human homolog of rheb*. FEBS Lett, 1995. **377**(2): p. 221-6.
61. Yamagata, K., et al., *rheb, a growth factor- and synaptic activity-regulated gene, encodes a novel Ras-related protein*. J Biol Chem, 1994. **269**(23): p. 16333-9.
62. Clark, G.J., et al., *The Ras-related protein Rheb is farnesylated and antagonizes Ras signaling and transformation*. J Biol Chem, 1997. **272**(16): p. 10608-15.
63. Mach, K.E., K.A. Furge, and C.F. Albright, *Loss of Rhb1, a Rheb-related GTPase in fission yeast, causes growth arrest with a terminal phenotype similar to that caused by nitrogen starvation*. Genetics, 2000. **155**(2): p. 611-22.
64. Yang, W., et al., *Failure to farnesylate Rheb protein contributes to the enrichment of G0/G1 phase cells in the Schizosaccharomyces pombe farnesyltransferase mutant*. Mol Microbiol, 2001. **41**(6): p. 1339-47.
65. Heard, J.J., et al., *Recent progress in the study of the Rheb family GTPases*. Cell Signal, 2014. **26**(9): p. 1950-7.

66. Saito, K., et al., *Novel role of the small GTPase Rheb: its implication in endocytic pathway independent of the activation of mammalian target of rapamycin*. J Biochem, 2005. **137**(3): p. 423-30.
67. Wittinghofer, A. and I.R. Vetter, *Structure-function relationships of the G domain, a canonical switch motif*. Annu Rev Biochem, 2011. **80**: p. 943-71.
68. Yu, Y., et al., *Structural basis for the unique biological function of small GTPase RHEB*. J Biol Chem, 2005. **280**(17): p. 17093-100.
69. Cherfils, J. and M. Zeghouf, *Regulation of small GTPases by GEFs, GAPs, and GDIs*. Physiol Rev, 2013. **93**(1): p. 269-309.
70. De Cicco, M., Kiss L., Dames S.A., *NMR analysis of the backbone dynamics of the small GTPase Rheb and its interaction with the regulatory protein FKBP38*. FEBS Lett, 2017.
71. Mizuki, N., et al., *Isolation of cDNA and genomic clones of a human Ras-related GTP-binding protein gene and its chromosomal localization to the long arm of chromosome 7, 7q36*. Genomics, 1996. **34**(1): p. 114-8.
72. Buerger, C., B. DeVries, and V. Stambolic, *Localization of Rheb to the endomembrane is critical for its signaling function*. Biochem Biophys Res Commun, 2006. **344**(3): p. 869-80.
73. Flinn, R.J., et al., *The late endosome is essential for mTORC1 signaling*. Mol Biol Cell, 2010. **21**(5): p. 833-41.
74. Hanker, A.B., et al., *Differential requirement of CAAX-mediated posttranslational processing for Rheb localization and signaling*. Oncogene, 2010. **29**(3): p. 380-91.
75. Maestre-Martinez, M., et al., *Solution structure of the FK506-binding domain of human FKBP38*. J Biomol NMR, 2006. **34**(3): p. 197-202.
76. Maestre-Martinez, M., et al., *A charge-sensitive loop in the FKBP38 catalytic domain modulates Bcl-2 binding*. J Mol Recognit, 2011. **24**(1): p. 23-34.
77. Karassek, S., et al., *Ras homolog enriched in brain (Rheb) enhances apoptotic signaling*. J Biol Chem, 2010. **285**(44): p. 33979-91.
78. Bos, J.L., H. Rehmann, and A. Wittinghofer, *GEFs and GAPs: critical elements in the control of small G proteins*. Cell, 2007. **129**(5): p. 865-77.
79. Petsko, G.A.a.D.R., *Protein Structure and Function, in Protein Structure and Function*. E. Lawrence and M. Robertson, Editors, New Science Press Ltd., 2004: p. 98-101.
80. Garami, A., et al., *Insulin activation of Rheb, a mediator of mTOR/S6K/4E-BP signaling, is inhibited by TSC1 and 2*. Mol Cell, 2003. **11**(6): p. 1457-66.
81. Tee, A.R., J. Blenis, and C.G. Proud, *Analysis of mTOR signaling by the small G-proteins, Rheb and RhebL1*. FEBS Lett, 2005. **579**(21): p. 4763-8.
82. Castro, A.F., et al., *Rheb binds tuberous sclerosis complex 2 (TSC2) and promotes S6 kinase activation in a rapamycin- and farnesylation-dependent manner*. J Biol Chem, 2003. **278**(35): p. 32493-6.
83. Zhang, Y., et al., *Rheb is a direct target of the tuberous sclerosis tumour suppressor proteins*. Nat Cell Biol, 2003. **5**(6): p. 578-81.
84. Li, Y., et al., *TSC2: filling the GAP in the mTOR signaling pathway*. Trends Biochem Sci, 2004. **29**(1): p. 32-8.
85. Hsu, Y.C., et al., *Drosophila TCTP is essential for growth and proliferation through regulation of dRheb GTPase*. Nature, 2007. **445**(7129): p. 785-8.
86. Rehmann, H., et al., *Biochemical characterisation of TCTP questions its function as a guanine nucleotide exchange factor for Rheb*. FEBS Lett, 2008. **582**(20): p. 3005-10.
87. Long, X., et al., *The Rheb switch 2 segment is critical for signaling to target of rapamycin complex 1*. J Biol Chem, 2007. **282**(25): p. 18542-51.

88. Tabancay, A.P., Jr., et al., *Identification of dominant negative mutants of Rheb GTPase and their use to implicate the involvement of human Rheb in the activation of p70S6K*. J Biol Chem, 2003. **278**(41): p. 39921-30.
89. Li, Y., K. Inoki, and K.L. Guan, *Biochemical and functional characterizations of small GTPase Rheb and TSC2 GAP activity*. Mol Cell Biol, 2004. **24**(18): p. 7965-75.
90. Smith, E.M., et al., *The tuberous sclerosis protein TSC2 is not required for the regulation of the mammalian target of rapamycin by amino acids and certain cellular stresses*. J Biol Chem, 2005. **280**(19): p. 18717-27.
91. Lam, E., M. Martin, and G. Wiederrecht, *Isolation of a cDNA encoding a novel human FK506-binding protein homolog containing leucine zipper and tetratricopeptide repeat motifs*. Gene, 1995. **160**(2): p. 297-302.
92. Fischer, G., et al., *Cyclophilin and peptidyl-prolyl cis-trans isomerase are probably identical proteins*. Nature, 1989. **337**(6206): p. 476-8.
93. Edlich, F., et al., *Bcl-2 regulator FKBP38 is activated by Ca²⁺/calmodulin*. EMBO J, 2005. **24**(14): p. 2688-99.
94. Kang, C.B., et al., *The flexible loop of Bcl-2 is required for molecular interaction with immunosuppressant FK-506 binding protein 38 (FKBP38)*. FEBS Lett, 2005. **579**(6): p. 1469-76.
95. Wang, H.Q., et al., *Interaction of presenilins with FKBP38 promotes apoptosis by reducing mitochondrial Bcl-2*. Hum Mol Genet, 2005. **14**(13): p. 1889-902.
96. Kang, C.B., et al., *FKBP family proteins: immunophilins with versatile biological functions*. Neurosignals, 2008. **16**(4): p. 318-25.
97. Kang, C.B., et al., *Molecular characterization of FK-506 binding protein 38 and its potential regulatory role on the anti-apoptotic protein Bcl-2*. Biochem Biophys Res Commun, 2005. **337**(1): p. 30-8.
98. Edlich, F., et al., *The specific FKBP38 inhibitor N-(N',N'-dimethylcarboxamidomethyl)cycloheximide has potent neuroprotective and neurotrophic properties in brain ischemia*. J Biol Chem, 2006. **281**(21): p. 14961-70.
99. Edlich, F., et al., *A novel calmodulin-Ca²⁺ target recognition activates the Bcl-2 regulator FKBP38*. J Biol Chem, 2007. **282**(50): p. 36496-504.
100. Shirane, M. and K.I. Nakayama, *Inherent calcineurin inhibitor FKBP38 targets Bcl-2 to mitochondria and inhibits apoptosis*. Nat Cell Biol, 2003. **5**(1): p. 28-37.
101. Partovian, C., et al., *Syndecan-4 regulates subcellular localization of mTOR Complex2 and Akt activation in a PKC α -dependent manner in endothelial cells*. Mol Cell, 2008. **32**(1): p. 140-9.
102. Wedaman, K.P., et al., *Tor kinases are in distinct membrane-associated protein complexes in Saccharomyces cerevisiae*. Mol Biol Cell, 2003. **14**(3): p. 1204-20.
103. Withers, D.J., et al., *Expression, enzyme activity, and subcellular localization of mammalian target of rapamycin in insulin-responsive cells*. Biochem Biophys Res Commun, 1997. **241**(3): p. 704-9.
104. Keith, C.T. and S.L. Schreiber, *PIK-related kinases: DNA repair, recombination, and cell cycle checkpoints*. Science, 1995. **270**(5233): p. 50-1.
105. Bosotti, R., A. Isacchi, and E.L. Sonnhammer, *FAT: a novel domain in PIK-related kinases*. Trends Biochem Sci, 2000. **25**(5): p. 225-7.
106. Dames, S.A., et al., *The solution structure of the FATC domain of the protein kinase target of rapamycin suggests a role for redox-dependent structural and cellular stability*. J Biol Chem, 2005. **280**(21): p. 20558-64.
107. Neklesa, T.K. and R.W. Davis, *Superoxide anions regulate TORC1 and its ability to bind Fpr1:rapamycin complex*. Proc Natl Acad Sci U S A, 2008. **105**(39): p. 15166-71.
108. Sarbassov, D.D., S.M. Ali, and D.M. Sabatini, *Growing roles for the mTOR pathway*. Curr Opin Cell Biol, 2005. **17**(6): p. 596-603.

109. Yoshida, S., et al., *Redox regulates mammalian target of rapamycin complex 1 (mTORC1) activity by modulating the TSC1/TSC2-Rheb GTPase pathway*. J Biol Chem, 2011. **286**(37): p. 32651-60.
110. Dames, S.A., *Structural basis for the association of the redox-sensitive target of rapamycin FATC domain with membrane-mimetic micelles*. J Biol Chem, 2010. **285**(10): p. 7766-75.
111. Berman, H., K. Henrick, and H. Nakamura, *Announcing the worldwide Protein Data Bank*. Nat Struct Biol, 2003. **10**(12): p. 980.
112. Sommer, L.A.M., M.A. Meier, and S.A. Dames, *A fast and simple method for probing the interaction of peptides and proteins with lipids and membrane-mimetics using GB1 fusion proteins and NMR spectroscopy*. Protein Sci, 2012. **21**(10): p. 1566-70.
113. Sommer, L.A. and S.A. Dames, *Characterization of residue-dependent differences in the peripheral membrane association of the FATC domain of the kinase 'target of rapamycin' by NMR and CD spectroscopy*. FEBS Lett, 2014. **2014**.
114. Sommer, L.A., M. Schaad, and S.A. Dames, *NMR- and Circular Dichroism-monitored Lipid Binding Studies Suggest a General Role for the FATC Domain as Membrane Anchor of Phosphatidylinositol 3-Kinase-related Kinases (PIKK)*. J Biol Chem, 2013. **288**(27): p. 20046-63.
115. Cavanagh, J.F., W. J.; Palmer, A. G.; Skelton, N. J.; Rance, M., *Protein NMR Spectroscopy*. Academic Press, 2006. **Second Edition: Principles and Practice, 2nd ed.**
116. Keeler, J., *Understanding NMR Spectroscopy*. John Wiley & Sons, 2005. **1st ed.**
117. Evans, J.N.S., *Biomolecular NMR Spectroscopy*
Oxford University Press, USA, 1995. **1st. ed.**
118. Dyson, H.J.P.I., A. G, *Comprehensive Biophysics*. Elsevier: Amsterdam, 2012. **Edward H. Egelman, Ed:** p. 136-159.
119. Pavia, D.L., Lampman, G. M., Kriz, G. S., and Vyvyan R. , *Introduction to Spectroscopy*. 4th Edition ed. Vol. 3. 2009.
120. Williamson, M.P., *Using chemical shift perturbation to characterise ligand binding*. Prog Nucl Magn Reson Spectrosc, 2013. **73**: p. 1-16.
121. McCoy, M.A. and D.F. Wyss, *Spatial localization of ligand binding sites from electron current density surfaces calculated from NMR chemical shift perturbations*. J Am Chem Soc, 2002. **124**(39): p. 11758-63.
122. Pervushin, K., et al., *Attenuated T2 relaxation by mutual cancellation of dipole-dipole coupling and chemical shift anisotropy indicates an avenue to NMR structures of very large biological macromolecules in solution*. Proc Natl Acad Sci U S A, 1997. **94**(23): p. 12366-71.
123. Michael Sattler, J.S., and Christian Griesinger, *Heteronuclear multidimensional NMR experiments for the structure determination of proteins in solution*. Progress in nuclear magnetic resonance spectroscopy, 1999. **34**(93): p. 158.
124. Lipari, G. and A. Szabo, *Model-free approach to the interpretation of nuclear magnetic resonance relaxation in macromolecules. 1. Theory and range of validity*. Journal of the American Chemical Society, 1982. **104**(17): p. 4546-4559.
125. Dosset, P., et al., *Efficient analysis of macromolecular rotational diffusion from heteronuclear relaxation data*. J Biomol NMR, 2000. **16**(1): p. 23-8.
126. Kleckner, I.R. and M.P. Foster, *An introduction to NMR-based approaches for measuring protein dynamics*. Biochim Biophys Acta, 2011. **1814**(8): p. 942-68.
127. Zeeb, M. and J. Balbach, *Protein folding studied by real-time NMR spectroscopy*. Methods, 2004. **34**(1): p. 65-74.
128. Grzesiek, S., J. Anglister, and A. Bax, *Correlation of Backbone Amide and Aliphatic Side-Chain Resonances in ¹³C/¹⁵N-Enriched Proteins by Isotropic Mixing of ¹³C Magnetization*. Journal of Magnetic Resonance, Series B, 1993. **101**(1): p. 114-119.

129. John, J., et al., *Kinetics of interaction of nucleotides with nucleotide-free H-ras p21*. *Biochemistry*, 1990. **29**(25): p. 6058-65.
130. Lazaridis, T., B. Mallik, and Y. Chen, *Implicit solvent simulations of DPC micelle formation*. *J Phys Chem B*, 2005. **109**(31): p. 15098-106.
131. Delaglio, F., et al., *NMRPipe: a multidimensional spectral processing system based on UNIX pipes*. *J Biomol NMR*, 1995. **6**(3): p. 277-93.
132. Johnson, B.A., *Using NMRView to visualize and analyze the NMR spectra of macromolecules*. *Methods Mol Biol*, 2004. **278**: p. 313-52.
133. Berghaus, C., et al., *Sequence-specific 1H, 13C, and 15N backbone assignment of the GTPase rRheb in its GDP-bound form*. *Biomol NMR Assign*, 2007. **1**(1): p. 45-7.
134. Schwarten, M., et al., *Sequence-specific 1H, 13C, and 15N backbone assignment of the activated 21 kDa GTPase rRheb*. *Biomol NMR Assign*, 2007. **1**(1): p. 105-8.
135. Marshall, C.B., et al., *Characterization of the intrinsic and TSC2-GAP-regulated GTPase activity of Rheb by real-time NMR*. *Sci Signal*, 2009. **2**(55): p. ra3.
136. Mandel, A.M., M. Akke, and A.G. Palmer, 3rd, *Backbone dynamics of Escherichia coli ribonuclease HI: correlations with structure and function in an active enzyme*. *J Mol Biol*, 1995. **246**(1): p. 144-63.
137. Mazhab-Jafari, M.T., et al., *Structure-guided mutation of the conserved G3-box glycine in Rheb generates a constitutively activated regulator of mammalian target of rapamycin (mTOR)*. *J Biol Chem*, 2014. **289**(18): p. 12195-201.
138. Wittinghofer, F., *Ras signalling. Caught in the act of the switch-on*. *Nature*, 1998. **394**(6691): p. 317, 319-20.
139. De Cicco, M., L.G. Milroy, and S.A. Dames, *Target of rapamycin FATC domain as a general membrane anchor: the FKBP-12 like domain of FKBP38 as a case study*. *Protein Sci*, 2017.
140. Sommer, L.A., et al., *Characterization of the immersion properties of the peripheral membrane anchor of the FATC domain of the kinase "target of rapamycin" by NMR, oriented CD spectroscopy, and MD simulations*. *J Phys Chem B*, 2014. **118**(18): p. 4817-31.
141. Tieleman, D.P.v.d.S., D.; Berendsen, H.J.C., *Molecular Dynamics Simulations of Dodecylphosphocholine Micelles at Three Different Aggregate Sizes: Micellar Structure and Chain Relaxation*. *J. Phys. Chem. B*, 2000. **104**: p. 6380-6388.
142. Warschawski, D.E., et al., *Choosing membrane mimetics for NMR structural studies of transmembrane proteins*. *Biochim Biophys Acta*, 2011. **1808**(8): p. 1957-74.
143. Geyer, M., et al., *Conformational transitions in p21ras and in its complexes with the effector protein Raf-RBD and the GTPase activating protein GAP*. *Biochemistry*, 1996. **35**(32): p. 10308-20.
144. Spoerner, M., et al., *Conformational states of Ras complexed with the GTP analogue GppNHp or GppCH2p: implications for the interaction with effector proteins*. *Biochemistry*, 2005. **44**(6): p. 2225-36.
145. Spoerner, M., et al., *Conformational states of human rat sarcoma (Ras) protein complexed with its natural ligand GTP and their role for effector interaction and GTP hydrolysis*. *J Biol Chem*, 2010. **285**(51): p. 39768-78.
146. Long, D., et al., *A comparative CEST NMR study of slow conformational dynamics of small GTPases complexed with GTP and GTP analogues*. *Angew Chem Int Ed Engl*, 2013. **52**(41): p. 10771-4.
147. Chandrashekar, R., et al., *A switch I mutant of Cdc42 exhibits less conformational freedom*. *Biochemistry*, 2011. **50**(28): p. 6196-207.
148. Ma, D., et al., *The Switch I Region of Rheb Is Critical for Its Interaction with FKBP38*. *J Biol Chem*, 2008. **283**: p. 25963-25970.
149. Ito, Y., et al., *Regional polyesterism in the GTP-bound form of the human c-Ha-Ras protein*. *Biochemistry*, 1997. **36**(30): p. 9109-19.

150. Mazhab-Jafari, M.T., et al., *Membrane-dependent modulation of the mTOR activator Rheb: NMR observations of a GTPase tethered to a lipid-bilayer nanodisc*. J Am Chem Soc, 2013. **135**(9): p. 3367-70.
151. Gasmi-Seabrook, G.M., et al., *Real-time NMR study of guanine nucleotide exchange and activation of RhoA by PDZ-RhoGEF*. J Biol Chem, 2010. **285**(8): p. 5137-45.
152. Goody, R.S. and W. Hofmann-Goody, *Exchange factors, effectors, GAPs and motor proteins: common thermodynamic and kinetic principles for different functions*. Eur Biophys J, 2002. **31**(4): p. 268-74.
153. Dibble, C.C. and L.C. Cantley, *Regulation of mTORC1 by PI3K signaling*. Trends Cell Biol, 2015. **25**(9): p. 545-55.
154. Avruch, J., et al., *Amino acid regulation of TOR complex 1*. Am J Physiol Endocrinol Metab, 2009. **296**(4): p. E592-602.
155. Zheng, M., et al., *Inactivation of Rheb by PRAK-mediated phosphorylation is essential for energy-depletion-induced suppression of mTORC1*. Nat Cell Biol, 2011. **13**(3): p. 263-72.
156. Hu, J., et al., *Structural biology of transmembrane domains: efficient production and characterization of transmembrane peptides by NMR*. Protein Sci, 2007. **16**(10): p. 2153-65.
157. Sahdev, S., S.K. Khattar, and K.S. Saini, *Production of active eukaryotic proteins through bacterial expression systems: a review of the existing biotechnology strategies*. Mol Cell Biochem, 2008. **307**(1-2): p. 249-64.
158. Eshaghi, S., *High-throughput expression and detergent screening of integral membrane proteins*. Methods Mol Biol, 2009. **498**: p. 265-71.
159. Hagn, F., et al., *Optimized phospholipid bilayer nanodiscs facilitate high-resolution structure determination of membrane proteins*. J Am Chem Soc, 2013. **135**(5): p. 1919-25.
160. Gomes, A.Q., et al., *Membrane targeting of Rab GTPases is influenced by the prenylation motif*. Mol Biol Cell, 2003. **14**(5): p. 1882-99.
161. Fres, J.M., S. Muller, and G.J. Praefcke, *Purification of the CaaX-modified, dynamin-related large GTPase hGBP1 by coexpression with farnesyltransferase*. J Lipid Res, 2010. **51**(8): p. 2454-9.
162. Losonczi, J.A., et al., *NMR studies of the anti-apoptotic protein Bcl-xL in micelles*. Biochemistry, 2000. **39**(36): p. 11024-33.
163. Dames, S.A., et al., *Structure, dynamics, lipid binding, and physiological relevance of the putative GTPase-binding domain of Dictyostelium formin C*. J Biol Chem, 2011. **286**(42): p. 36907-20.
164. Rodriguez Camargo, D.C., N.M. Link, and S.A. Dames, *The FKBP-rapamycin binding domain of human TOR undergoes strong conformational changes in the presence of membrane mimetics with and without the regulator phosphatidic acid*. Biochemistry, 2012. **51**(24): p. 4909-21.
165. McMahon, H.T. and E. Boucrot, *Membrane curvature at a glance*. J Cell Sci, 2015. **128**(6): p. 1065-70.
166. Stafford, R.E., T. Fanni, and E.A. Dennis, *Interfacial properties and critical micelle concentration of lysophospholipids*. Biochemistry, 1989. **28**(12): p. 5113-20.
167. Sprong, H., P. van der Sluijs, and G. van Meer, *How proteins move lipids and lipids move proteins*. Nat Rev Mol Cell Biol, 2001. **2**(7): p. 504-13.
168. Liu, W. and M. Caffrey, *Interactions of tryptophan, tryptophan peptides, and tryptophan alkyl esters at curved membrane interfaces*. Biochemistry, 2006. **45**(39): p. 11713-26.
169. Thorgeirsson, T.E., et al., *Direct determination of the membrane affinities of individual amino acids*. Biochemistry, 1996. **35**(6): p. 1803-9.
170. Mocklinghoff, S., et al., *Synthesis and crystal structure of a phosphorylated estrogen receptor ligand binding domain*. ChemBiochem, 2010. **11**(16): p. 2251-4.
171. Tharun, I.M., et al., *Subtype-specific modulation of estrogen receptor-coactivator interaction by phosphorylation*. ACS Chem Biol, 2015. **10**(2): p. 475-84.

172. Crankshaw, M.W. and G.A. Grant, *Modification of cysteine*. Curr Protoc Protein Sci, 2001. **Chapter 15**: p. Unit15 1.
173. Corpet, F., *Multiple sequence alignment with hierarchical clustering*. Nucleic Acids Res, 1988. **16**(22): p. 10881-90.
174. Robert, X. and P. Gouet, *Deciphering key features in protein structures with the new ENDscript server*. Nucleic Acids Res, 2014. **42**(Web Server issue): p. W320-4.

APPENDIX

Table 1: ^{15}N -relaxation times T_1 and T_2 , and $\{^1\text{H}\}$ - ^{15}N NOE values and corresponding errors for the GDP-bound form of Rheb Δ CT

Residue	^{15}N - T_1 [ms] \pm error	^{15}N - T_2 [ms] \pm error	$\{^1\text{H}\}$ - ^{15}N NOE \pm error
6	724 \pm 2	100 \pm 0	0.70 \pm 0.03
7	673 \pm 1	95 \pm 0	0.80 \pm 0.03
8	690 \pm 1	100 \pm 1	0.81 \pm 0.03
9	641 \pm 1	100 \pm 1	0.76 \pm 0.03
10	614 \pm 1	94 \pm 1	0.81 \pm 0.04
11	655 \pm 1	91 \pm 1	0.74 \pm 0.03
12	651 \pm 1	88 \pm 1	0.75 \pm 0.03
14	666 \pm 2	88 \pm 1	0.78 \pm 0.04
15	657 \pm 5	96 \pm 1	0.87 \pm 0.10
16	677 \pm 2	81 \pm 1	0.80 \pm 0.04
18	616 \pm 2	87 \pm 1	0.78 \pm 0.04
19	677 \pm 3	86 \pm 1	0.92 \pm 0.05
20	694 \pm 2	76 \pm 0	0.86 \pm 0.03
21	729 \pm 2	78 \pm 1	0.92 \pm 0.03
22	650 \pm 1	85 \pm 0	0.85 \pm 0.02
24	665 \pm 2	78 \pm 0	0.85 \pm 0.03
25	651 \pm 2	84 \pm 0	0.93 \pm 0.04
26	663 \pm 2	79 \pm 0	0.91 \pm 0.03
27	670 \pm 1	77 \pm 0	0.83 \pm 0.03
28	698 \pm 2	80 \pm 1	0.80 \pm 0.03
29	644 \pm 2	90 \pm 0	0.83 \pm 0.04
31	721 \pm 1	95 \pm 0	0.74 \pm 0.03
32	720 \pm 2	96 \pm 0	0.74 \pm 0.05
33	670 \pm 1	108 \pm 0	0.71 \pm 0.02
34	671 \pm 1	114 \pm 0	0.73 \pm 0.03

35	694 ± 1	143 ± 0	0.48 ± 0.03
36	764 ± 4	103 ± 1	0.78 ± 0.04
38	684 ± 2	81 ± 1	0.78 ± 0.03
39	640 ± 6	85 ± 0	0.62 ± 0.08
40	668 ± 1	86 ± 1	0.78 ± 0.06
41	755 ± 2	86 ± 1	0.71 ± 0.03
42	726 ± 2	76 ± 0	0.86 ± 0.04
43	654 ± 2	78 ± 1	0.76 ± 0.03
44	717 ± 1	85 ± 0	0.82 ± 0.03
45	665 ± 1	81 ± 0	0.75 ± 0.03
46	703 ± 1	78 ± 0	0.81 ± 0.02
47	675 ± 1	84 ± 0	0.78 ± 0.03
48	692 ± 1	79 ± 0	0.83 ± 0.03
51	769 ± 4	80 ± 1	0.81 ± 0.02
52	745 ± 1	90 ± 0	0.77 ± 0.03
53	735 ± 1	84 ± 1	0.74 ± 0.03
54	667 ± 1	95 ± 0	0.82 ± 0.03
55	693 ± 1	96 ± 0	0.82 ± 0.03
56	670 ± 1	108 ± 0	0.77 ± 0.03
57	662 ± 1	114 ± 0	0.78 ± 0.03
58	655 ± 1	143 ± 0	0.83 ± 0.03
59	667 ± 1	103 ± 1	0.84 ± 0.04
60	701 ± 2	97 ± 1	0.70 ± 0.07
61	677 ± 4	103 ± 1	0.85 ± 0.03
62	708 ± 1	90 ± 0	0.58 ± 0.05
63	664 ± 2	118 ± 1	0.85 ± 0.08
64	634 ± 3	90 ± 1	0.87 ± 0.03
65	720 ± 2	86 ± 0	0.84 ± 0.05
66	718 ± 3	88 ± 1	0.76 ± 0.03
68	668 ± 1	86 ± 0	0.78 ± 0.03
69	708 ± 2	89 ± 0	0.79 ± 0.04

74	609 ± 2	73 ± 0	0.77 ± 0.03
75	609 ± 1	92 ± 0	0.80 ± 0.04
76	680 ± 3	92 ± 0	0.45 ± 0.05
77	670 ± 1	71 ± 0	0.78 ± 0.05
78	669 ± 2	92 ± 0	0.81 ± 0.05
79	666 ± 1	89 ± 1	0.76 ± 0.03
83	664 ± 1	93 ± 0	0.72 ± 0.03
84	647 ± 1	92 ± 1	0.77 ± 0.03
85	650 ± 1	87 ± 1	0.87 ± 0.03
86	701 ± 2	89 ± 1	0.80 ± 0.04
87	682 ± 1	74 ± 0	0.79 ± 0.03
88	675 ± 2	85 ± 0	0.91 ± 0.04
89	673 ± 1	79 ± 0	0.83 ± 0.02
90	660 ± 1	85 ± 0	0.83 ± 0.03
91	643 ± 1	87 ± 0	0.92 ± 0.02
92	675 ± 1	83 ± 0	0.83 ± 0.03
93	639 ± 2	85 ± 0	0.78 ± 0.04
94	701 ± 1	80 ± 0	0.87 ± 0.03
95	660 ± 1	81 ± 0	0.84 ± 0.03
96	64 ± 1	68 ± 0	0.86 ± 0.04
97	650 ± 4	72 ± 0	0.81 ± 0.07
98	674 ± 3	86 ± 1	0.76 ± 0.06
99	687 ± 1	83 ± 0	0.82 ± 0.03
101	656 ± 3	77 ± 0	0.82 ± 0.05
105	688 ± 1	82 ± 0	0.78 ± 0.03
106	100 ± 1	89 ± 0	0.74 ± 0.03
107	686 ± 1	89 ± 0	0.77 ± 0.03
108	672 ± 1	96 ± 0	0.75 ± 0.03
109	733 ± 2	109 ± 1	0.66 ± 0.04
110	729 ± 1	133 ± 0	0.43 ± 0.03
111	736 ± 1	122 ± 0	0.56 ± 0.03

112	771 ± 1	125 ± 0	0.43 ± 0.03
115	647 ± 1	95 ± 1	0.74 ± 0.03
116	647 ± 1	93 ± 1	0.89 ± 0.03
118	659 ± 2	90 ± 1	0.83 ± 0.04
119	661 ± 1	85 ± 1	0.78 ± 0.02
120	746 ± 6	84 ± 1	0.95 ± 0.08
121	685 ± 1	79 ± 0	0.78 ± 0.03
122	622 ± 1	80 ± 0	0.86 ± 0.03
123	692 ± 2	90 ± 0	0.89 ± 0.04
124	665 ± 2	88 ± 0	0.79 ± 0.03
125	735 ± 2	85 ± 1	0.74 ± 0.03
127	647 ± 3	87 ±	0.75 ± 0.05
128	670 ± 2	79 ± 1	0.86 ± 0.05
129	690 ± 3	98 ± 1	0.81 ± 0.05
130	694 ± 1	88 ± 0	0.84 ± 0.03
131	654 ± 2	88 ± 0	0.88 ± 0.03
132	683 ± 1	83 ± 0	0.88 ± 0.02
133	691 ± 1	85 ± 0	0.80 ± 0.03
134	654 ± 3	93 ± 1	0.74 ± 0.6
135	649 ± 2	83 ± 0	0.85 ± 0.03
136	658 ± 1	79 ± 0	0.84 ± 0.03
137	610 ± 3	88 ± 0	0.74 ± 0.05
138	649 ± 1	82 ± 0	0.86 ± 0.03
139	676 ± 1	80 ± 0	0.83 ± 0.02
140	650 ± 1	80 ± 0	0.80 ± 0.03
141	677 ± 2	94 ± 1	0.75 ± 0.04
142	711 ± 1	82 ± 0	0.44 ± 0.07
143	714 ± 1	81 ± 0	0.86 ± 0.03
144	720 ± 1	100 ± 0	0.73 ± 0.03
145	685 ± 1	93 ± 0	0.87 ± 0.03
146	653 ± 2	89 ± 0	0.86 ± 0.03

147	678 ± 2	93 ± 0	0.78 ± 0.04
148	666 ± 1	83 ± 1	0.91 ± 0.03
149	737 ± 2	84 ± 0	0.85 ± 0.04
150	689 ± 1	90 ± 0	0.90 ± 0.03
151	660 ± 3	86 ± 0	0.79 ± 0.05
152	660 ± 2	90 ± 0	0.78 ± 0.04
154	753 ± 2	88 ± 0	0.83 ± 0.03
155	646 ± 3	96 ± 0	0.81 ± 0.05
156	654 ± 1	93 ± 0	0.86 ± 0.05
157	677 ± 1	82 ± 0	0.76 ± 0.02
158	654 ± 3	81 ± 0	0.83 ± 0.02
159	650 ± 5	82 ± 0	0.77 ± 0.05
160	661 ± 1	83 ± 1	0.77 ± 0.10
161	686 ± 5	83 ± 0	0.82 ± 0.02
163	626 ± 5	82 ± 0	0.70 ± 0.03
164	684 ± 1	81 ± 1	0.83 ± 0.08
165	637 ± 1	82 ± 0	0.72 ± 0.03
166	657 ± 1	83 ± 0	0.81 ± 0.03
167	649 ± 1	94 ± 0	0.81 ± 0.02
168	649 ± 1	95 ± 0	0.67 ± 0.03
169	606 ± 0	117 ± 0	0.50 ± 0.02
170	614 ± 0	194 ± 0	0.37 ± 0.02

Table 2: ^{15}N -relaxation times T_1 and T_2 , and $\{^1\text{H}\}$ - ^{15}N NOE values and corresponding errors for the GppNHp-bound form of Rheb Δ CT

Residue	^{15}N - T_1 [ms] ± error	^{15}N - T_2 [ms] ± error	$\{^1\text{H}\}$ - ^{15}N NOE ± error
4	87 ± 3	170 ± 1	0.12 ± 0.06
5	773 ± 3	124 ± 1	0.39 ± 0.06
6	756 ± 1	94 ± 0	0.74 ± 0.04
7	709 ± 1	95 ± 0	0.86 ± 0.05

8	702 ± 1	93 ± 0	0.81 ± 0.05
9	668 ± 1	88 ± 0	0.74 ± 0.05
10	696 ± 2	93 ± 1	0.69 ± 0.07
11	671 ± 1	87 ± 0	0.77 ± 0.06
12	725 ± 1	90 ± 0	0.84 ± 0.05
13	682 ± 1	97 ± 0	0.78 ± 0.05
14	655 ± 2	80 ± 1	0.89 ± 0.10
16	638 ± 1	79 ± 0	0.88 ± 0.07
17	675 ± 2	95 ± 0	0.77 ± 0.06
18	828 ± 3	88 ± 1	0.82 ± 0.08
20	710 ± 3	73 ± 0	0.79 ± 0.05
21	728 ± 2	68 ± 1	0.87 ± 0.10
22	715 ± 1	85 ± 1	0.81 ± 0.06
23	794 ± 6	77 ± 0	0.86 ± 0.05
26	697 ± 1	75 ± 0	0.82 ± 0.04
27	732 ± 1	75 ± 0	0.78 ± 0.06
28	698 ± 1	73 ± 0	0.78 ± 0.05
29	698 ± 1	91 ± 0	0.88 ± 0.05
43	695 ± 2	77 ± 1	0.81 ± 0.07
44	708 ± 1	91 ± 0	0.30 ± 0.04
45	705 ± 1	88 ± 0	0.77 ± 0.04
46	724 ± 1	99 ± 0	0.76 ± 0.04
47	708 ± 1	83 ± 0	0.76 ± 0.03
48	760 ± 1	94 ± 0	0.81 ± 0.03
49	735 ± 1	97 ± 0	0.75 ± 0.04
51	823 ± 1	98 ± 0	0.70 ± 0.04
52	804 ± 1	82 ± 0	0.74 ± 0.03
53	764 ± 1	92 ± 0	0.73 ± 0.03
54	755 ± 1	87 ± 0	0.69 ± 0.04
55	734 ± 1	90 ± 0	0.78 ± 0.04
56	689 ± 1	89 ± 0	0.71 ± 0.05

57	698 ± 1	87 ± 0	0.73 ± 0.06
58	699 ± 1	93 ± 0	0.86 ± 0.06
59	674 ± 1	91 ± 0	0.88 ± 0.06
63	827 ± 6	82 ± 1	0.96 ± 0.13
65	775 ± 1	91 ± 0	0.71 ± 0.04
66	733 ± 4	81 ± 1	0.72 ± 0.16
67	684 ± 1	81 ± 0	0.85 ± 0.04
68	781 ± 1	87 ± 0	0.80 ± 0.03
77	713 ± 2	91 ± 1	0.77 ± 0.10
79	695 ± 1	90 ± 0	0.67 ± 0.06
80	661 ± 1	100 ± 0	0.65 ± 0.05
81	690 ± 1	81 ± 0	0.88 ± 0.06
82	654 ± 1	85 ± 0	0.77 ± 0.05
83	668 ± 1	94 ± 0	0.84 ± 0.05
84	693 ± 1	89 ± 0	0.90 ± 0.05
85	670 ± 1	81 ± 0	0.87 ± 0.05
86	692 ± 2	83 ± 0	0.98 ± 0.08
87	702 ± 1	66 ± 0	0.89 ± 0.05
88	721 ± 1	80 ± 0	0.84 ± 0.05
90	702 ± 1	86 ± 0	0.79 ± 0.05
92	695 ± 1	86 ± 0	0.85 ± 0.04
93	714 ± 1	84 ± 0	0.86 ± 0.05
94	699 ± 1	78 ± 0	0.85 ± 0.04
95	708 ± 1	79 ± 0	0.80 ± 0.04
96	717 ± 1	72 ± 0	0.77 ± 0.04
97	673 ± 1	79 ± 0	0.77 ± 0.06
98	678 ± 1	75 ± 0	0.92 ± 0.05
99	710 ± 1	74 ± 0	0.80 ± 0.05
100	782 ± 1	71 ± 0	0.84 ± 0.04
101	692 ± 1	80 ± 0	0.98 ± 0.06
102	732 ± 1	79 ± 0	0.85 ± 0.04

107	744 ± 1	79 ± 0	0.66 ± 0.04
108	752 ± 1	102 ± 0	0.66 ± 0.04
109	774 ± 2	91 ± 1	0.72 ± 0.10
110	801 ± 1	129 ± 0	0.44 ± 0.03
111	725 ± 1	119 ± 0	0.54 ± 0.04
112	805 ± 0	124 ± 0	0.40 ± 0.03
114	701 ± 1	93 ± 0	0.73 ± 0.05
115	668 ± 1	87 ± 0	0.74 ± 0.04
116	653 ± 1	96 ± 0	0.73 ± 0.05
117	651 ± 1	90 ± 0	0.82 ± 0.04
118	734 ± 2	83 ± 0	0.97 ± 0.06
119	687 ± 1	84 ± 0	0.82 ± 0.03
120	732 ± 2	84 ± 0	0.81 ± 0.07
121	723 ± 1	74 ± 0	0.90 ± 0.04
122	647 ± 1	77 ± 0	0.92 ± 0.05
123	704 ± 1	82 ± 0	0.93 ± 0.04
124	738 ± 1	85 ± 0	0.81 ± 0.03
126	748 ± 1	85 ± 0	0.70 ± 0.04
127	692 ± 1	85 ± 0	0.83 ± 0.05
128	681 ± 2	70 ± 1	0.86 ± 0.08
129	712 ± 1	96 ± 0	0.73 ± 0.06
130	742 ± 1	88 ± 0	0.79 ± 0.04
131	724 ± 1	86 ± 0	0.82 ± 0.04
132	736 ± 1	82 ± 0	0.86 ± 0.03
133	724 ± 1	79 ± 0	0.81 ± 0.04
134	682 ± 1	91 ± 0	0.85 ± 0.05
135	707 ± 1	76 ± 0	0.84 ± 0.04
136	718 ± 1	76 ± 0	0.84 ± 0.03
137	679 ± 1	75 ± 0	0.81 ± 0.04
138	706 ± 1	80 ± 0	0.86 ± 0.04
139	710 ± 0	76 ± 0	0.83 ± 0.03

140	748 ± 1	78 ± 0	0.81 ± 0.03
141	732 ± 1	88 ± 0	0.85 ± 0.04
142	745 ± 1	76 ± 0	0.81 ± 0.03
143	742 ± 1	78 ± 0	0.77 ± 0.03
144	753 ± 1	99 ± 0	0.71 ± 0.03
145	720 ± 1	88 ± 0	0.90 ± 0.04
146	709 ± 1	84 ± 0	0.79 ± 0.03
147	729 ± 1	89 ± 0	0.77 ± 0.03
148	700 ± 1	79 ± 0	0.80 ± 0.04
149	777 ± 1	84 ± 0	0.84 ± 0.05
150	705 ± 1	86 ± 0	0.91 ± 0.05
151	716 ± 1	84 ± 0	0.79 ± 0.06
152	718 ± 1	82 ± 0	0.81 ± 0.04
154	727 ± 2	84 ± 0	0.76 ± 0.04
155	693 ± 1	80 ± 0	0.76 ± 0.05
156	707 ± 1	89 ± 0	0.77 ± 0.04
157	720 ± 1	80 ± 0	0.81 ± 0.04
158	713 ± 1	77 ± 0	0.85 ± 0.03
159	693 ± 1	77 ± 0	0.85 ± 0.04
160	644 ± 2	82 ± 0	0.89 ± 0.07
162	692 ± 1	75 ± 0	0.80 ± 0.04
164	706 ± 1	80 ± 0	0.83 ± 0.06
165	690 ± 1	78 ± 0	0.75 ± 0.04
166	699 ± 1	83 ± 0	0.79 ± 0.03
167	696 ± 0	84 ± 0	0.82 ± 0.03
168	723 ± 0	87 ± 0	0.73 ± 0.02
169	683 ± 0	98 ± 0	0.60 ± 0.01
170	660 ± 0	186 ± 0	0.38 ± 0.02

Table 3: ^{15}N -relaxation times T_1 and T_2 , and $\{^1\text{H}\}$ - ^{15}N NOE values and corresponding errors for the GppCp-bound form of Rheb Δ CT.

Residue	^{15}N - T_1 [ms] \pm error	^{15}N - T_2 [ms] \pm error	$\{^1\text{H}\}$ - ^{15}N NOE \pm error
5	863 \pm 7	151 \pm 3	0.58 \pm 0.12
6	746 \pm 4	105 \pm 1	0.73 \pm 0.08
7	657 \pm 3	85 \pm 2	0.77 \pm 0.09
8	725 \pm 5	118 \pm 3	0.91 \pm 0.13
9	806 \pm 7	104 \pm 3	0.82 \pm 0.12
10	680 \pm 4	105 \pm 3	0.86 \pm 0.15
11	672 \pm 4	92 \pm 3	0.81 \pm 0.13
13	640 \pm 6	113 \pm 3	0.67 \pm 0.13
14	857 \pm 12	83 \pm 3	0.62 \pm 0.13
17	644 \pm 3	99 \pm 2	0.76 \pm 0.13
18	606 \pm 5	103 \pm 3	0.79 \pm 0.11
20	804 \pm 7	70 \pm 1	0.65 \pm 0.12
22	731 \pm 4	78 \pm 1	0.73 \pm 0.12
23	763 \pm 5	77 \pm 1	0.78 \pm 0.13
26	665 \pm 5	73 \pm 2	0.92 \pm 0.09
29	656 \pm 3	115 \pm 3	0.79 \pm 0.11
44	815 \pm 4	92 \pm 2	0.73 \pm 0.09
46	767 \pm 4	116 \pm 2	0.83 \pm 0.13
47	716 \pm 3	85 \pm 1	0.71 \pm 0.09
49	750 \pm 4	113 \pm 3	0.75 \pm 0.10
52	773 \pm 4	93 \pm 1	0.76 \pm 0.14
53	747 \pm 3	93 \pm 1	0.60 \pm 0.12
54	694 \pm 4	117 \pm 3	0.70 \pm 0.14
55	733 \pm 6	94 \pm 2	0.91 \pm 0.13
56	718 \pm 5	92 \pm 2	0.94 \pm 0.13
58	627 \pm 5	104 \pm 3	0.83 \pm 0.13
59	682 \pm 5	95 \pm 2	0.79 \pm 0.12

79	623 ± 4	92 ± 3	0.75 ± 0.12
80	678 ± 4	104 ± 2	0.70 ± 0.12
81	722 ± 6	79 ± 2	0.89 ± 0.12
82	596 ± 3	102 ± 3	0.77 ± 0.13
85	788 ± 8	90 ± 2	0.63 ± 0.11
87	681 ± 7	70 ± 1	0.89 ± 0.12
88	621 ± 4	95 ± 2	0.75 ± 0.11
90	852 ± 5	105 ± 3	0.89 ± 0.11
93	738 ± 6	94	0.71 ± 0.11
94	697 ± 3	91 ± 2	0.79 ± 0.10
95	722 ± 4	103 ± 2	0.93 ± 0.17
96	735 ± 4	66 ± 1	0.72 ± 0.13
97	611 ± 5	69 ± 2	0.86 ± 0.12
98	699 ± 4	83 ± 2	0.93 ± 0.11
99	750 ± 5	89 ± 2	0.82 ± 0.09
101	610 ± 3	102 ± 2	0.75 ± 0.10
102	709 ± 4	80 ± 2	0.77 ± 0.10
103	690 ± 4	78 ± 1	0.99 ± 0.08
105	810 ± 6	90 ± 2	0.66 ± 0.07
107	732 ± 3	82 ± 1	0.86 ± 0.07
108	743 ± 3	96 ± 1	0.81 ± 0.08
109	782 ± 5	103 ± 2	0.86 ± 0.13
110	764 ± 2	139 ± 1	0.52 ± 0.13
111	805 ± 5	127 ± 3	0.44 ± 0.15
112	767 ± 2	119 ± 1	0.36 ± 0.11
114	753 ± 3	111 ± 1	0.89 ± 0.10
115	805 ± 5	94 ± 2	0.78 ± 0.11
116	730 ± 7	106 ± 4	0.80 ± 0.08
117	703 ± 5	103 ± 3	0.77 ± 0.16
120	672 ± 9	69 ± 2	0.68 ± 0.13
121	685 ± 4	69 ± 1	0.90 ± 0.08

122	755 ± 5	93 ± 2	1.02 ± 0.07
123	631 ± 4	84 ± 1	0.95 ± 0.09
124	737 ± 4	79 ± 1	0.79 ± 0.12
125	406 ± 17	85 ± 1	0.71 ± 0.10
126	792 ± 4	80 ± 1	0.77 ± 0.08
127	954 ± 10	91 ± 2	0.61 ± 0.12
128	787 ± 6	69 ± 1	0.69 ± 0.10
129	798 ± 7	74 ± 2	0.76 ± 0.10
132	802 ± 4	89 ± 1	0.87 ± 0.07
133	657 ± 3	78 ± 1	0.84 ± 0.10
134	698 ± 6	102 ± 2	0.69 ± 0.07
135	752 ± 4	82 ± 1	0.87 ± 0.11
136	715 ± 3	81 ± 1	0.70 ± 0.10
137	861 ± 6	87 ± 1	0.92 ± 0.11
138	725 ± 3	80 ± 2	0.89 ± 0.11
139	861 ± 6	75 ± 1	0.90 ± 0.10
140	725 ± 3	78 ± 1	0.80 ± 0.16
141	765 ± 3	91 ± 2	0.69 ± 0.11
143	728 ± 5	69 ± 1	0.74 ± 0.11
144	836 ± 4	105 ± 1	0.91 ± 0.09
145	781 ± 4	85 ± 1	0.98 ± 0.12
146	747 ± 3	87 ± 2	0.89 ± 0.10
148	621 ± 2	113 ± 3	0.83 ± 0.08
149	711 ± 3	96 ± 2	0.83 ± 0.13
150	778 ± 6	99 ± 2	0.81 ± 0.20
152	729 ± 4	81 ± 1	0.85 ± 0.07
154	741 ± 4	89 ± 1	0.69 ± 0.16
155	759 ± 5	89 ± 2	0.86 ± 0.09
156	608 ± 4	81 ± 1	0.90 ± 0.08
157	673 ± 3	84 ± 2	0.74 ± 0.06
158	799 ± 3	80 ± 1	0.80 ± 0.04

159	732 ± 4	71 ± 1	0.82 ± 0.06
162	736 ± 4	93 ± 2	0.77 ± 0.00
164	699 ± 8	80 ± 2	0.80 ± 0.01
165	681 ± 3	80 ± 1	0.78 ± 0.12
166	672 ± 4	132 ± 3	0.68 ± 0.08
167	698 ± 2	94 ± 1	0.69 ± 0.09
168	678 ± 1	84 ± 1	0.72 ± 0.13
169	667 ± 1	99 ± 0	0.58 ± 0.12
170	638 ± 1	192 ± 1	0.29 ± 0.15

Table 4: ^{15}N -relaxation times T_1 and T_2 , and $\{^1\text{H}\}$ - ^{15}N NOE values and corresponding errors for the GppNHp-bound form of Rheb Δ CT in the presence of FKBP38-BD

Residue	^{15}N - T_1 [ms] \pm error	^{15}N - T_2 [ms] \pm error	$\{^1\text{H}\}$ - ^{15}N NOE \pm error
4	726 ± 2	170 ± 0	0.43 ± 0.08
5	663 ± 2	118 ± 0	0.67 ± 0.10
6	771 ± 2	93 ± 0	0.69 ± 0.06
7	710 ± 2	88 ± 1	0.80 ± 0.06
8	755 ± 2	93 ± 1	0.89 ± 0.06
9	720 ± 2	90 ± 1	0.84 ± 0.07
10	700 ± 3	106 ± 1	0.81 ± 0.08
12	665 ± 2	89 ± 1	0.84 ± 0.07
13	756 ± 3	97 ± 1	0.80 ± 0.07
14	718 ± 8	98 ± 2	0.92 ± 0.12
16	795 ± 6	88 ± 1	0.73 ± 0.09
17	570 ± 2	84 ± 1	1.08 ± 0.08
18	574 ± 4	77 ± 1	1.01 ± 0.11
20	705 ± 3	75 ± 1	0.73 ± 0.07
21	844 ± 7	75 ± 2	0.84 ± 0.12

22	620 ± 3	87 ± 1	0.69 ± 0.07
23	728 ± 3	71 ± 1	0.90 ± 0.07
24	717 ± 3	60 ± 1	0.59 ± 0.08
25	704 ± 1	74 ± 0	0.92 ± 0.05
26	706 ± 2	76 ± 0	0.78 ± 0.05
27	719 ± 3	74 ± 1	0.81 ± 0.08
28	707 ± 2	90 ± 1	0.95 ± 0.07
29	688 ± 2	117 ± 5	0.66 ± 0.06
44	777 ± 1	91 ± 0	0.91 ± 0.05
46	703 ± 1	97 ± 1	0.77 ± 0.06
47	672 ± 1	85 ± 0	0.83 ± 0.05
48	713 ± 1	92 ± 0	0.81 ± 0.04
49	711 ± 2	90 ± 0	0.68 ± 0.05
51	801 ± 3	95 ± 0	0.85 ± 0.08
52	820 ± 2	81 ± 0	0.68 ± 0.04
53	717 ± 1	87 ± 0	0.74 ± 0.05
54	693 ± 2	86 ± 0	0.70 ± 0.07
56	689 ± 2	85 ± 1	0.78 ± 0.04
57	686 ± 3	92 ± 1	0.73 ± 0.07
58	588 ± 2	85 ± 1	0.87 ± 0.08
59	652 ± 2	91 ± 1	0.81 ± 0.08
63	770 ± 8	86 ± 2	0.84 ± 0.07
65	703 ± 2	88 ± 1	0.77 ± 0.07
67	645 ± 2	76 ± 0	0.67 ± 0.05
68	722 ± 2	88 ± 0	0.86 ± 0.03
78	786 ± 4	90 ± 1	0.75 ± 0.07
79	669 ± 2	81 ± 1	0.69 ± 0.06
84	655 ± 2	81 ± 1	0.83 ± 0.07
85	635 ± 2	76 ± 1	0.83 ± 0.06

86	763 ± 5	79 ± 1	0.90 ± 0.10
87	691 ± 2	68 ± 0	0.86 ± 0.06
88	701 ± 2	76 ± 0	0.82 ± 0.06
90	686 ± 2	80 ± 0	0.83 ± 0.06
92	720 ± 2	78 ± 0	0.82 ± 0.06
93	727 ± 3	76 ± 1	0.83 ± 0.06
94	711 ± 2	74 ± 0	0.78 ± 0.05
95	691 ± 2	74 ± 0	0.81 ± 0.05
96	687 ± 2	68 ± 0	0.89 ± 0.05
97	632 ± 3	29 ± 1	0.73 ± 0.08
98	718 ± 2	77 ± 1	0.71 ± 0.07
99	607 ± 3	74 ± 1	0.84 ± 0.06
100	618 ± 2	63 ± 0	0.71 ± 0.05
101	754 ± 2	72 ± 1	0.80 ± 0.07
106	700 ± 1	85 ± 1	0.80 ± 0.03
107	703 ± 1	76 ± 0	0.85 ± 0.05
108	662 ± 1	84 ± 0	0.77 ± 0.06
110	756 ± 1	121 ± 0	0.42 ± 0.04
112	777 ± 1	114 ± 0	0.48 ± 0.04
114	755 ± 3	89 ± 1	0.98 ± 0.08
115	651 ± 1	83 ± 0	0.76 ± 0.06
116	707 ± 2	83 ± 1	0.84 ± 0.07
117	673 ± 1	86 ± 0	0.75 ± 0.06
118	643 ± 2	80 ± 0	0.95 ± 0.08
121	722 ± 2	69 ± 0	0.85 ± 0.05
122	628 ± 2	75 ± 1	0.73 ± 0.06
123	731 ± 2	79 ± 0	0.70 ± 0.06
124	650 ± 1	81 ± 0	0.84 ± 0.05
127	658 ± 2	81 ± 0	0.74 ± 0.07

128	820 ± 4	70 ± 1	0.80 ± 0.10
129	691 ± 2	92 ± 1	0.86 ± 0.07
131	681 ± 2	82 ± 0	0.75 ± 0.05
132	738 ± 1	73 ± 0	0.74 ± 0.04
133	730 ± 2	74 ± 0	0.72 ± 0.05
134	634 ± 2	84 ± 0	0.88 ± 0.07
135	705 ± 2	71 ± 0	0.85 ± 0.05
136	702 ± 1	68 ± 0	0.89 ± 0.04
137	636 ± 2	72 ± 0	0.83 ± 0.06
139	752 ± 1	71 ± 0	0.79 ± 0.04
140	724 ± 1	73 ± 0	0.79 ± 0.04
141	708 ± 2	82 ± 0	0.82 ± 0.05
142	757 ± 1	76 ± 0	0.74 ± 0.04
143	738 ± 1	77 ± 0	0.84 ± 0.05
144	754 ± 1	91 ± 0	0.77 ± 0.05
146	682 ± 2	82 ± 0	0.72 ± 0.04
147	671 ± 1	86 ± 0	0.88 ± 0.06
148	710 ± 2	77 ± 0	0.78 ± 0.06
149	782 ± 3	78 ± 0	0.72 ± 0.07
150	662 ± 2	86 ± 1	0.75 ± 0.06
152	700 ± 1	82 ± 0	0.91 ± 0.06
154	807 ± 3	79 ± 0	0.69 ± 0.07
155	689 ± 2	80 ± 0	0.94 ± 0.07
156	694 ± 2	87 ± 0	0.78 ± 0.06
157	739 ± 1	79 ± 0	0.80 ± 0.05
158	676 ± 1	74 ± 0	0.79 ± 0.04
159	690 ± 2	74 ± 0	0.86 ± 0.06
160	709 ± 3	78 ± 0	0.75 ± 0.10
161	729 ± 2	78 ± 0	0.83 ± 0.09

162	705 ± 3	73 ± 0	0.77 ± 0.05
164	778 ± 1	73 ± 0	0.79 ± 0.09
165	696 ± 1	75 ± 0	0.77 ± 0.05
166	662 ± 1	82 ± 0	0.87 ± 0.05
167	660 ± 1	86 ± 0	0.82 ± 0.05
169	688 ± 1	97 ± 0	0.65 ± 0.02
170	640 ± 0	178 ± 0	0.42 ± 0.03

Table 5: Results from the Lipari and Szabo model-free analysis of the ^{15}N -relaxation data of Rheb Δ CT bound to GDP with TENSOR2

Residue	Model	χ^2	$S^2 \pm \text{error}$	$\tau_i [\text{ns}] \pm \text{error}$	$R_{\text{ex}} [\text{s}^{-1}] \pm \text{error}$
6	5	0.00(0)	0.94 ± 0.01	0.940 ± 0.451	0.0 ± 0.0
7	5	0.00(0)	0.94 ± 0.01	5.140 ± 3.320	0.0 ± 0.0
8	(6)5	0.17(4)	0.90 ± 0.01	9.900 ± 3.390	0.0 ± 0.0
9	5	0.00(0)	0.87 ± 0.02	3.730 ± 2.920	0.0 ± 0.0
10	(6)5	0.13(8)	0.84 ± 0.02	9.900 ± 3.050	0.0 ± 0.0
11	5	0.00(0)	0.95 ± 0.01	1.460 ± 2.420	0.0 ± 0.0
12	5	0.00(0)	0.97 ± 0.01	1.080 ± 2.560	0.0 ± 0.0
14	1	0.67(7)	0.85 ± 0.00	0.000 ± 0.000	0.0 ± 0.0
15	(6)5	0.51(5)	0.89 ± 0.02	9.900 ± 3.880	0.8 ± 0.0
16	3	0.00(6)	0.84 ± 0.00	0.000 ± 0.000	1.1 ± 0.1
18	5	0.00(0)	0.95 ± 0.01	3.000 ± 3.430	0.0 ± 0.0
19	(6)5	5.68(0)	1.03 ± 0.01	9.900 ± 4.150	0.0 ± 0.0
20	(6)3	3.54(0)	0.82 ± 0.00	0.000 ± 0.000	2.2 ± 0.1
21	(3)3	11.40(0)	0.78 ± 0.00	0.000 ± 0.000	2.3 ± 0.0
22	1	4.59(0)	0.87 ± 0.00	0.000 ± 0.000	0.0 ± 0.0
24	3	1.57(0)	0.85 ± 0.00	0.000 ± 0.000	1.2 ± 0.1
25	(3)3	10.70(0)	0.87 ± 0.00	0.000 ± 0.000	0.2 ± 0.0
26	(6)5	10.50(0)	1.09 ± 0.01	9.900 ± 3.130	0.0 ± 0.0

27	3	1.04(0)	0.84 ± 0.00	0.000 ± 0.000	1.5 ± 0.1
28	3	0.01(8)	0.81 ± 0.00	0.000 ± 0.000	1.5 ± 0.1
29	(6)5	0.69(2)	0.93 ± 0.01	9.840 ± 3.760	0.0 ± 0.0
31	2	0.99(4)	0.78 ± 0.00	0.010 ± 0.004	0.0 ± 0.0
32	2	0.24(5)	0.77 ± 0.00	0.021 ± 0.007	0.0 ± 0.0
33	5	0.00(0)	0.84 ± 0.01	2.330 ± 0.472	0.0 ± 0.0
34	5	0.00(0)	0.81 ± 0.01	3.330 ± 1.350	0.0 ± 0.0
35	5	0.00(0)	0.65 ± 0.00	1.580 ± 0.075	0.0 ± 0.0
36	5	0.00(0)	0.97 ± 0.01	1.720 ± 3.760	0.0 ± 0.0
38	3	0.61(8)	0.83 ± 0.00	0.000 ± 0.000	1.2 ± 0.1
39	2	1.30(0)	0.87 ± 0.00	0.054 ± 0.023	0.0 ± 0.0
40	1	1.69(0)	0.85 ± 0.00	0.000 ± 0.000	0.0 ± 0.0
41	4	0.00(0)	0.73 ± 0.01	0.019 ± 0.006	1.7 ± 0.1
42	3	2.14(0)	0.78 ± 0.00	0.000 ± 0.000	2.6 ± 0.1
43	3	1.94(0)	0.87 ± 0.00	0.000 ± 0.000	1.1 ± 0.1
44	3	0.44(7)	0.79 ± 0.00	0.000 ± 0.000	1.1 ± 0.1
45	3	3.83(0)	0.85 ± 0.00	0.000 ± 0.000	0.8 ± 0.1
46	3	0.01(7)	0.81 ± 0.00	0.000 ± 0.000	1.9 ± 0.1
47	3	1.21(0)	0.84 ± 0.00	0.000 ± 0.000	0.6 ± 0.1
48	3	0.62(1)	0.82 ± 0.00	0.000 ± 0.000	1.6 ± 0.1
51	3	0.03(3)	0.74 ± 0.00	0.000 ± 0.000	2.5 ± 0.1
52	3	1.59(0)	0.76 ± 0.00	0.000 ± 0.000	0.8 ± 0.1
53	4	0.00(0)	0.76 ± 0.01	0.015 ± 0.007	1.7 ± 0.1
54	(6)5	0.83(4)	0.92 ± 0.01	9.900 ± 3.00	0.0 ± 0.0
55	(6)5	0.47(7)	0.94 ± 0.01	9.900 ± 3.500	0.0 ± 0.0
56	5	0.00(0)	0.84 ± 0.03	5.500 ± 2.840	0.0 ± 0.0
57	5	0.00(0)	0.76 ± 0.03	7.530 ± 2.780	0.0 ± 0.0
58	(6)5	2.73(0)	0.48 ± 0.05	9.890 ± 2.100	0.0 ± 0.0
59	(6)5	1.66(0)	0.83 ± 0.02	9.900 ± 3.000	0.0 ± 0.0
60	5	0.00(0)	0.94 ± 0.03	0.794 ± 2.000	0.0 ± 0.0
61	(6)5	4.06(0)	0.85 ± 0.02	9.900 ± 2.940	0.0 ± 0.0

62	4	0.00(0)	0.76 ± 0.01	0.055 ± 0.009	0.8 ± 0.1
63	(6)5	0.73(0)	0.69 ± 0.04	9.890 ± 3.000	0.0 ± 0.0
64	(6)5	4.94(0)	0.92 ± 0.01	9.900 ± 3.420	0.0 ± 0.0
65	3	0.52(9)	0.79 ± 0.00	0.000 ± 0.000	1.0 ± 0.1
66	3	2.49(0)	0.79 ± 0.00	0.000 ± 0.000	0.7 ± 0.1
68	3	0.12(1)	0.80 ± 0.00	0.000 ± 0.000	0.4 ± 0.1
69	6 (4)	1.06(0)	0.20 ± 0.07	9.090 ± 1.740	8.3 ± 0.5
74	3	0.73(6)	0.93 ± 0.00	0.000 ± 0.000	1.2 ± 0.1
75	(6)5	0.08(9)	0.86 ± 0.02	9.900 ± 3.080	0.0 ± 0.0
76	4	0.00(0)	0.77 ± 0.01	0.097 ± 0.012	0.4 ± 0.1
77	3	0.36(5)	0.84 ± 0.00	0.000 ± 0.000	2.7 ± 0.1
78	(6)5	0.04(6)	0.95 ± 0.01	9.840 ± 4.050	0.0 ± 0.0
79	2	3.52(0)	0.83 ± 0.00	0.029 ± 0.008	0.0 ± 0.0
83	5	0.00(0)	0.93 ± 0.01	1.270 ± 1.370	0.0 ± 0.0
84	5	0.00(0)	0.94 ± 0.01	2.560 ± 3.000	0.0 ± 0.0
85	(6)5	5.09(0)	0.98 ± 0.01	9.810 ± 4.000	0.0 ± 0.0
86	3	0.00(5)	0.81 ± 0.00	0.000 ± 0.000	0.3 ± 0.1
87	3	0.18(4)	0.83 ± 0.00	0.000 ± 0.000	2.2 ± 0.1
88	(3)3	8.03(0)	0.84 ± 0.00	0.000 ± 0.000	0.5 ± 0.0
89	3	1.53(0)	0.84 ± 0.00	0.000 ± 0.000	1.3 ± 0.0
90	3	0.81(7)	0.86 ± 0.00	0.000 ± 0.000	0.2 ± 0.1
91	(6)5	21.30(0)	0.97 ± 0.00	9.900 ± 3.790	0.0 ± 0.0
92	3	0.68(1)	0.84 ± 0.00	0.000 ± 0.000	0.7 ± 0.1
93	2	3.29(0)	0.87 ± 0.00	0.037 ± 0.011	0.0 ± 0.0
94	(6)3	5.98(0)	0.81 ± 0.00	0.000 ± 0.000	1.6 ± 0.1
95	3	2.03(0)	0.86 ± 0.00	0.000 ± 0.000	0.8 ± 0.1
96	3	1.96(0)	0.87 ± 0.00	0.000 ± 0.000	2.9 ± 0.1
97	3	0.00(3)	0.87 ± 0.01	0.000 ± 0.000	2.1 ± 0.1
98	3	0.48(4)	0.84 ± 0.00	0.000 ± 0.000	0.3 ± 0.1
99	3	0.32(3)	0.82 ± 0.00	0.000 ± 0.000	0.9 ± 0.1
101	3	0.12(2)	0.86 ± 0.00	0.000 ± 0.000	1.3 ± 0.0

105	3	0.41(4)	0.82 ± 0.00	0.000 ± 0.000	1.1 ± 0.0
106	3	4.00(0)	0.81 ± 0.00	0.000 ± 0.000	0.3 ± 0.0
107	3	0.94(5)	0.82 ± 0.00	0.000 ± 0.000	0.1 ± 0.0
108	5	0.00(0)	0.93 ± 0.01	2.000 ± 0.741	0.0 ± 0.0
109	5	0.00(0)	0.89 ± 0.01	1.280 ± 0.240	0.0 ± 0.0
110	5	0.00(0)	0.71 ± 0.00	1.200 ± 0.062	0.0 ± 0.0
111	5	0.00(0)	0.79 ± 0.01	1.340 ± 0.117	0.0 ± 0.0
112	5	0.00(0)	0.79 ± 0.00	0.899 ± 0.055	0.0 ± 0.0
115	5	0.00(0)	0.91 ± 0.01	2.130 ± 2.210	0.0 ± 0.0
116	(6)5	6.86(0)	0.90 ± 0.01	9.900 ± 3.280	0.0 ± 0.0
118	(6)5	0.43(7)	0.96 ± 0.01	9.900 ± 3.910	0.0 ± 0.0
119	3	1.32(0)	0.86 ± 0.00	0.000 ± 0.000	0.2 ± 0.1
120	3	2.99(0)	0.76 ± 0.01	0.000 ± 0.000	1.7 ± 0.1
121	3	0.54(5)	0.83 ± 0.00	0.000 ± 0.000	1.5 ± 0.1
122	(6)5	4.11(0)	1.01 ± 0.01	7.680 ± 4.110	0.0 ± 0.0
123	(6)5	5.54(0)	1.01 ± 0.01	3.880 ± 4.480	0.0 ± 0.0
124	2	1.54(0)	0.84 ± 0.00	0.016 ± 0.006	0.0 ± 0.0
125	3	3.19(0)	0.77 ± 0.00	0.000 ± 0.000	1.4 ± 0.1
127	2	2.25(0)	0.85 ± 0.00	0.051 ± 0.013	0.0 ± 0.0
128	3	1.43(0)	0.84 ± 0.00	0.000 ± 0.000	1.3 ± 0.1
129	(6)5	0.12(2)	0.91 ± 0.01	9.900 ± 3.730	0.0 ± 0.0
130	3	1.18(0)	0.82 ± 0.00	0.000 ± 0.000	0.4 ± 0.1
131	(6)5	9.35(0)	0.97 ± 0.00	9.760 ± 3.860	0.0 ± 0.0
132	(6)5	13.40(0)	1.07 ± 0.01	9.900 ± 3.240	0.0 ± 0.0
133	3	0.00(0)	0.82 ± 0.00	0.000 ± 0.000	0.6 ± 0.0
134	5	0.00(0)	0.93 ± 0.01	1.850 ± 2.590	0.0 ± 0.0
135	3	1.56(0)	0.87 ± 0.00	0.000 ± 0.000	0.3 ± 0.1
136	3	2.37(0)	0.86 ± 0.00	0.000 ± 0.000	1.1 ± 0.0
137	5	0.00(0)	0.93 ± 0.01	1.830 ± 3.000	0.0 ± 0.0
138	(6)5	3.74(0)	1.04 ± 0.01	9.900 ± 3.680	0.0 ± 0.0
139	3	2.14(0)	0.84 ± 0.00	0.000 ± 0.000	1.2 ± 0.0

140	3	0.06(1)	0.87 ± 0.00	0.000 ± 0.000	0.8 ± 0.0
141	5	0.00(0)	0.95 ± 0.01	1.720 ± 2.850	0.0 ± 0.0
142	4	0.00(0)	0.73 ± 0.01	0.082 ± 0.012	2.2 ± 0.1
143	(6)3	4.15(0)	0.79 ± 0.00	0.000 ± 0.000	1.6 ± 0.1
144	5	0.00(0)	0.94 ± 0.01	1.300 ± 0.463	0.0 ± 0.0
145	(6)5	4.74(0)	0.96 ± 0.01	9.870 ± 3.660	0.0 ± 0.0
146	(6)5	2.80(0)	0.96 ± 0.01	9.900 ± 3.830	0.0 ± 0.0
147	5	0.00(0)	0.96 ± 0.01	2.540 ± 3.770	0.0 ± 0.0
148	(3)3	11.00(0)	0.85 ± 0.00	0.000 ± 0.000	0.6 ± 0.0
149	3	1.79(0)	0.77 ± 0.00	0.000 ± 0.000	1.5 ± 0.1
150	(6)5	13.20(0)	1.00 ± 0.01	9.900 ± 4.480	0.0 ± 0.0
151	1	2.40(0)	0.86 ± 0.00	0.000 ± 0.000	0.0 ± 0.0
152	5	0.00(0)	0.97 ± 0.01	2.340 ± 3.940	0.0 ± 0.0
154	3	0.73(2)	0.75 ± 0.00	0.000 ± 0.000	1.2 ± 0.1
155	(6)5	0.06(4)	0.87 ± 0.02	9.900 ± 3.450	0.0 ± 0.0
156	(6)5	1.17(0)	0.92 ± 0.01	9.900 ± 3.700	0.0 ± 0.0
157	3	3.25(0)	0.84 ± 0.00	0.000 ± 0.000	0.9 ± 0.1
158	3	1.32(0)	0.87 ± 0.00	0.000 ± 0.000	0.6 ± 0.1
159	3	0.49(6)	0.87 ± 0.01	0.000 ± 0.000	0.5 ± 0.1
160	3	0.11(1)	0.86 ± 0.00	0.000 ± 0.000	0.5 ± 0.1
161	3	0.71(5)	0.83 ± 0.01	0.000 ± 0.000	0.9 ± 0.1
163	4	0.00(0)	0.88 ± 0.01	0.059 ± 0.016	0.2 ± 0.1
164	3	0.13(6)	0.83 ± 0.00	0.000 ± 0.000	1.2 ± 0.1
165	4	0.00(0)	0.87 ± 0.01	0.044 ± 0.013	0.4 ± 0.1
166	3	0.19(9)	0.86 ± 0.00	0.000 ± 0.000	0.5 ± 0.0
167	(6)5	0.27(5)	0.89 ± 0.01	9.900 ± 3.000	0.0 ± 0.0
168	5	0.00(0)	0.90 ± 0.01	1.200 ± 0.175	0.0 ± 0.0
169	5	0.00(0)	0.69 ± 0.01	1.540 ± 0.102	0.0 ± 0.0
170	5	0.00(0)	0.39 ± 0.00	1.810 ± 0.085	0.0 ± 0.0

Table 6: Results from the Lipari and Szabo model-free analysis of the ^{15}N -relaxation data of Rheb Δ CT bound to GppNHp with TENSOR2

Residue	Model	χ^2	$S^2 \pm \text{error}$	$\tau_i [\text{ns}] \pm \text{error}$	$R_{\text{ex}} [\text{s}^{-1}] \pm \text{error}$
4	5	0.00(0)	0.59 ± 0.01	0.95 ± 0.07	0.0 ± 0.0
5	5	0.00(0)	0.74 ± 0.01	1.00 ± 0.12	0.0 ± 0.0
6	2	4.46(0)	0.75 ± 0.00	0.03 ± 0.00	0.0 ± 0.0
7	(6)5	1.61(0)	0.88 ± 0.02	10.40 ± 3.67	0.0 ± 0.0
8	(6)5	0.06(5)	0.86 ± 0.02	10.40 ± 3.62	0.0 ± 0.0
9	5	0.00(0)	0.92 ± 0.01	1.82 ± 2.57	0.0 ± 0.0
10	5	0.00(0)	0.90 ± 0.01	1.36 ± 2.64	0.0 ± 0.0
11	5	0.00(0)	0.94 ± 0.01	2.33 ± 3.66	0.0 ± 0.0
12	(6)5	0.57(5)	0.96 ± 0.01	10.40 ± 4.23	0.0 ± 0.0
13	5	0.00(0)	0.87 ± 0.02	5.90 ± 3.56	0.0 ± 0.0
14	(6)5	0.85(0)	0.97 ± 0.01	10.40 ± 4.54	0.0 ± 0.0
16	(6)5	1.35(0)	0.79 ± 0.03	10.40 ± 3.38	0.0 ± 0.0
17	5	0.00(0)	0.94 ± 0.01	2.86 ± 4.10	0.0 ± 0.0
18	3	0.03(0)	0.71 ± 0.00	0.00 ± 0.00	1.9 ± 0.1
20	3	0.15(7)	0.83 ± 0.00	0.00 ± 0.00	2.9 ± 0.1
21	3	0.37(2)	0.81 ± 0.00	0.00 ± 0.00	0.3 ± 0.1
22	3	0.00(0)	0.83 ± 0.00	0.00 ± 0.00	1.3 ± 0.0
23	3	1.37(0)	0.75 ± 0.01	0.00 ± 0.00	0.5 ± 0.2
26	3	0.12(4)	0.85 ± 0.00	0.00 ± 0.00	1.4 ± 0.1
27	3	0.15(2)	0.81 ± 0.00	0.00 ± 0.00	2.2 ± 0.1
28	5	0.00(0)	0.94 ± 0.01	4.00 ± 0.00	0.0 ± 0.0
29	(6)5	2.62(0)	0.91 ± 0.01	10.40 ± 3.84	0.0 ± 0.0
43	3	0.01(2)	0.85 ± 0.00	0.00 ± 0.00	0.9 ± 0.1
44	(6)5	7.07(0)	0.92 ± 0.01	10.40 ± 3.90	0.0 ± 0.0
45	5	0.00(0)	0.97 ± 0.01	1.86 ± 3.84	0.0 ± 0.0
46	5	0.00(0)	0.91 ± 0.02	2.93 ± 3.51	0.0 ± 0.0
47	3	2.14(0)	0.84 ± 0.00	0.00 ± 0.00	0.2 ± 0.0

48	(6)5	0.05(4)	0.97 ± 0.00	10.40 ± 4.14	0.0 ± 0.0
49	5	0.00(0)	0.93 ± 0.01	2.08 ± 2.81	0.0 ± 0.0
51	4	0.00(0)	0.70 ± 0.01	0.02 ± 0.01	0.3 ± 0.1
52	3	4.46(0)	0.74 ± 0.00	0.00 ± 0.00	1.7 ± 0.0
53	2	0.13(5)	0.76 ± 0.00	0.01 ± 0.00	0.0 ± 0.0
54	4	0.00(0)	0.76 ± 0.01	0.03 ± 0.00	0.7 ± 0.1
55	5	0.00(0)	0.98 ± 0.01	1.61 ± 0.00	0.0 ± 0.0
56	5	0.00(0)	0.93 ± 0.01	1.25 ± 0.00	0.0 ± 0.0
57	5	0.00(0)	0.96 ± 0.01	0.91 ± 3.00	0.0 ± 0.0
58	(6)5	1.20(0)	0.89 ± 0.01	10.40 ± 3.89	0.0 ± 0.0
59	(6)5	1.94(0)	0.88 ± 0.02	10.40 ± 3.76	0.0 ± 0.0
63	3	1.37(0)	0.72 ± 0.00	0.00 ± 0.00	2.0 ± 0.1
65	4	0.00(0)	0.75 ± 0.01	0.02 ± 0.01	0.4 ± 0.1
66	3	0.28(4)	0.81 ± 0.01	0.00 ± 0.00	0.9 ± 0.2
67	1	4.42(0)	0.87 ± 0.00	0.00 ± 0.00	0.0 ± 0.0
68	3	0.08(0)	0.76 ± 0.00	0.00 ± 0.00	0.7 ± 0.0
77	5	0.00(0)	0.95 ± 0.01	2.11 ± 4.14	0.0 ± 0.0
79	5	0.00(0)	0.92 ± 0.01	1.00 ± 0.64	0.0 ± 0.0
80	5	0.00(0)	0.83 ± 0.01	1.77 ± 0.63	0.0 ± 0.0
81	3	1.74(0)	0.86 ± 0.00	0.00 ± 0.00	0.2 ± 0.1
82	5	0.00(0)	0.94 ± 0.01	2.48 ± 3.63	0.0 ± 0.0
83	(6)5	0.58(6)	0.84 ± 0.02	10.40 ± 3.63	0.0 ± 0.0
84	(6)5	3.59(0)	0.93 ± 0.01	10.40 ± 4.14	0.0 ± 0.0
85	(6)5	1.79(0)	0.99 ± 0.01	10.40 ± 4.67	0.0 ± 0.0
86	1	6.31(0)	0.85 ± 0.00	17 ± 0.00	0.0 ± 0.0
87	(6)3	3.49(0)	0.84 ± 0.00	0.00 ± 0.00	3.2 ± 0.1
88	3	0.42(3)	0.82 ± 0.00	0.00 ± 0.00	0.9 ± 0.0
90	5	0.00(0)	0.98 ± 0.01	2.17 ± 4.56	0.0 ± 0.0
92	(6)5	1.13(0)	0.96 ± 0.01	10.40 ± 4.17	0.0 ± 0.0
93	3	1.22(0)	0.83 ± 0.00	0.00 ± 0.00	0.2 ± 0.0
94	3	1.47(0)	0.85 ± 0.00	0.00 ± 0.00	0.8 ± 0.0

95	3	0.00(1)	0.84 ± 0.00	0.00 ± 0.00	0.9 ± 0.0
96	3	0.70(5)	0.83 ± 0.00	0.00 ± 0.00	2.2 ± 0.0
97	3	0.45(5)	0.88 ± 0.00	0.00 ± 0.00	0.2 ± 0.1
98	5	0.00(0)	1.07 ± 0.01	1.09 ± 1.78	0.0 ± 0.0
99	3	0.01(5)	0.83 ± 0.00	0.00 ± 0.00	1.7 ± 0.0
100	3	0.70(2)	0.76 ± 0.00	0.00 ± 0.00	3.4 ± 0.0
101	(3)3	10.60(0)	0.86 ± 0.00	0.00 ± 0.00	0.5 ± 0.0
102	3	1.37(0)	0.81 ± 0.00	0.00 ± 0.00	1.2 ± 0.0
107	4	0.00(0)	0.77 ± 0.01	0.03 ± 0.01	1.8 ± 0.1
108	5	0.00(0)	0.89 ± 0.01	1.23 ± 0.26	0.0 ± 0.0
109	3	0.67(1)	0.76 ± 0.00	0.00 ± 0.00	0.2 ± 0.1
110	5	0.00(0)	0.75 ± 0.01	1.11 ± 0.07	0.0 ± 0.0
111	5	0.00(0)	0.75 ± 0.01	1.47 ± 0.17	0.0 ± 0.0
112	5	0.00(0)	0.77 ± 0.01	0.92 ± 0.06	0.0 ± 0.0
114	5	0.00(0)	0.92 ± 0.01	1.71 ± 3.21	0.0 ± 0.0
115	5	0.00(0)	0.93 ± 0.01	1.66 ± 2.44	0.0 ± 0.0
116	5	0.00(0)	0.86 ± 0.02	2.80 ± 2.78	0.0 ± 0.0
117	(6)5	0.20(0)	0.86 ± 0.02	10.40 ± 3.56	0.0 ± 0.0
118	(6)3	7.98(0)	0.81 ± 0.00	0.00 ± 0.00	0.7 ± 0.1
119	(6)5	0.29(5)	0.98 ± 0.00	10.40 ± 4.25	0.0 ± 0.0
120	3	0.01(3)	0.81 ± 0.00	0.00 ± 0.00	0.0 ± 0.5
121	(6)3	5.65(0)	0.82 ± 0.00	0.00 ± 0.00	1.9 ± 0.0
122	(6)5	3.12(0)	1.02 ± 0.04	0.19 ± 3.84	0.0 ± 0.0
123	(3)3	8.72(0)	0.84 ± 0.00	0.00 ± 0.00	0.3 ± 0.0
124	3	0.00(9)	0.80 ± 0.00	0.00 ± 0.00	0.4 ± 0.0
126	4	0.00(0)	0.77 ± 0.01	0.03 ± 0.01	0.8 ± 0.1
127	(6)5	0.28(0)	0.98 ± 0.00	10.30 ± 4.17	0.0 ± 0.0
128	3	0.61(6)	0.87 ± 0.00	0.00 ± 0.00	1.9 ± 0.1
129	5	0.00(0)	0.91 ± 0.01	1.91 ± 3.32	0.0 ± 0.0
130	3	0.25(2)	0.80 ± 0.00	0.00 ± 0.00	0.1 ± 0.0
131	1	4.94(0)	0.82 ± 0.00	0.00 ± 0.00	0.0 ± 0.0

132	3	2.69(0)	0.80 ± 0.00	0.00 ± 0.00	0.8 ± 0.0
133	3	0.05(3)	0.82 ± 0.00	0.00 ± 0.00	1.1 ± 0.0
134	(6)5	1.34(0)	0.89 ± 0.02	10.40 ± 3.62	0.0 ± 0.0
135	3	0.81(1)	0.84 ± 0.00	0.00 ± 0.00	1.3 ± 0.0
136	3	1.36(0)	0.82 ± 0.00	0.00 ± 0.00	1.5 ± 0.0
137	3	0.00(2)	0.87 ± 0.00	0.00 ± 0.00	1.0 ± 0.0
138	3	2.73(0)	0.84 ± 0.00	0.00 ± 0.00	0.6 ± 0.0
139	3	0.66(0)	0.83 ± 0.00	0.00 ± 0.00	1.3 ± 0.0
140	3	0.03(5)	0.79 ± 0.00	0.00 ± 0.00	1.7 ± 0.0
141	1	1.89(0)	0.81 ± 0.00	0.00 ± 0.00	0.0 ± 0.0
142	3	0.01(6)	0.79 ± 0.00	0.00 ± 0.00	1.9 ± 0.0
143	3	1.06(0)	0.80 ± 0.00	0.00 ± 0.00	1.5 ± 0.0
144	5	0.00(0)	0.92 ± 0.01	1.39 ± 0.67	0.0 ± 0.0
145	(6)5	6.19(0)	0.98 ± 0.00	10.40 ± 4.23	0.0 ± 0.0
146	3	0.19(4)	0.84 ± 0.00	0.00 ± 0.00	0.1 ± 0.0
147	5	0.00(0)	0.98 ± 0.01	1.06 ± 3.25	0.0 ± 0.0
148	3	0.03(5)	0.85 ± 0.00	0.00 ± 0.00	0.7 ± 0.0
149	3	0.49(7)	0.76 ± 0.00	0.00 ± 0.00	1.1 ± 0.1
150	(6)5	4.01(0)	0.98 ± 0.01	10.40 ± 4.53	0.0 ± 0.0
151	3	0.09(7)	0.83 ± 0.00	0.00 ± 0.00	0.3 ± 0.0
152	3	0.03(7)	0.82 ± 0.00	0.00 ± 0.00	0.5 ± 0.0
154	3	1.05(0)	0.81 ± 0.00	0.00 ± 0.00	0.5 ± 0.1
155	3	0.96(6)	0.85 ± 0.00	0.00 ± 0.00	0.5 ± 0.0
156	5	0.00(0)	0.96 ± 0.01	2.00 ± 3.44	0.0 ± 0.0
157	3	0.00(2)	0.82 ± 0.00	0.00 ± 0.00	0.9 ± 0.0
158	3	2.50(0)	0.83 ± 0.00	0.00 ± 0.00	1.3 ± 0.0
159	3	1.12(0)	0.85 ± 0.00	0.00 ± 0.00	0.9 ± 0.0
160	(6)5	1.38(0)	0.94 ± 0.01	10.40 ± 4.26	0.0 ± 0.0
162	3	0.02(4)	0.86 ± 0.00	0.00 ± 0.00	1.2 ± 0.0
164	3	0.14(7)	0.84 ± 0.00	0.00 ± 0.00	0.6 ± 0.0
165	3	1.78(0)	0.86 ± 0.00	0.00 ± 0.00	0.8 ± 0.0

166	3	0.13(9)	0.85 ± 0.00	0.00 ± 0.00	0.1 ± 0.0
167	(6)5	0.31(4)	0.99 ± 0.00	10.40 ± 4.54	0.0 ± 0.8
168	2	1.28(0)	0.81 ± 0.00	0.02 ± 0.00	0.0 ± 0.0
169	5	0.00(0)	0.84 ± 0.00	1.23 ± 0.06	0.0 ± 0.0
170	5	0.00(0)	0.42 ± 0.00	1.77 ± 0.06	0.0 ± 0.0

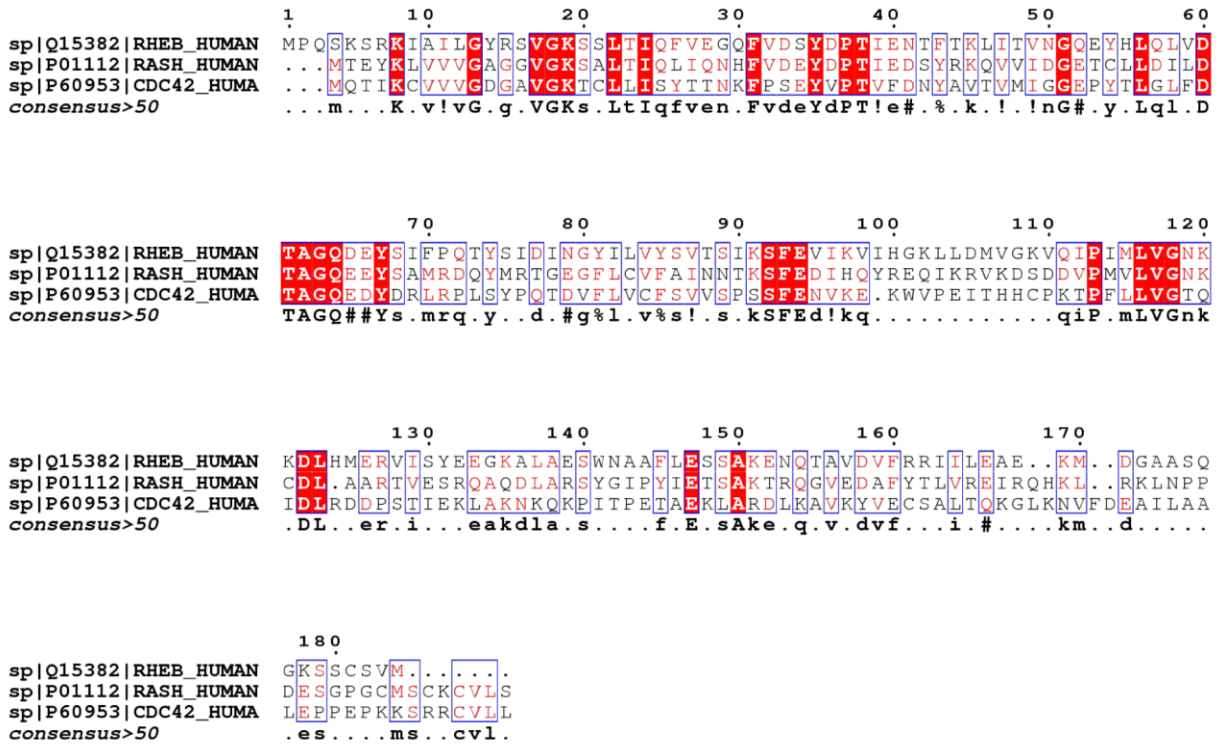


Figure 1: Picture of the alignment of the amino acid sequences of human Rheb, Ras (p21ras), and Cdc42. The respective Uniprot codes are given at the beginning of each line. The figure was made using MultAlin [173] for the alignment and ESPrict [174] for the illustration of the alignment. Adapted from [70]

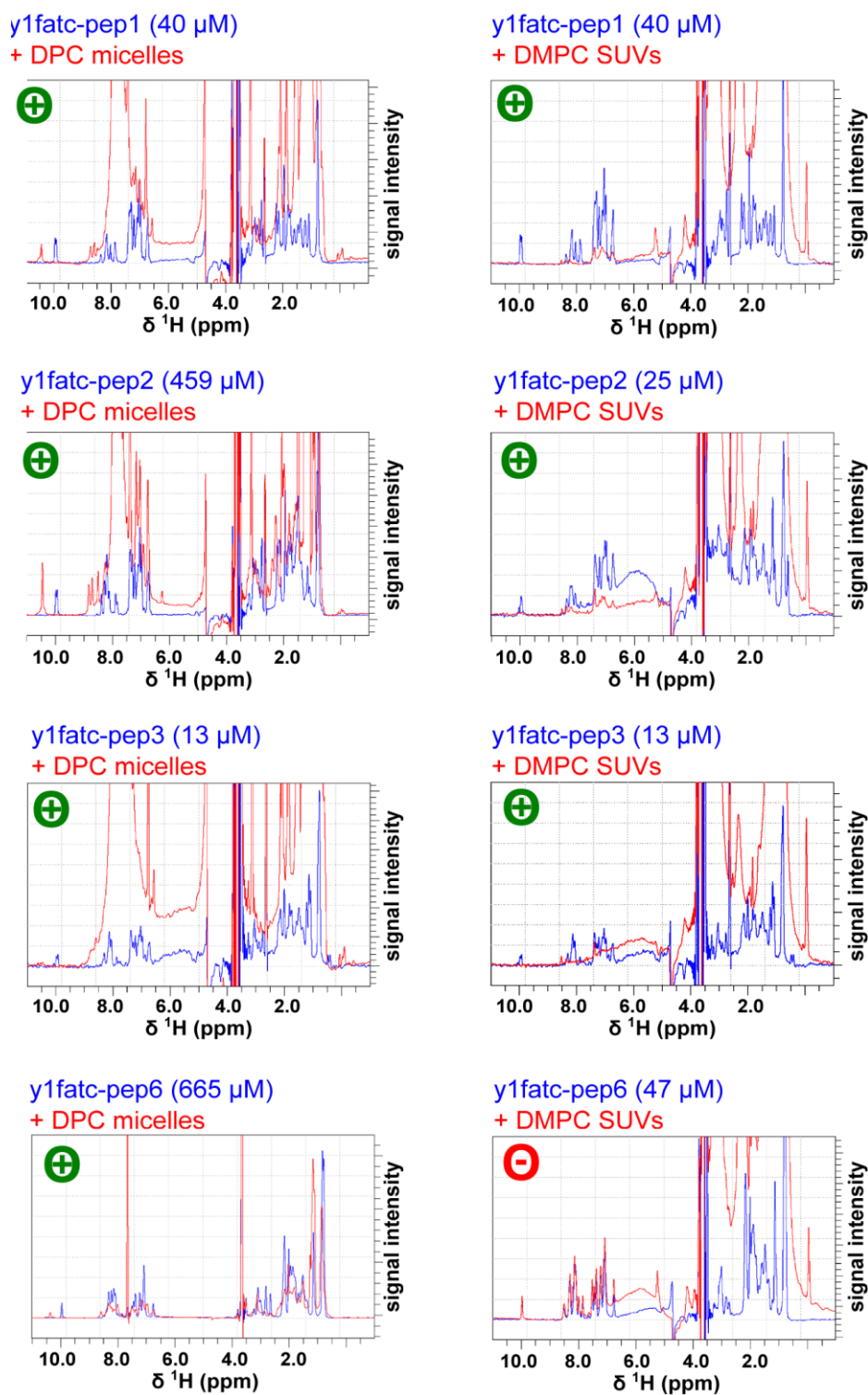


Figure 2: Monitoring of the interaction of the unlabeled y1fatc peptides with membrane mimetics by 1D ^1H NMR spectroscopy. The shown spectra picture display the full spectral region from 11 to -1 ppm for the interaction studies with DPC micelles and DMPC SUVs. In the presence of bicelles the aliphatic region is dominated by lipid signals and thus not shown. The spectra of the peptides in buffer are shown in blue and those in the additional presence of micelles (100 mM d38-DPC) or SUVs (<42 mM DMPC) in red. If the spectral changes indicate and interaction with the

respective membrane mimetic a circled green plus sign is shown in the upper left. If there are no significant spectral changes and thus interactions, a circled red minus sign is shown instead. The peptide concentrations are indicated at the top of each spectrum. Since y1fatc-pep3mutant showed a higher solubility in aqueous buffer than the other peptides, a second sample with a concentration of 0.665 mM was used to record ^1H - ^{15}N HSQC spectra at natural abundance of the peptide in buffer and in the additional presence of DPC and SUVs (only half peptide concentration due to sample preparation method, Figure 4.22 Results part in main text). Adapted from [139]

ACKNOWLEDGEMENTS

First of all I would like to thank PD. Dr. Sonja Dames for presenting me with the opportunity to undertake this project, with continued support and advice throughout my whole doctoral period. When I first came, I had any experience in biochemistry and you allowed me to work for this project. You gave me a chance to prove my qualities and I really hope I paid you back for everything you were doing for me. It was not easy, but you always gave me the time to learn how to do science. I cannot forget your human and professional guidance. Thanks for the trust, I hope to have succeeded on her expectation.

Then, thanks a lot to my colleagues Matthias and Munirah for giving always suggestions and support. It was a big pleasure for me to work with you.

I would like to acknowledge all my students who worked with me: Jonas, Leo, Lisa, Anthea, Eva Maria, Florian, Balazs. I wish you all the best for your career.

My special acknowledge also to Prof. Dr. Bernd Reif and Prof. Dr. Michael Sattler for giving me the opportunity to work in their labs. And thanks their groups for their valuable suggestions during my work.

Thanks to the Prof. Dr. Reif's group, especially Diana, Elke, Manuel, Riddhiman, Maria, Markus, Teji, Zheng, Antje for the nice time spent together in the lab. A special thank to Carina, who was a real guide for me in the last 2 years. You are a really good lab manager and I have learned a lot from you! Thank you for your huge patience.

Thanks also the Prof. Dr. Madl's group: Ben, Christoph H. and G., Gesa, Martin, Sandra. You are really good scientists and moreover you create always a positive and fruitful atmosphere. But special thank to Sandra, for all her instructions at the beginning of my project and her valuable guidance on NMR and, obviously, for her friendship. And thanks to Giannina for the pleasant moments and wine testing after work!

I thank all my Italian friends in Munich, Valeria, Marco, Filippo, Enrico, Carlo, Luca to have taking part in my German experience and to be good friends. Thanks to Irene and Francesca to share painful moments at gym!

Last but not least I would like to thank the most important persons in my life: mamma, papà, Federica e Mario. And thank you Davide for all your support, encouragement and for making me a better person. Grazie!

Thanks to all of you!

CURRICULUM VITAE

Maristella De Cicco, Mobile: +49(0)1639404169, E-mail: maristelladecicco@hotmail.com



Date of birth: 26/09/1987 in Avellino

Citizenship: Italian

Address: Brunnenweg, 23, 85748 Garching bei München

Mobile: +49 (0)163 9404169

E-mail: maristelladecicco@hotmail.com

Education

since 03/2014

Ph.D candidate

Technische Universität München. Germany.

Chair of Biomolecular NMR Spectroscopy Group of PD Dr. Sonja A. Dames

17/03/2014

Masters of II level "Drug development and design".

University of Pavia. Italy

25/01/2012

Master of Science degree in Analytical Chemistry .

University La Sapienza, Rome.

Thesis title: *Development of new stationary phases SPE constituted of biomimic ligands for the analysis of cocaine on biological samples.*

16/12/2009

Bachelor degree in Chemistry

University Federico II, Naples.

Thesis title: *Phosphines from glucose for the synthesis of organometallics drugs.*

Professional experiences

09/2013-02/2014 **Research assistant.**

BASF SE, Ludwigshafen, Germany.

Six months practical internship within the program of the II level Master at University of Pavia.R&D department, working on Lead Optimization Fungicides.

- Synthesis
- purification

01/2013-07/2013 **Quality Assurance specialist. BSP pharmaceuticals S.p.A., Latina, Italy.**

BSP Pharmaceuticals S.p.A. is focused on the development and manufacturing of anticancer drugs with high potency and cytotoxic characteristics for the Pharmaceuticals Industry.

- Manage Supplier qualification
- Manage Quality agreement flow
- SOPs updating
- Annual product review
- Internal audit

11/2012-01/2013 **Quality Assurance assistant. ITC farma s.r.l. , Pomezia (RM), Italy**

Italian company involved in the pharmaceutical production for third parties

- Support investigations on issues generated by nonconformities, customer complaints.
- Assist with the risk assessment process and evaluating product impact.
- Analyze and organize data from multiple sources by utilizing statistical tools to identify trends and recommend updates or changes when necessary.
- Provide support on Nonconformance and CAPA investigations by providing data analysis tools and assistance.
- Assist in training production personnel as needed.
- Support investigation activities and Nonconformity board review meetings
- Annual product review

Conferences and workshops

08/2016 **International Conference on Magnetic Resonance in Biological Systems**, Kyoto, Japan

07/2015 **29th Annual Symposium Protein Science**, Barcelona, Spain.

06/2015 **EMBO Practical Course on Modern biophysical methods for protein-ligand interactions**, Oulu, Finland

05/2015 **International Conference on 'Conformational transitions in proteins'** Venice International University in San Servolo, Venice

10/2014 **German-Austrian NMR meeting**, Helmholtz Zentrum, Munich